Molecular and Surface Interaction Mechanisms of Asphaltenes in Organic and Aqueous Media

by

Ling Zhang

A thesis submitted in partial fulfillment of the requirements for the degree of

Doctor of Philosophy

in

Chemical Engineering

Department of Chemical and Materials Engineering
University of Alberta

ABSTRACT

Asphaltenes are the heaviest component in crude oil and bitumen. The molecular interactions and interfacial behaviours of asphaltenes are closely related to many challenging issues in oil production, which are believed to play an important role in stabilizing water-in-oil (W/O) and oil-in-water (O/W) emulsions, surface wettability change of clays, stabilizing solid particles, and fouling problems. In this work, the intermolecular and surface interactions of asphaltenes, extracted from different oil resources, in both organic and aqueous media have been experimentally investigated using several complementary techniques including surface forces apparatus (SFA), atomic force microscope (AFM), quartz crystal microbalance with dissipation monitoring (QCM-D), contact angle goniometer and in-house built computer-controlled 4-roll mill fluidic device.

The interactions between asphaltenes were measured using SFA in heptol solvent with different ratio of n-heptane. The results showed that the interactions gradually changed from pure repulsion to weak adhesion as the ratio of toluene increased and theoretical fitting of the force curves also determined the force origin. Micropipette tests results showed asphaltenes at water/oil interfaces inhibited the coalescence of the emulsion drops and 4-roll mill tests revealed that the interfacial sliding between emulsion drops was required to destabilize the asphaltene layer at interface which could increase the probability of emulsion coalescence. The adsorption mechanisms of asphaltenes on silica surface were studied in toluene using QCM-D and SFA. It was found the adsorption of asphaltenes was dependent on the

sources of the asphaltenes and showed various behaviours under different flow and static conditions. The asphaltenes precipitated from a crude oil was found to be able to continuously adsorb on silica surface under flow condition whereas the adsorption reached the equilibrium state under static condition. Combined with the elemental and X-ray photoelectron spectroscopy (XPS) analysis, Ca and O might play an important role in the aggregation of asphaltenes even at a low concentration in toluene resulting in continuous adsorption behaviour.

The interaction mechanisms between asphaltene surfaces in aqueous solutions were investigated using SFA and AFM. The SFA results showed repulsion was measured during approach while adhesion was detected during separation. The measured long-range repulsion could be affected by the solution pH, salinity and Ca^{2+} addition whereas could not be described by the Derjaguin–Landau–Verwey–Overbeek (DLVO) theory. However, theoretical calculations based on the DLVO theory reasonably agreed with the measured force curves between AFM tip and asphaltene surfaces, indicating the DLVO interaction origin of asphaltenes in aqueous solutions at nanoscale. Pancake-like domains were observed on asphaltene films in aqueous solutions and were significantly affected by the solution conditions, which might be due to the interactions of asphaltene molecules (particularly the polar groups), water, and the supporting solid substrate. van der Waals interaction was calculated between water and mica surface across the asphaltene film and a water diffusing process was proposed for the paterning phenomena observed.

The results in this work provide insights into the fundamental understanding of molecular and surface interaction mechanisms of asphaltenes in both organic

solvents and aqueous solutions, with important implications to the stabilization/destabilization mechanisms of emulsion drops and fine solids in the presence of asphaltenes in oil production.

PREFACE

Chapter 3 of this thesis has been published as Ling Zhang, Chen Shi, Qingye Lu, Qingxia Liu, and Hongbo Zeng, "Probing Molecular Interactions of Asphaltenes in Heptol Using a Surface Forces Apparatus: Implications on Stability of Water-in-Oil Emulsions," Langmuir, vol. 32, issue 19, 4886–4895. I was responsible for the SFA and micropipette experiment and data analysis as well as the manuscript composition. Dr. Qingye Lu and I collaborated to conduct the 4-roll mill tests and data analysis. Chen Shi and Dr. Qingxia Liu contributed to manuscript edits. Dr. Hongbo Zeng was the corresponding author and was involved in the manuscript composition.

Chapter 4 of this thesis was composed by Ling Zhang. I was responsible for the QCM-D tests and all the SFA and AFM work including data analysis. Shanshan Wang helped conduct some of the QCM-D tests. Chen Shi and Dr. Qingxia Liu contributed to manuscript edits. Dr. Cesar A. Mantilla and Dr. Frans G.A. van den Berg are industrial collaborators and gave suggestions for revising the manuscript. Dr. Hongbo Zeng was the supervisor who was involved in the manuscript composition.

Chapter 5 of this thesis has been submitted as Ling Zhang, Lei Xie, Chen Shi, Jun Huang, Qingxia Liu, Cesar A. Mantilla, Frans G.A. van den Berg and Hongbo Zeng, "Interaction Mechanisms between Asphaltene Surfaces in Aqueous Solutions Studied by Surface Forces Apparatus and Atomic Force Microscope," Energy & Fuels. I was responsible for the SFA experiments, AFM imaging, data analysis as

well as the manuscript composition. Lei Xie completed the AFM force measurement and data analysis. Chen Shi and Dr. Qingxia Liu contributed to manuscript edits. Dr. Cesar A. Mantilla and Dr. Frans G.A. van den Berg are industrial collaborators and gave suggestions for revising the manuscript. Dr. Hongbo Zeng was the supervisor and corresponding author, and was involved in the manuscript composition.

Chapter 6 of this thesis was composited by Ling Zhang. I was responsible for all the experiments and data analysis. Chen Shi and Dr. Qingxia Liu contributed to manuscript edits. Dr. Hongbo Zeng was the supervisor who was involved in the manuscript composition.

Chapter 1, Chapter 2 and Chapter 7 are all origianlly written by Ling Zhang.

Dedicate to

My husband Xinwei Cui, my son Chris Cui, & my family members

ACKNOWLEDGEMENT

First of all, I would like to express my sincere gratitude to Professor Hongbo Zeng for his solid support and excellent guidance during my graduate studies. It was Prof. Zeng who guided me into the research focusing on the surface science and intermolecular forces of polymers, asphaltenes and emulsions. Every time I discussed the research work with Prof. Zeng, the most important thing I got is the way how he thinks about questions as well as his attention to the details. Besides that, he also gave me opportunities to be involved in other research fields which helped me gain more and also beneficial for my further study.

I also wish to thank Professor Qingxia Liu who has been more like a senior to me teaching me from the research to life. Prof. Liu is a very experienced and knowledgeable man from whom I learned the attitude to the scientific research. We need critical thinking, an open mind, creativity, and teamwork.

Second, I would like to thank my lovely group members who helped me in different ways to finish my project. I am so grateful to Dr. Qingye Lu who taught me how to operate the SFA step by step at the very beginning and her valuable suggestion during the SFA experiments. Thank Mr. Chen Shi for his teamwork and discussion on the experiments as well as his helpful suggestions in revising the manuscripts. Thank Mr. Jun Huang for his discussion on designing the surface force measurement and Ms. Shanshan Wang for her great help on the demonstration of QCM-D experiments. Thank Professor Zhenghe Xu for accessing his lab to use the

facilities and post doctors in Prof. Xu's group for the micropipette. The kind help from other group members is also very much appreciated.

Finally, I would like to thank my parents, parents-in-law and my twin brother as well as my husband, Xinwei Cui and my son, Chris Cui for their faith in me. Without their patience and encouragement, I would never be able to finish my Ph.D. studies.

TABLE OF CONTENTS

LIST OF TABLES

LISTS OF FIGURES

xxiii

SYMBOLS AND NOMENCLATURE

SFA   surface forces apparatus

AFM   atomic force microscope

QCM-D   quartz crystal microbalance with dissipation monitoring

DLVO   Derjaguin –Landau –Verwey –Overbeek theory

A Hamaker constant, J

D separation distance between surfaces, m

D_{jump} distance one surface jump apart from the other surface, m

$D_{applied}$ the distance to move the surfaces at the base of the double-
                      cantilever force springs, m

D_{actual} the actual distance that the surfaces move relative to each other, m

MBI   multiple beam interferometry

R_1, R_2 curvature of the surfaces, m

$\lambda_n^0, \lambda_{n-1}^0$ wavelength move of the nth and (n-1)th fringe, m

K_s spring constant, N/m

F_{ad} adhesion force, N

W_{ad} adhesion energy, mJ/m^2

ω	weight fraction
A	Hamaker constant
ψ	surface potential, V
σ	surface charge density, C/m^2
κ^{-1}	Debye length, m^{-1}
e	elementary charge, C
c_0	bulk ion-number concentration
k_B	Boltzmann constant, $m^2 \cdot kg \cdot s^{-2} \cdot K^{-1}$
ε_0	permittivity of vacuum, F/m
$P(D)$	repulsive pressure between two surfaces, Pa
R	radius of the cylindrical silica disc, m
T	temperature, C°
L	brush layer thickness, m
k	Boltzmann constant, 1.381×10^{-23} J K^{-1}
s	mean distance between two grafting points on the surface, m
Δf	frequency change, Hz
Δm	mass change on sensor surface, ng/cm^2

ΔD	dissipation change, 1E-6
ρ_q	specific density in quartz, ng/cm^3
v_q	shear wave velocity in quartz, cm/s
t_q	thickness of the quartz crystal, cm
f_0	fundamental resonance frequency, Hz
f	oscillation frequency, Hz
h	thickness, m
ρ	density, kg/m^3
η	viscosity, Pa·s
μ	shear modulus, Pa
ω	circular frequency, Hz
δ	fluid penetration depth, m
γ	surface energy, mJ/m^2
γ^d	the dispersive component (Lifshitz-van der Waals interactions), mJ/m^2
γ^+, γ^-	the polar components (Lewis acid-base), mJ/m^2
θ	contact angle, °

CHAPTER 1   **INTRODUCTION**

1.1 Overview

The crude oil industry has been shifting the oil production from conventional oil (light oil) to heavy oil and bitumen due to depletion of conventional oil reservoir and increase of the world demand. Canada, especially Alberta, relies much on the extraction of heavy oil and bitumen for the crude oil industry. Asphaltenes, the heaviest fraction in the crude oil, have raised many challenging issues for the oil industry and attracted lots of attention in the research field due to the increase in production of the high asphaltenic heavy oils and bitumen as well as its difficulties and high cost in remediation processes.

Asphaltenes precipitation and deposition problem can start from the reservoir to the downstream operations. The destabilization of asphaltenes due to pressure changes and temperature variations can lead to the asphaltenes precipitation and deposition causing wellbores and pipelines plugging.[1,2] The build-up of the precipitates can also damage the reservoir rocks and alter the wettability of the reservoir solids, finally sacrificing the oil recovery.[3] Additionally, during the heavy oil processing, the dilution of heavy oil using a paraffinic solvent for transportation can cause the asphaltenes precipitation in pipelines, tubular, and surface facilities. In the oil sands industry, the precipitation of asphaltenes happens during the paraffin-based bitumen froth treatment. Moreover, the deposition of asphaltenes in the crude oil upgrading and refinery process can lead to the fouling issues to the downstream operations.

The adsorption of asphaltenes at water/oil and solid/oil interfaces can cause many problems as well. Asphaltenes are known to play a key role in enhancing the stability of emulsions resulting in fouling and corrosion issues to the operating facilities.[4-6] The adsorption of asphaltenes on fine solids can assist their dispersion in the organic medium (i.e. a good solvent for asphaltenes) which can have detrimental impacts on the oil quality.[7] Significant efforts have been made to deal with the asphaltenes related problems, such as removing/cleaning the asphaltenes precipitation and deposition, and destabilizing the emulsion droplets either using chemical or physical treatment.[8,9] Therefore, it is of great importance for us to understand the mechanisms of asphaltenes aggregation, precipitation and adsorption at water/oil/solids interfaces, which drives us to investigate the molecular and surface interactions of asphaltenes in complex liquid media and which is also essential to ultimately solve these challenging issues caused by the asphaltenes.

1.2 Literature review

1.2.1 Asphaltenes

Asphaltenes are not a pure component and consist of different molecules with similar solubility behaviour but with different chemical structures, shapes and sizes. So asphaltenes are operationally defined as a solubility class which are soluble in aromatic solvents, such as toluene and benzene, but not soluble in n-alkanes, such as n-pentane and n-heptane.[10] Therefore, asphaltenes are generally precipitated from n-pentane or n-heptane and named after its n-alkane precipitant, such as pentane-asphaltenes and heptane-asphaltenes, in short of C5-asphaltenes and C7-asphaltenes,

respectively. Variation of the standard procedure used to extract asphaltenes will lead to the different fractions of asphaltenes obtained with different properties. Lots of techniques have been used to characterize the asphaltenes and quantities of information of asphaltenes have been achieved. Due to its complex nature, asphaltenes are usually dealt with using its average properties. A brief introduction of asphaltenes in term of its chemical composition and molecular structure is given in the following two sections.

Chemical composition

Asphaltenes is a hydrocarbon mixture containing heteroatoms, sulphur (S), oxygen (O) and nitrogen (N), as well as trace metals of iron, nickel, and vanadium.[11] The heteroatoms account for a variety of functional groups. Sulphur can be in the form of thiophenes, thiols, sulphides, disulphides and oxidized forms. Oxygen comprises the groups of carbonyls, carboxylic and ketonic. Nitrogen can exist as pyrroles and pyridines structures. Metal elements are found mainly in the form of porphyrin.[12] The carbon content and H/C molar ratio of asphaltenes can vary much depending on the sources as well as the precipitants. The carbon percent can range from around 40-80% and the molar ratio of H/C can be in the range of 1-1.2.[11] Therefore, different types of asphaltenes can have entirely different behaviours regarding their adsorption at water/oil and solid/oil interfaces and self-aggregation ability in solvents.

3

Molecular structure and molecular weight

Since asphaltenes is a mixture, there is no single well-defined molecular structure for asphaltenes molecules. Therefore, the debate always exists regarding the chemical structure of the asphaltenes. Asphaltenes consist of polycondensed aromatic rings interconnected or decorated with cyclic or linear alkanes and heteroatoms whereas two fundamental models have been proposed throughout the literature: the island model and the archipelago model.[13-15] The island structure is also called condensed structure which has a large condensed polyaromatic core with aliphatic chains on the periphery.[16-18] The archipelago structure is also known as dispersed structure which has a collection of small polyaromatic structures bridged by aliphatic chains or connected by heteroatoms.[19-21] Both models have supportive evidence from different research groups and have been successfully applied in explaining some of the asphaltenes properties. It has been reported that the archipelago model can well explain the polymer-like properties of asphaltenes while the island model corresponds well with the molecular weight of about 750 Daltons for asphaltenes proposed by Mullin.[22,23]

The molecular weight of the asphaltenes has also been under debate for many years due to the polydispersity of the asphaltenes as well as the aggregation behaviours of the asphaltenes. The molecular weight of asphaltene aggregates was measured sometimes rather than the individual asphaltene molecule. Therefore, a wide range of molecular weight of asphaltenes is expected from several hundred of Daltons to more than ten thousand Daltons depending on lots of variables such as solvent, asphaltenes concentration, temperature and even analytical techniques

applied.[24,25] Not just for the molecular weight determination, it is always very crucial to consider the self-association behaviour of asphaltenes to analyze the asphaltenes properties.

1.2.2 Asphaltenes aggregation and precipitation

There are lots of problems during oil production associated with asphaltenes aggregation behaviour and precipitation. The mechanisms of the aggregation behaviour of asphaltenes are not completely understood yet and are generally believed to attribute to π-π interactions, acid-base interactions and hydrogen bonding between asphaltene molecules. Different models are used to describe the aggregation behaviors of asphaltenes. Colloids and micelles are two commonly used terms to describe the self-association behaviors of asphaltenes. The modified Yen model (also known as Yen-Mullins model) well described the colloidal-like properties of asphaltenes in the solvents.[26,27] Due to the amphiphilic nature of the asphaltenes, asphaltenes can form micelle-like aggregates similar with surfactants. Therefore, analogous to the critical micelle concentration (CMC), a critical nano-aggregation concentration (CNAC) existed for asphaltenes solutions and was determined using different techniques, such as high-Q ultrasonic, AC and DC conductivity and NMR.[26,28-31] The modified Yen model shows that the asphaltene nanoaggregate is around 2 nm in size and composed of about six asphaltene molecules stacked through the aromatic sheets. In some literature, CMC was also used to describe the aggregation of asphaltenes.[32-35] Both experimental and theoretical methods were utilized to investigate the adsorption behaviour of asphaltenes. For example, Rogel reported a CMC of asphaltenes in various solvents using surface tension

measurement and also used a molecular thermodynamic model for predicting the CMC of asphaltenes in different solvents.[32,35,36] The CMC is slightly different from CNAC which normally shows a higher asphaltenes concentration in solution. The sudden change observed in surface tension or heat of dissociation should be due to the change of the asphaltenes aggregation behaviour which might be the formation of asphaltene clusters.[32,34] In modified Yen model, asphaltene clusters with a size of ~5 nm can form due to the further aggregation of asphaltene nano-aggregates. All these observations of CNAC and CMC of asphaltenes in solutions correspond to the colloidal-like properties of asphaltenes.

The self-association of the asphaltenes is sometimes believed to behave as polymers by some researchers.[25,37-40] Merino-Garcia found that the self-association of asphaltenes was a step-wise process and proposed a model which based on the model of polymerization. Isothermal titration calorimetry was also used by the same researcher (Merino-Garcia) and proved that CMC did not exist and association of asphaltenes was further believed to be step-wise.[37,40] "Linear Polymerization" model was also proposed by Agrawala et al. to describe the self-association of asphaltenes and they think resin could act as the terminator to asphaltenes association which was also the evidence that resin was capable of stabilizing the asphaltenes.[38]

The aggregation of asphaltenes can be affected by many factors such as the source of asphaltenes, concentrations, solvent conditions, temperature, pressure and in the presence of resin. Concentrations above 50-100 mg/L are believed for asphaltenes forming nano-aggregates.[29,41,42] The amount of the aggregation was found to increase as the solubility parameter of the solvent decreased.[43] The size of

6

asphaltene aggregates or numbers of asphaltenes in one aggregates decreased as the temperature was increased.[44-46] As reported by Espinat et al., the pressure impact on the asphaltene aggregates was not as significant as temperature.[46] However, people did find that the pressure depletion can cause the asphaltenes to precipitate.[2,47] With the addition of resin into the asphaltene solution, the size of asphaltene aggregates can also be reduced either by disrupting the interaction between asphaltene monomers or solvating the asphaltenes in solution.[48,49] Speight and Long also reported that the asphaltenes would be destabilized once the resin was removed from the oil phase.[50] The subfraction of crude oil resins, naphthenic acid, can also increase the solubility of asphaltenes in toluene in a similar way as the resins.[51,52]

As stated above, asphaltene nano-aggregates can further aggregate to clusters which are believed to be the precursors of the asphaltene flocculates leading to the asphaltenes precipitation. The precipitation of asphaltenes can result in the wellbores and pipelines plugging and equipment fouling which attracted lots of attention on studying the mechanisms of asphaltenes precipitation. Similar with the aggregation of asphaltenes, precipitation of asphaltenes occurs upon changes in solvents/oil compositions, temperature, pressure and addition of resins.[53-58] The most common methods to determine the precipitation onset of asphaltenes at atmospheric pressure are titration and microscopic examination.[59,60] At high pressure or elevated temperature, people normally used near-infrared (NIR) spectroscopy, small-angle X-ray scattering (SAXS), small-angle neutron scattering (SANS), and dynamic light scattering (DLS) to determine precipitation onset.[46,57] However, the optical methods are usually limited to light oils with low asphaltenes content due to the lower light

transmittance through the oil. The precipitated amount of asphaltenes is generally determined by filtration.[59,61,62] Many researchers proposed that van der Waals force be responsible for the flocculation of asphaltenes aggregates.[63-65] Based on the assumption of van der Waals force, the onset of the asphaltene precipitation was also predicted by measuring the refractive index (RI) of the oil mixture. Buckley used RI measurement to predict the onset of precipitations in asphaltenes solutions and studied the effects of solvents, the addition of resin and with different asphaltene fractions.[58,66] Flory-Huggins model was also used to predict the phase separation behaviour of asphaltenes in crude oil when adding different solvents.[67-70] Wang and Buckley developed a two-component asphaltene solubility model (ASM) to predict the asphaltene precipitation and defined the phase equilibrium in asphaltene solutions using Flory-Huggins model. They found that the precipitated asphaltenes increased with increasing the amount of n-alkane added, reached a maximum value, then decreased with keeping adding n-alkane in the oil.[68] A modified Flory-Huggins model was developed by Pazuki et al. and was found to calculate the precipitated amount of asphaltenes successfully by adding n-alkanes which was in a good agreement with the Flory-Huggins model and experimental data.[69]

Although the asphaltene aggregation and precipitation in solutions have been extensively studied experimentally and theoretically, the force to drive the asphaltenes to associate is still under debate and the direct force measurements between asphaltenes in solvents remain limited.

1.2.3 Asphaltenes adsorption at water/oil/solids interfaces

Asphaltenes are believed to be able to adsorb to lots of types of surfaces as well as the water/oil interfaces. As mentioned above, the fouling of the facilities surfaces and mineral surfaces as well as the stabilization of the W/O or O/W emulsions bring severe problems to the oil industry.

The adsorption of asphaltenes onto solid surfaces has been extensively studied in the model oil solutions by using different experimental techniques such as UV-vis spectrometry and quartz crystal microbalance with dissipation (QCM-D).[71-75] The adsorption process is extremely complex which can be impacted by lots of variables, such as absorbent types, asphaltenes sources, oil types, the addition of other surfactants, water contents and temperature. The solid surfaces or particles frequently used for the asphaltenes adsorption can be mainly classified into minerals, silica and alumina, metal and metal oxides. Depending on the sources of the asphaltenes, different solvents used and asphaltene concentrations, the adsorption capacity of asphaltene on various surfaces could vary from 0.2 mg/m^2 [76] to more than 100 mg/m^2.[77] Decreasing the solvent strength would normally increase the adsorbed amount of asphaltenes. Most of the studies showed that the adsorption capacity was larger in heptol solvent than that in toluene.[73] However, the reverse trend was also found that the adsorption of asphaltene on silica, alumina and TiO_2 was sometimes less in heptol compared to toluene solvent.[74] Besides the quantification of adsorbed amount, the adsorption kinetics was usually obtained and adsorption isotherm was analyzed. Non-equilibrium and equilibrium state were both reported from literature. Xie et al., reported the asphaltenes adsorption on metal surface did not reach the

equilibrium even after 700 min under flow conditions.[78] Goual used asphaltenes from five different sources and found equilibrium adsorption for four of them whereas one of them could not reach the steady state within the experiment time in 0.1 wt% asphaltenes toluene solution.[79] Ekholm et al. also reported that no equilibrium was reached for the asphaltenes adsorption on the gold surface both from toluene and heptol solvents.[73] Both monolayer and multilayer adsorption were reported throughout the related literature. Many researchers reported the Langmuir-type adsorption isotherm which represents the homogeneous monolayer adsorption.[43,71,74,76,80-82] Multilayers were also found in lots of cases, especially in high concentration of asphaltene solutions, or with longer adsorption time or in n-alkane solutions.[83-85] A QCM-D study showed asphaltene multilayer formation on the metal surface in toluene-pentane and toluene-heptane solutions.[78] Another QCM study was reported that monolayer adsorption was found at early times on gold surface in heptol solutions whereas multilayer formation was observed at much longer adsorption time.[86] However, there is also study showing that the possible multilayer formation of asphaltenes in pure toluene solvent using QCM-D.[87]

The adsorption of asphaltenes showed differences and inconsistencies throughout the literature. Therefore a thorough understanding the adsorption mechanism between asphaltenes and the solid surface is very vital for the ultimate prevention of the asphaltenes from adsorbing onto the surfaces or removal of the adsorbed asphaltenes. There are always arguments on the dominant driving force between asphaltenes and solid surface. Some researchers think it is primarily dependent on the adsorbent surfaces which include the roughness, pore size, surface

area and it is less sensitive to the asphaltenes sources (the asphaltenes composition). The adsorption of the asphaltenes on the metal surface is believed to be more likely a physical adsorption process; hence the surface characteristics mainly determine the adsorption amount of asphaltenes under the same conditions.[71,82] Other studies show that functional groups and heteroatoms contained in asphaltenes can contribute to the interaction between asphaltenes and surface.[72,75,88-91] An XPS and TOF-SIMS study showed that as the adsorbed asphaltene layer was sputtered, the concentration of S and N increased as approaching to the surface which indicates that the functional groups with these heteroatoms contributed to the initial adsorption.[89] By investigating the adsorption of asphaltenes on hydrophilic silica and hydrophobic silica surfaces, Jouault, N. et al. found that the adsorption mechanism of asphaltenes was dominated by the polar entities.[91] Moreover, the π-π interactions and H-bonding have also been reported to be responsible for the asphaltenes adsorption on solid surfaces. An early asphaltenes adsorption study on Fe_2O_3 showed that the H-bonding dominated the interactions between asphaltenes and Fe_2O_3 surface evident from the FTIR measurements and water desorption tests.[92] It is much easier to think of the π-π interactions involved in the asphaltenes adsorption because of the aromaticity of the asphaltenes. Asphaltenes with higher aromaticity showed higher tendency to form multilayers on the surface leading to the precipitations.[84] Another simulation studied also revealed that the increased aromaticity would make asphaltenes more attractive to the Fe_2O_3 surface.[93]

Asphaltenes are also known to adsorb to the water/oil interface due to the amphiphilic nature hence play a major role in stabilizing the W/O and O/W

11

emulsions. It is believed that a rigid asphaltene film formed at the interface which results in the steric hindrance between emulsions leading to the stabilization of the emulsions. To destabilize the W/O or O/W emulsions, it is vital to understand the stabilization mechanism of emulsion drops. Therefore, the properties of the adsorbed asphaltenes at interfaces have been extensively studied by various techniques, including micropipette, Langmuir trough, surface/interfacial tension measurement and pendant drop oscillation.[44,94-100] The micropipette technique is able to manipulate a pair of micrometer-size emulsion droplets and accurately obtain the surface tension at the surfaces of the emulsion drops by fitting the measured force-deformation relation.[95] Langmuir trough study showed that the asphaltene monolayer formed at the water and toluene interface was rigid and hard to be washed away by the addition of fresh toluene as well as difficulty to be displaced by other molecules which were the reasons for the extremely stable emulsion drops.[96] The rheology study of the adsorbed asphaltene film showed that a cross-linked and viscoelastic network was formed through polar interactions between asphaltenes at the interface.[48,97,100] The above techniques have provided valuable information relating to the stabilization mechanism of the W/O or O/W emulsions mainly in terms of the surface/interfacial tension or the film rheological properties. However, due to the limited work on the direct force measurement between asphaltenes or emulsion drops, the stabilization and destabilization mechanism remains unclear.

1.2.4 Interaction forces measurement of asphaltenes

The colloidal technique of AFM has been successfully applied to measure the interactions for asphaltenes/bitumen-asphaltenes/bitumen, asphaltenes/bitumen-silica

surfaces both in aqueous solutions and organic solvent.[22,101-107] Liu et al. found that the forces between asphaltenes or between bitumen surfaces were well fitted by the extended DLVO theory by incorporate with hydrophobic force and short-range steric force.[102,104] The steric force was found to dominate the interactions between asphaltenes in the organic solvent.[105,106] However, the studies on the direct force measurement of asphaltenes are still limited and only a few studies are available for measuring the interactions of asphaltenes using SFA which only focuses on the organic solvent system.[108] No SFA work has been done on the interactions of asphaltenes systematically in aqueous solutions. Therefore, it is necessary for us to further investigate the interactions of asphaltenes in various liquid surroundings which will help us improve the understanding of the interaction mechanisms of asphaltenes.

1.3 Objectives

As discussed above, asphaltenes bring many problems to the oil industry, both economically and environmentally. The main objective of this thesis is to improve our understanding of the molecular and surface interaction mechanisms of asphaltenes in various liquid media, with implications for the stabilization mechanisms of W/O and O/W emulsions in the presence of asphaltenes, aggregation and deposition behaviours of asphaltenes as well as the wettability change mechanisms of the clay surface due to asphaltenes. The key parameters which govern the interactions of asphaltenes were explored including solvent types, water chemistry and the properties of the asphaltenes. The detailed objectives are listed below.

13

(1) Measure the molecular interactions between asphaltenes in heptol solvents to provide a fundamental understanding of the aggregation behaviour of asphaltenes and micropipette and 4-roll mill fluidic device were also applied to give implications on the stabilization and destabilization of W/O emulsions in the presence of asphaltenes.

(2) Investigate the adsorption kinetics of asphaltenes on model clay surface using quartz crystal microbalance with dissipation (QCM-D). The adsorption behaviour of two different types of asphaltenes was compared. Surface forces were measured between model clay surfaces in asphaltene solutions to further elucidate the adsorption mechanisms of asphaltenes on solid surfaces in toluene.

(3) Measure the interactions between asphaltene surfaces in aqueous solutions to provide some insights into the stability mechanisms of O/W emulsions due to asphaltenes. SFA was applied to directly measure the surface forces between two asphaltene films and the effects of solution pH, salinity and Ca^{2+} addition were investigated. Atomic force microscope (AFM) imaging was applied to monitor the morphology of asphaltene films under various aqueous solution conditions which were further correlated to the SFA force measurements. The interactions between AFM tip and asphaltene film were also measured to provide more information on the interaction behaviours of asphaltenes at nanoscale.

(4) Investigate the stability of the asphaltene films on substrates with varying wettability in aqueous solutions to provide implications on the wettability change of

the reservoir solids due to adsorption of asphaltenes as well as the bitumen liberation process in oil sands industry.

1.4 Structure of the Thesis

Chapter 1 overviews the background of this project and introduces the objectives of this work. The related literature on asphaltenes is reviewed.

Chapter 2 describes the materials and the techniques used in this study. The working principle of the instruments and the experimental setup are provided.

In Chapter 3, the results of the molecular interactions between asphaltenes in heptol solvent are presented. Alexander-de Gennes model was used to describe the nature of the interaction force. Micropipettes and an in-house built 4-roll mill device were also applied to provide a further understanding of the stability of water-in-diluted bitumen emulsions.

The adsorption of asphaltenes on silica surface was investigated and presented in Chapter 4. Dynamic and static conditions were compared and the adsorption mechanism was proposed.

Chapter 5 elucidates the interactions between asphaltene surfaces in aqueous solutions. Effects of solution pH, salinity, the addition of Ca^{2+} were investigated.

Chapter 6 presents the study on the stability of asphaltene film on mica surface which is based on the work in Chapter 5. The hydrophobicity of the mica surface was varied and effects of solution pH and Ca^{2+} addition were investigated.

The overall conclusions of the study and suggestions for future work are outlined in Chapter 7.

References

(1) Hirschberg, A.; Dejong, L. N. J.; Schipper, B. A.; Meijer, J. G. *Soc Petrol Eng J* **1984**, *24*, 283-293.

(2) Hammami, A.; Phelps, C. H.; Monger-McClure, T.; Little, T. M. *Energ Fuel* **2000**, *14*, 14-18.

(3) Buckley, J. S. *Rev I Fr Petrol* **1998**, *53*, 303-312.

(4) Sjoblom, J.; Aske, N.; Auflem, I. H.; Brandal, O.; Havre, T. E.; Saether, O.; Westvik, A.; Johnsen, E. E.; Kallevik, H. *Adv Colloid Interfac* **2003**, *100*, 399-473.

(5) Czarnecki, J.; Moran, K. *Energ Fuel* **2005**, *19*, 2074-2079.

(6) Czarnecki, J. *Energ Fuel* **2009**, *23*, 1253-1257.

(7) Yan, J. N.; Plancher, H.; Morrow, N. R. *Spe Prod Facil* **1997**, *12*, 259-266.

(8) Chang, C. L.; Fogler, H. S. *Fuel Sci Techn Int* **1996**, *14*, 75-100.

(9) Al-Sahhaf, T. A.; Fahim, M. A.; Elkilani, A. S. *Fluid Phase Equilibr* **2002**, *194*, 1045-1057.

(10) Tharanivasan, A. K., UNIVERSITY OF CALGARY, 2012.

(11) Mullins, O. C.; Sheu, E. Y. *Structures and dynamics of asphaltenes*; Springer Science & Business Media, 2013.

(12) Yen, T. F.; Boucher, L. J.; Dickie, J. P.; Tynan, E. C.; Vaughan, G. B. *J I Petrol* **1969**, *55*, 87-&.

(13) Kuznicki, T.; Masliyah, J. H.; Bhattacharjee, S. *Energ Fuel* **2008**, *22*, 2379-2389.

(14) Durand, E.; Clemancey, M.; Lancelin, J. M.; Verstraete, J.; Espinat, D.; Quoineaud, A. A. *Energ Fuel* **2010**, *24*, 1051-1062.

(15) Aguilera-Mercado, B.; Herdes, C.; Murgich, J.; Muller, E. A. *Energ Fuel* **2006**, *20*, 327-338.

(16) Ruiz-Morales, Y.; Mullins, O. C. *Energ Fuel* **2007**, *21*, 256-265.

(17) Schneider, M. H.; Andrews, A. B.; Mitra-Kirtley, S.; Mullins, O. C. *Energ Fuel* **2007**, *21*, 2875-2882.

(18) Groenzin, H.; Mullins, O. C. *Energ Fuel* **2000**, *14*, 677-684.

(19) Gawrys, K. L.; Blankenship, G. A.; Kilpatrick, P. K. *Langmuir* **2006**, *22*, 4487-4497.

(20) Gray, M. R. *Energ Fuel* **2003**, *17*, 1566-1569.

(21) Murgich, J.; Abanero, J. A.; Strausz, O. P. *Energ Fuel* **1999**, *13*, 278-286.

(22) Long, J.; Xu, Z. H.; Masliyah, J. H. *Langmuir* **2007**, *23*, 6182-6190.

(23) Mullins, O. C. *Spe J* **2008**, *13*, 48-57.

(24) Mullins, O. C.; Sheu, E. Y.; Hammami, A.; Marshall, A. G. *Asphaltenes, heavy oils, and petroleomics*; Springer Science & Business Media, 2007.

(25) Yarranton, H. W. *J Disper Sci Technol* **2005**, *26*, 5-8.

(26) Mullins, O. C. *Energ Fuel* **2010**, *24*, 2179-2207.

(27) Mullins, O. C. *Annu Rev Anal Chem* **2011**, *4*, 393-418.

(28) Andreatta, G.; Bostrom, N.; Mullins, O. C. *Langmuir* **2005**, *21*, 2728-2736.

(29) Andreatta, G.; Goncalves, C. C.; Buffin, G.; Bostrom, N.; Quintella, C. M.; Arteaga-Larios, F.; Perez, E.; Mullins, O. C. *Energ Fuel* **2005**, *19*, 1282-1289.

(30) Zeng, H.; Song, Y. Q.; Johnson, D. L.; Mullins, O. C. *Energ Fuel* **2009**, *23*, 1201-1208.

(31) Lisitza, N. V.; Freed, D. E.; Sen, P. N.; Song, Y. Q. *Energ Fuel* **2009**, *23*, 1189-1193.

(32) Rogel, E.; Leon, O.; Torres, G.; Espidel, J. *Fuel* **2000**, *79*, 1389-1394.

(33) Castillo, J.; Fernandez, A.; Ranaudo, M. A.; Acevedo, S. *Petrol Sci Technol* **2001**, *19*, 75-106.

(34) Andersen, S. I.; Christensen, S. D. *Energ Fuel* **2000**, *14*, 38-42.

(35) Rogel, E. *Langmuir* **2004**, *20*, 1003-1012.

(36) Rogel, E. *Langmuir* **2002**, *18*, 1928-1937.

(37) Merino-Garcia, D.; Murgich, J.; Andersen, S. I. *Petrol Sci Technol* **2004**, *22*, 735-758.

(38) Agrawala, M.; Yarranton, H. W. *Ind Eng Chem Res* **2001**, *40*, 4664-4672.

(39) Duda, Y.; Lira-Galeana, C. *Fluid Phase Equilibr* **2006**, *241*, 257-267.

(40) Merino-Garcia, D.; Andersen, S. I. *J Disper Sci Technol* **2005**, *26*, 217-225.

(41) Groenzin, H.; Mullins, O. C. *J Phys Chem A* **1999**, *103*, 11237-11245.

(42) Adams, J. J. *Energ Fuel* **2014**, *28*, 2831-2856.

(43) Simon, S.; Jestin, J.; Palermo, T.; Barre, L. *Energ Fuel* **2009**, *23*, 306-313.

(44) Yarranton, H. W.; Alboudwarej, H.; Jakher, R. *Ind Eng Chem Res* **2000**, *39*, 2916-2924.

(45) Tanaka, R.; Sato, E.; Hunt, J. E.; Winans, R. E.; Sato, S.; Takanohashi, T. *Energ Fuel* **2004**, *18*, 1118-1125.

(46) Espinat, D.; Fenistein, D.; Barre, L.; Frot, D.; Briolant, Y. *Energ Fuel* **2004**, *18*, 1243-1249.

(47) Peramanu, S.; Singh, C.; Agrawala, M.; Yarranton, H. W. *Energ Fuel* **2001**, *15*, 910-917.

(48) Spiecker, P. M.; Gawrys, K. L.; Trail, C. B.; Kilpatrick, P. K. *Colloid Surface A* **2003**, *220*, 9-27.

(49) Gawrys, K. L.; Spiecker, P. M.; Kilpatrick, P. K. *Petrol Sci Technol* **2003**, *21*, 461-489.

(50) Speight, J. G.; Long, R. B. *Fuel Sci Techn Int* **1996**, *14*, 1-12.

(51) Carbonezi, C. A.; de Almeida, L. C.; Araujo, B. C.; Lucas, E. F.; Gonzalez, G. *Energ Fuel* **2009**, *23*, 1249-1252.

(52) Auflem, I. H.; Havre, T. E.; Sjoblom, J. *Colloid Polym Sci* **2002**, *280*, 695-700.

(53) Hong, E.; Watkinson, P. *Fuel* **2004**, *83*, 1881-1887.

(54) Angle, C. W.; Long, Y. C.; Hamza, H.; Lue, L. *Fuel* **2006**, *85*, 492-506.

(55) Maqbool, T.; Balgoa, A. T.; Fogler, H. S. *Energ Fuel* **2009**, *23*, 3681-3686.

(56) Pineda, L. A.; Trejo, F.; Ancheyta, J. *Petrol Sci Technol* **2007**, *25*, 105-119.

(57) Joshi, N. B.; Mullins, O. C.; Jamaluddin, A.; Creek, J.; McFadden, J. *Energ Fuel* **2001**, *15*, 979-986.

(58) Wang, J. X.; Buckley, J. S. *Energ Fuel* **2003**, *17*, 1445-1451.

(59) Andersen, S. I. *Energ Fuel* **1999**, *13*, 315-322.

(60) Buckley, J. S. *Fuel Sci Techn Int* **1996**, *14*, 55-74.

(61) Leontaritis, K. J.; Amaefule, J. O.; Charles, R. E. *Spe Prod Facil* **1994**, *9*, 157-164.

(62) Hammami, A.; Changyen, D.; Nighswander, J. A.; Stange, E. *Fuel Sci Techn Int* **1995**, *13*, 1167-1184.

(63) Stachowiak, C.; Viguie, J. R.; Grolier, J. P. E.; Rogalski, M. *Langmuir* **2005**, *21*, 4824-4829.

(64) Porte, G.; Zhou, H. G.; Lazzeri, V. *Langmuir* **2003**, *19*, 40-47.

(65) Buckley, J. S.; Hirasaki, G. J.; Liu, Y.; Von Drasek, S.; Wang, J. X.; Gil, B. S. *Petrol Sci Technol* **1998**, *16*, 251-285.

(66) Buckley, J. S. *Energ Fuel* **1999**, *13*, 328-332.

(67) Wang, J. X.; Buckley, J. S. *Energ Fuel* **2001**, *15*, 1004-1012.

(68) Wang, J. X.; Buckley, J. *J Disper Sci Technol* **2007**, *28*, 425-430.

(69) Pazuki, G. R.; Nikookar, M. *Fuel* **2006**, *85*, 1083-1086.

(70) Johansson, B.; Friman, R.; Hakanpaa-Laitinen, H.; Rosenholm, J. B. *Adv Colloid Interfac* **2009**, *147-48*, 132-143.

(71) Alboudwarej, H.; Pole, D.; Svrcek, W. Y.; Yarranton, H. W. *Ind Eng Chem Res* **2005**, *44*, 5585-5592.

(72) Dudasova, D.; Simon, S.; Hemmingsen, P. V.; Sjoblom, J. *Colloid Surface A* **2008**, *317*, 1-9.

(73) Ekholm, P.; Blomberg, E.; Claesson, P.; Auflem, I. H.; Sjoblom, J.; Kornfeldt, A. *J Colloid Interf Sci* **2002**, *247*, 342-350.

(74) Dudasova, D.; Silset, A.; Sjoblom, J. *J Disper Sci Technol* **2008**, *29*, 139-146.

(75) Farooq, U.; Sjoblom, J.; Oye, G. *J Disper Sci Technol* **2011**, *32*, 1388-1395.

(76) Kokal, S.; Tang, T.; Schramm, L.; Sayegh, S. *Colloid Surface A* **1995**, *94*, 253-265.

(77) Castro, M.; de la Cruz, J. L. M.; Buenrostro-Gonzalez, E.; Lopez-Ramirez, S.; Gil-Villegas, A. *Fluid Phase Equilibr* **2009**, *286*, 113-119.

(78) Xie, K.; Karan, K. *Energ Fuel* **2005**, *19*, 1252-1260.

(79) Goual, L.; Abudu, A. *Energ Fuel* **2010**, *24*, 469-474.

(80) Syunyaev, R. Z.; Balabin, R. M.; Akhatov, I. S.; Safieva, J. O. *Energ Fuel* **2009**, *23*, 1230-1236.

(81) Acevedo, S.; Ranaudo, M. A.; Garcia, C.; Castillo, J.; Fernandez, A. *Energ Fuel* **2003**, *17*, 257-261.

(82) Balabin, R. M.; Syunyaev, R. Z.; Schmid, T.; Stadler, J.; Lomakina, E. I.; Zenobi, R. *Energ Fuel* **2011**, *25*, 189-196.

(83) Acevedo, S.; Ranaudo, M. A.; Garcia, C.; Castillo, J.; Fernandez, A.; Caetano, M.; Goncalvez, S. *Colloid Surface A* **2000**, *166*, 145-152.

(84) Acevedo, S.; Ranaudo, M. A.; Escobar, G.; Gutierrez, L.; Ortega, P. *Fuel* **1995**, *74*, 595-598.

(85) Marczewski, A. W.; Szymula, M. *Colloid Surface A* **2002**, *208*, 259-266.

(86) Goual, L.; Horvath-Szabo, G.; Masliyah, J. H.; Xu, Z. H. *Langmuir* **2005**, *21*, 8278-8289.

(87) Zahabi, A.; Gray, M. R. *Energ Fuel* **2012**, *26*, 1009-1018.

(88) Drummond, C.; Israelachvili, J. *J Petrol Sci Eng* **2004**, *45*, 61-81.

(89) Abdallah, W. A.; Taylor, S. D. *J Phys Chem C* **2008**, *112*, 18963-18972.

(90) Rudrake, A.; Karan, K.; Horton, J. H. *J Colloid Interf Sci* **2009**, *332*, 22-31.

(91) Jouault, N.; Corvis, Y.; Cousin, F.; Jestin, J.; Barre, L. *Langmuir* **2009**, *25*, 3991-3998.

(92) Carbognani, L. *Petrol Sci Technol* **2000**, *18*, 335-360.

(93) Alvarez-Ramirez, F.; Garcia-Cruz, I.; Tavizon, G.; Martinez-Magadan, J. M. *Petrol Sci Technol* **2004**, *22*, 915-926.

(94) Yeung, A.; Dabros, T.; Masliyah, J.; Czarnecki, J. *Colloid Surface A* **2000**, *174*, 169-181.

(95) Moran, K.; Yeung, A.; Masliyah, J. *Langmuir* **1999**, *15*, 8497-8504.

(96) Zhang, L. Y.; Lopetinsky, R.; Xu, Z. H.; Masliyah, J. H. *Energ Fuel* **2005**, *19*, 1330-1336.

(97) Bouriat, P.; El Kerri, N.; Graciaa, A.; Lachaise, J. *Langmuir* **2004**, *20*, 7459-7464.

(98) Tsamantakis, C.; Masliyah, J.; Yeung, A.; Gentzis, T. *J Colloid Interf Sci* **2005**, *284*, 176-183.

(99) Rane, J. P.; Pauchard, V.; Couzis, A.; Banerjee, S. *Langmuir* **2013**, *29*, 4750-4759.

(100)   Sztukowski, D. M.; Yarranton, H. W. *Langmuir* **2005**, *21*, 11651-11658.

(101)   Liu, J. J.; Xu, Z. H.; Masliyah, J. *Can J Chem Eng* **2004**, *82*, 655-666.

(102)   Liu, J. J.; Xu, Z. H.; Masliyah, J. *Colloid Surface A* **2005**, *260*, 217-228.

(103)   Long, J.; Zhang, L. Y.; Xu, Z. H.; Masliyah, J. H. *Langmuir* **2006**, *22*, 8831-8839.

(104)   Liu, J. J.; Zhang, L. Y.; Xu, Z. H.; Masliyah, J. *Langmuir* **2006**, *22*, 1485-1492.

(105)   Wang, S. Q.; Liu, J. J.; Zhang, L. Y.; Xu, Z. H.; Masliyah, J. *Energ Fuel* **2009**, *23*, 862-869.

(106)   Wang, S. Q.; Liu, J. J.; Zhang, L. Y.; Masliyah, J.; Xu, Z. H. *Langmuir* **2010**, *26*, 183-190.

(107)   Abraham, T.; Christendat, D.; Karan, K.; Xu, Z.; Masliyah, J. *Ind Eng Chem Res* **2002**, *41*, 2170-2177.

(108)   Natarajan, A.; Xie, J. G.; Wang, S. Q.; Liu, Q. X.; Masliyah, J.; Zeng, H. B.; Xu, Z. H. *J Phys Chem C* **2011**, *115*, 16043-16051.

CHAPTER 2   MATERIALS AND EXPERIMENTAL

TECHNIQUES

2.1 Materials

Asphaltenes used in this study are all n-heptane extracted from different sources. Asphaltenes used in Chapter 3, Chapter 5 and Chapter 6 are from vacuum distillation feed bitumen and asphaltenes used in Chapter 4 was from crude oil and bitumen provided by the sponsor. The extraction processes for different types of asphaltenes were different and the details are as follows.

Asphaltenes precipitated from vacuum distillation feed bitumen [1]

First, the vacuum distillation feed bitumen was dissolved in toluene at a bitumen/toluene volume ratio of 1/5. Fine solids were removed using a centrifuge and the toluene-free bitumen was obtained allowing the toluene solvent to evaporate in a well-ventilated clean fume hood. The obtained toluene-free bitumen was mixed with certified ACS grade n-heptane at a bitumen/heptane volume ratio of 1/40 and the mixture was placed on a horizon shaker for 2 hours. The asphaltenes were allowed to precipitate overnight and the precipitated asphaltenes were washed using n-heptane until the supernatant of the solution was clear and colourless. During the every single wash, the asphaltenes and n-heptane mixture was shaken for 2 hours and left overnight for asphaltenes to precipitate. High-performance liquid chromatography (HPLC) grade n-heptane was used for the final two washes. The washed asphaltenes were left in the fume hood for 3 days to ensure that the n-heptane evaporated completely. Normally it took one month to obtain pure

asphaltene solid and the total mass of the dry asphaltene solids is ~12 wt% of that of the original bitumen.

Asphaltenes precipitated from crude oil and bitumen (provided by sponsor)

High-performance liquid chromatography (HPLC) grade n-heptane was firstly added into the crude oil or bitumen sample at a weight ratio of 30 to 1 using a flask 1 and the mixture was stirred and refluxed for 1 hour. Subsequently, the mixture was cooled down and then stored in the refrigerator for two and half hours allowing the asphaltenes to precipitate. Before the filtration, the mixture was required to return to room temperature. Decant the liquid carefully through a suitable funnel lined with Whatman No. 40 filter paper pre-wet with heptane, into a boiling flask 2. The flask 1 was rinsed three times with hot n-heptane and the remaining precipitated asphaltenes were carefully transferred to the filter paper. The filter paper was placed in a Soxhlet extractor and extracted by n-heptane until the solvent in the upper section of the Soxhlet was clear. Methylene chloride was used to extract the asphaltenes on the filter papers using another Soxhlet extractor. The asphaltenes in methylene chloride solution were then concentrated and fully dried under nitrogen flow. The obtained mass of the asphaltenes solid was about 10 wt% of the original crude oil or bitumen sample.

2.2 Surface forces apparatus (SFA)

Surface force apparatus (SFA) has been used for several decades to directly measure the intermolecular forces between surfaces. Since the pioneer work done by Tabor, Winterton and Israelachvili,[2-4] SFA has been being developed and

improved.[5-8] After the development of early versions of SFA, such as SFA Mk I and SFA Mk II, the most commonly used SFA are version Mk III and SFA 2000. The Mk III, developed by Israelachvili and McGuiggan (1985-1989), was much more compact than the previous versions and a new attachment called the bimorph slider was developed as well for the friction force measurement.[7,9]

SFA 2000 used in this study was shown in Figure 2.1. SFA 2000 is designed to have fewer parts and it is much more user-friendly and at the same time, it still retains the good performance as the previous versions. Figure 2.2 shows a schematic of the basic SFA 2000.[8] The main components are the micrometers, the main stage containing the central single cantilever spring, the lower disk holder and the upper disk holder. There are totally four different controls to determine the separation distance between the upper surface and the lower surface. The lower surface can be controlled by the differential micrometer and can be moved over a range of 2 mm with a position accuracy of 2 Å. The upper surface can be moved by a piezoelectric crystal over a range of 1000 Å with a precision of less than 1 Å.
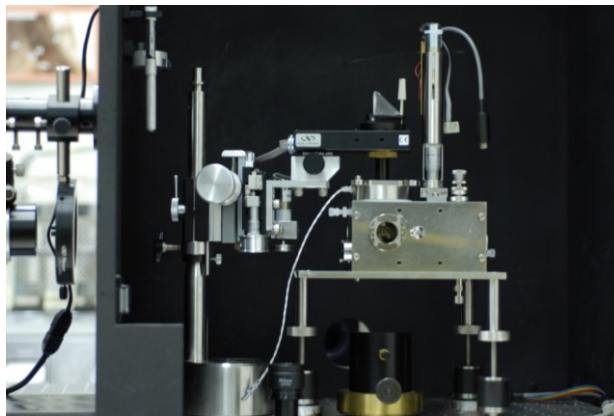
Figure 2.1 The picture of the SFA 2000 used in this study.
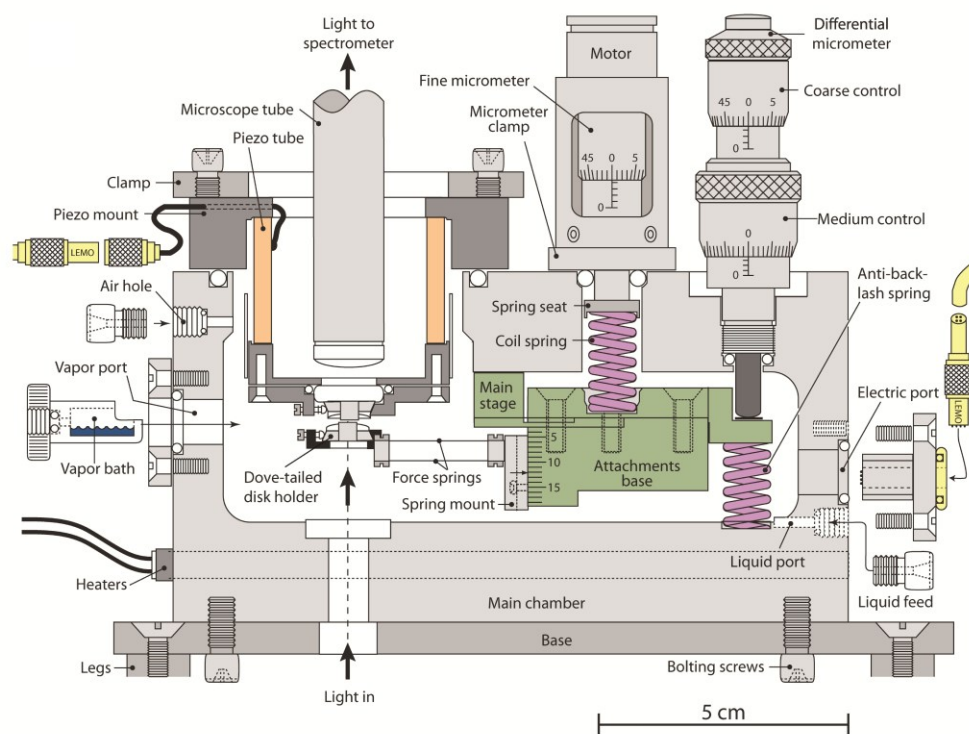
Figure 2.2 Schematic drawing of SFA 2000.[8]

2.2.1 Setup of the SFA measurement

Figure 2.3 shows a brief setup of a typical SFA experiment.[10-13] Two back silvered molecular smooth mica surfaces were glued onto two cylindrical silica discs (of radius R). For the surface force measurement between asphaltene surfaces, asphaltenes were coated on the mica surfaces that were already glued on the silica discs. The two asphaltene surfaces were placed in a crossed cylinder configuration in the SFA chamber which was locally equivalent to a sphere (of radius R) near a flat surface or two spheres (of radius $2R$) close together when the separation distance $D \ll R$. Solvents or solutions were injected in between the two surfaces and allowed to fill the gap between two surfaces. For the asphaltenes adsorption measurement,

the asphaltenes solutions were injected in-situ between two mica surfaces after the two mica surfaces were placed in the SFA chamber.
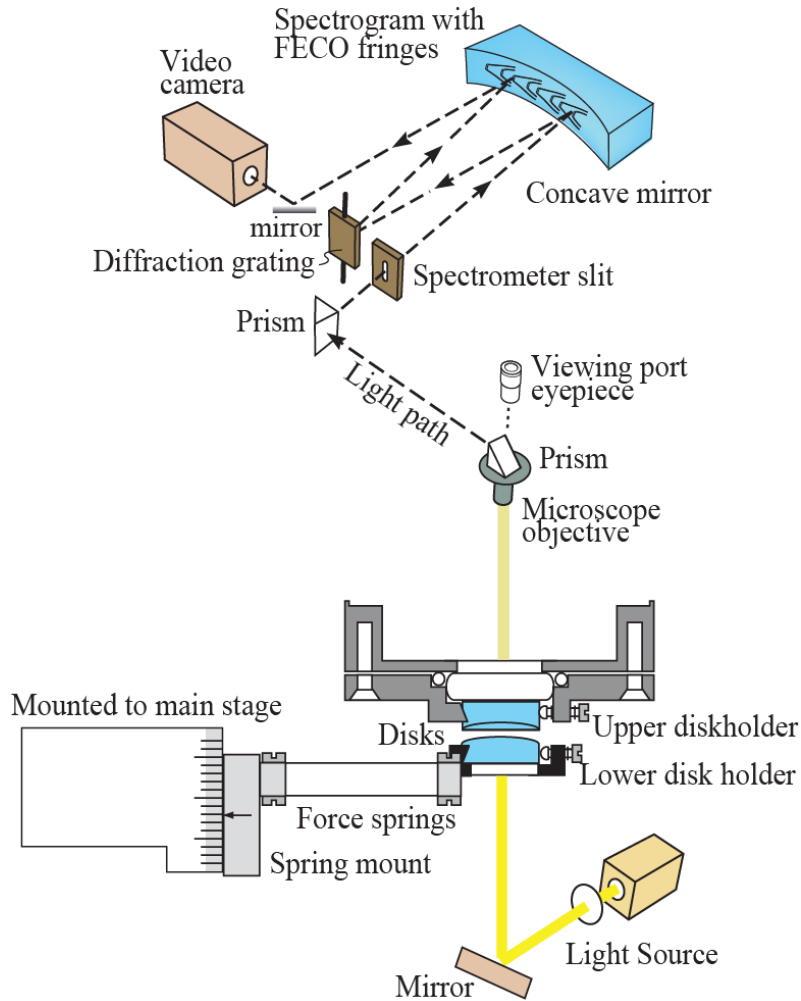
Figure 2.3 A schematic of brief SFA setup.[14]

2.2.2 Surface force measurement using SFA

Normal forces between two surfaces are determined based on the Hooke's law. The changed force $\Delta F = K_s \Delta x$, where K_s is the spring constant supporting the lower surface, and $\Delta x = D_{applied} - D_{actual}$. The applied separation $D_{applied}$ distance is measured by the differential micrometer and motor-driven fine micrometer. The actual

separation distance D_{actual} between two surfaces is determined using the multiple beam interferometry (MBI) technique by employing fringes of equal chromatic order (FECO).[15,16] The resolution of the force measured using SFA is 10 nN and the accuracy of distance measurement is 1 Å.

A typical force measurement is completed by approaching the two surfaces to a "hard wall" (defined as the surface-surface separation where the confined film thickness hardly changes with increasing normal load or pressure) for contacting for some time followed by a separation. The measured interaction force $F(D)$ is commonly normalized by R (the curvature of the surface) and can be related to the interaction energy per unit area between two flat surfaces by using the Derjaguin approximation (Eq. 2.1):[16]

$$W_{flat}(D) = \frac{F(D)}{2\pi\sqrt{R_1 R_2}} = \frac{F(D)}{2\pi R} \tag{2.1}$$

when $R_1 = R_2 = R$.

The measured adhesion force F_{ad} could be related to the adhesion energy per unit area W_{ad} using $F_{ad} = 1.5\pi R W_{ad}$ for soft deformable surfaces.[8]
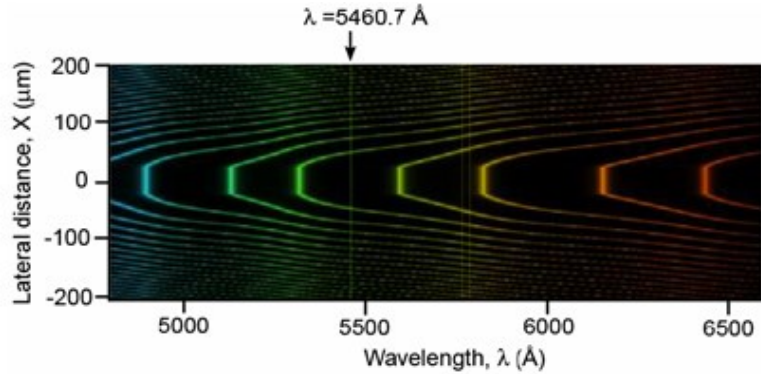
Figure 2.4 A colored FECO fringes in a typical force measurement (two surfaces in adhesive contact).[17]

2.2.3 Multiple beam interferometry (MBI)

MBI is an optical interference technique for determining the thickness and refractive index profiles of thin films which has been described in details by S. Tolansky in 1948 and J. Israelachvili in 1973.[15] The film thickness, surface separation and surface deformations can be monitored in the SFA experiments using the MBI technique. In a typical SFA measurement, when two surfaces come into contact and white light normally passes through the two surfaces, the emerging interference light is separated by a grating spectrometer into sharp fringes (FECO) consisting of discrete wavelengths λ_n^0 (n = 1, 2, 3, …), as shown in Figure 2.4. If the two mica sheets have the same thickness, the surface separation D and the fringe wavelength λ_n^D can be correlated by

$$\tan(2\pi\mu D / \lambda_n^D) = \frac{2\bar{\mu}\sin\left[\pi\left(1-\lambda_n^0/\lambda_n^D\right)/\left(1-\lambda_n^0/\lambda_{n-1}^0\right)\right]}{(1+\bar{\mu}^2)\cos\left[\pi\left(1-\lambda_n^0/\lambda_n^D\right)/\left(1-\lambda_n^0/\lambda_{n-1}^0\right)\right]\pm(\bar{\mu}^2-1)} \qquad (2.2)$$

where '+' refers to odd order fringes (n odd), and '-' refers to even order fringes (n even). μ is the refractive index of the medium between the two mica surfaces at λ_n^D, μ_{mica} is the refractive index of mica at λ_n^D, and $\bar{\mu} = \mu_{mica}/\mu$. The Eq. 2.2 can be simplified to the following two approximate equations when separation is less than 30 nm.

$$D = \frac{nF_n(\lambda_n^D - \lambda_n^0)}{2\mu_{mica}} \qquad \text{for n odd (positive sign in Eq.2.2)} \qquad (2.2a)$$

$$D = \frac{nF_n(\lambda_n^D - \lambda_n^0)\mu_{mica}}{2\mu^2} \qquad \text{for n even (negative sign in Eq.2.2)} \qquad (2.2b)$$

where $F_n = \lambda_{n-1}^0/(\lambda_{n-1}^0 - \lambda_n^0)$. By using the above equations, the distance D can be determined by measuring the shifts in wavelengths of an odd and adjacent even fringe. The accuracy is about 1 Å for measurement of D in the range of 0-200 nm.

2.3 Atomic force microscope (AFM)

Atomic force microscope (AFM) has been widely used for a lot of applications, such as in measuring the interaction forces, generating the topography of the surfaces and determining the mechanical and electrochemical properties of the surfaces.[18-21] It was invented by Binning et al. in 1986 after the success of scanning tunnelling microscope (STM).[22,23] As shown in Figure 2.5, the AFM mainly consists of a cantilever with a sharp tip, a piezo scanner, a laser beam source and a quadrant displacement sensor. In our study, tapping mode was used to obtain the topography

of the surfaces where the cantilever is externally oscillated at or close to its fundamental resonance frequency. Usually, the sample surface has bumps and depressions. To keep the oscillation amplitude constant to maintain a constant tip-sample separation, the adjustment of the sample surface can generate a 3-D mapping of the sample surface. The interaction force measurement is conducted in a contact mode and the force-distance profiles were obtained by approaching and retracting the AFM tip on the measured surface.
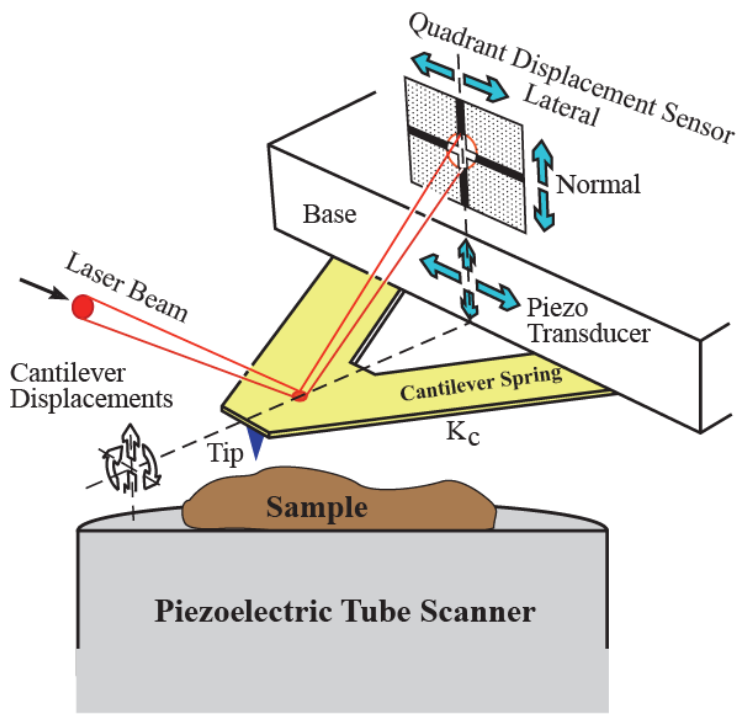
Figure 2.5 Schematic of AFM working principle.[24,25]

2.3.1 Setup of AFM imaging

The topographic images of the sample surfaces in this study were obtained using Asylum MFP-3D AFM (Asylum, Santa Barbara, CA, USA) under tapping mode in air or tapping mode in liquid as required. For the imaging in air, the sample

was fixed on a glass slide which could be immobilized on the sample stage. For the imaging in liquid, the solution was injected into a fluid cell where the sample was placed. For each surface, multiple positions were scanned to assure the reproducibility.

2.3.2 Setup of the AFM force measurement

The same AFM was carried out to conduct force measurement in aqueous solutions in this study. Silicon nitride AFM tip was used to measure the interactions between tip and surfaces. The surfaces were also fixed in a fluid cell as for the AFM imaging in liquid. The interactions were measured at different locations of the surfaces to ensure the reproducibility.

2.4 Quartz crystal microbalance with dissipation (QCM-D)

A QCM-D E1 system (Q-sense, Sweden) was used to quantify the adsorbed amount of asphaltenes on quartz crystal sensor coated with silica from different solvents. The quartz crystal used in this study is AT-cut crystals coated with silica with the resonance frequency of 5 MHz. The quartz crystal sensor is a thin piezoelectric plate with gold coated on each side as electrodes (Figure 2.6). So the crystal sensor can oscillate at its resonance frequency when an AC voltage is applied. The mass adsorbed on the sensor surface can induce the drop of sensor's resonance frequency Δf. The equation that correlates frequency change (Δf) and mass change (Δm) named Sauerbrey equation:

$$\Delta m = -\frac{\rho_q t_q \Delta f}{f_0 n} = -\frac{\rho_q \upsilon_q \Delta f}{2 f_0^2 n} = -\frac{C \Delta f}{n} \tag{2.3}$$

where ρ_q and v_q are the specific density and the shear wave velocity in quartz respectively; t_q is the thickness of the quartz crystal, and f_0 is the fundamental resonance frequency (when n = 1). C equals 17.7 ng Hz^{-1} cm^{-2} for the quartz crystal used in this study. However, the Sauerbrey equation is only valid under the following three conditions: 1) the mass adsorbed is evenly distributed; 2) the Δm is much smaller than that of quartz crystal itself and 3) the adsorbed layer is rigidly attached to the crystal surface.[26-28] The third condition can be satisfied only when there is negligible energy dissipation (ΔD) observed. The dissipation change ΔD can also be monitored simultaneously which is a result of energy loss due to the viscous dissipation when the crystal oscillates with the adsorbed materials. In this study, the liquid association with the adsorbed asphaltenes layer was very substantial which gave a significant rise to the dissipation factor. Therefore, the Sauerbrey equation is no longer valid for these cases and Voigt viscoelastic model embedded in Q-sense Qtools was used to obtain the relationship between the mass of the adsorbed asphaltenes layer and both changes of frequency and dissipation.[29,30] The Voigt model can be expressed as follows by correlating the oscillation frequency Δf, dissipation factor ΔD, layer thickness h, density ρ, viscosity η, shear modulus μ and circular frequency ω for a viscoelastic layer (index 1) on quartz crystal (index 0) immersed in a bulk Newtonian fluid (index 2) as well as the penetration depth δ of this fluid.

$$\Delta f \approx -\frac{1}{2\pi\rho_0 h_0}\left\{ \frac{\eta_2}{\delta_2} + \left[h_1\rho_1\omega - 2h_1\left(\frac{\eta_2}{\delta_2}\right)^2 \frac{\eta_1\omega^2}{\mu_1^2+\eta_1\omega^2} \right] \right\} \qquad (2.4)$$

32

$$\Delta D \approx -\frac{1}{2\pi f \rho_0 h_0}\left\{\frac{\eta_2}{\delta_2} + \left[2h_1\left(\frac{\eta_2}{\delta_2}\right)^2 \frac{\eta_1 \omega^2}{\mu_1^2 + \eta_1 \omega^2}\right]\right\} \tag{2.5}$$

$$\delta_2 = \sqrt{\frac{2\eta_2}{\rho_2 \omega}} \tag{2.6}$$

2.4.1 QCM-D experiment setup

A detailed operational procedure of QCM-D experiment has been reported elsewhere.[29,31] First of all, the crystal sensor surface should be thoroughly cleaned following the standard cleaning procedure for silica sensor surface which required a 10-min UV/Ozone clean, 30-min immersion in 2 wt% of sodium dodecyl sulfate (SDS) solution and another 10-min UV/Ozone clean. After the sensor was cleaned and carefully placed in the flow module, a baseline was then established by injecting the background solvent using the pump where the frequency and dissipation changes were defined as zero points. The main components of the QCM-D E1 system are shown in Figure 2.6. After a steady baseline was reached, the asphaltenes solution was injected into the flow module. When the asphaltenes adsorbed on the sensor surface, there was a negative change in frequency and a positive change in dissipation. The background solvent was injected again at the end of adsorption to rinse off the unbounded or loosely bounded asphaltenes.

(a)

(b)
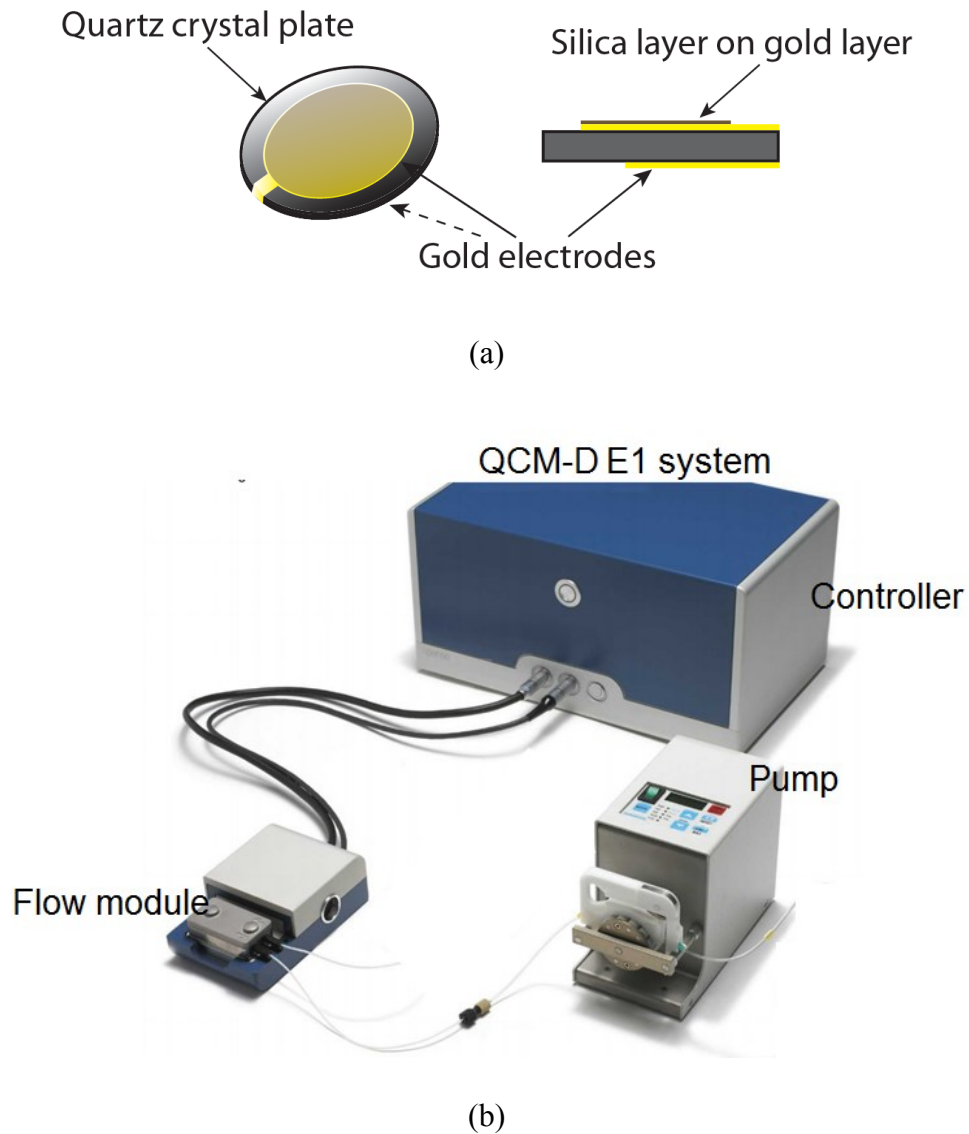
Figure 2.6 (a) The quartz crystal sensors; (b) The main components of the QCM-D E1 system. (http://www.biolinscientific.com/product/q-sense-explorer/)

2.5 Other techniques

2.5.1 Contact angle measurement

The contact angles of water on different sample surfaces were characterized by a sessile drop method using a standard goniometer (Model 250, Ramé-hart, USA). A

droplet of Milli-Q water or aqueous solution was placed on the surface and the shape of the drop was fitted by image processing software to determine the contact angle.

2.5.2 Micropipette tests

The micropipette technique was used to investigate the interactions between water-in-oil emulsion droplets in the presence of asphaltenes.[32] In a typical micropipette experiment, individual emulsion droplets can be manipulated using two small suction pipettes. Using an inverted microscope, micropipette experiments can be monitored in real time and recorded on video for further analysis. Figure 2.7, Figure 2.8 and Figure 2.9 show the main stage of the instrument, a brief schematic of the micropipette experimental setup, and a schematic of two water droplets interacting in asphaltenes-toluene solution, respectively. Briefly, about 50 µl of emulsified solution was placed in a sample cell that was assembled from microscope cover slips. Micron-sized droplets in the emulsion could be observed with the inverted microscope utilizing transmission bright-field illumination. Two small suction pipettes were extended into the sample cell from opposite sides to manipulate individual droplets. The pipettes were mounted on micromanipulators to enable their continuous motions on a micrometer scale. To grasp individual droplets with controlled forces, adjustable suction pressures were applied at the pipette tips, which were accomplished by connecting the other ends of the pipettes to the syringes through flexible tubings. The sequences were also recorded for subsequent analysis. In this study, thirty pairs of droplets were collected for statistics analysis under each fixed experimental condition.
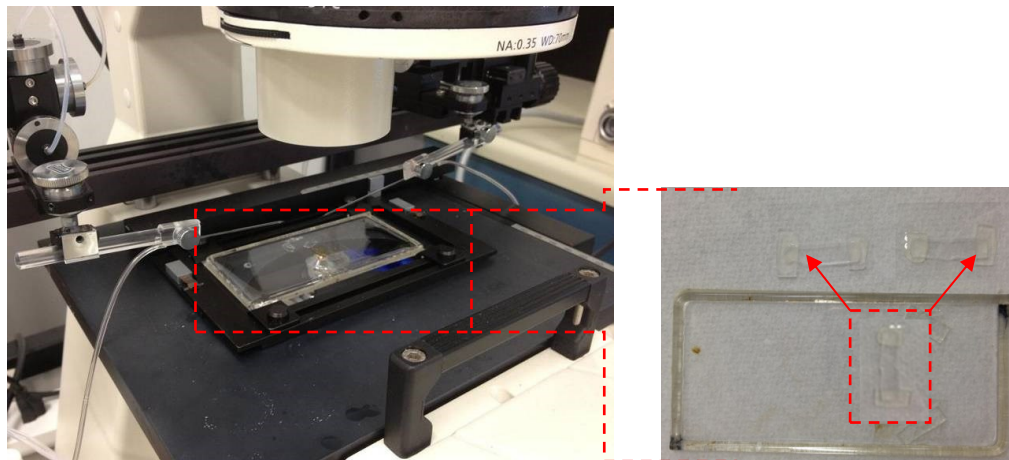
Figure 2.7 The left picture shows the main stage of the instrument. The part in the red dash line is the in-house made cell for capturing the emulsion solution.
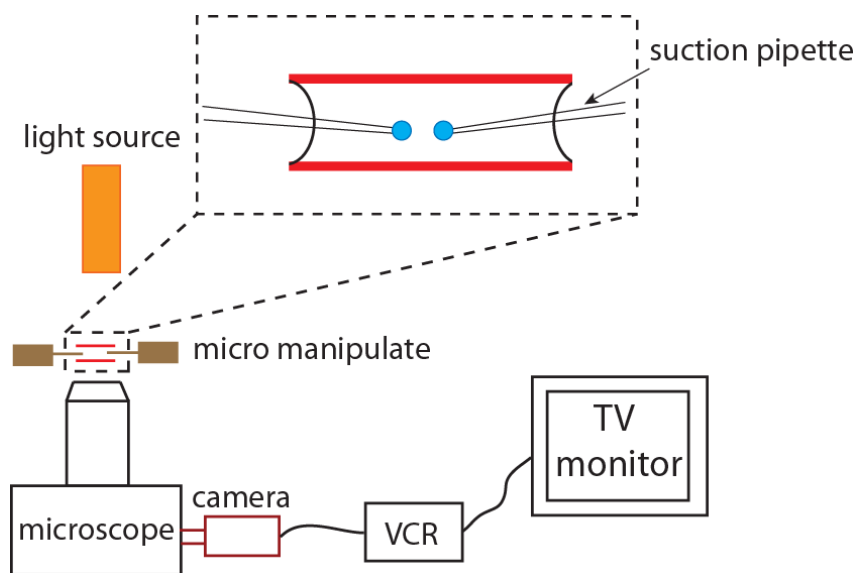
Figure 2.8 A brief schematic of the micropipette experimental setup.

asphaltene film

water   water

asphaltene in toluene solution
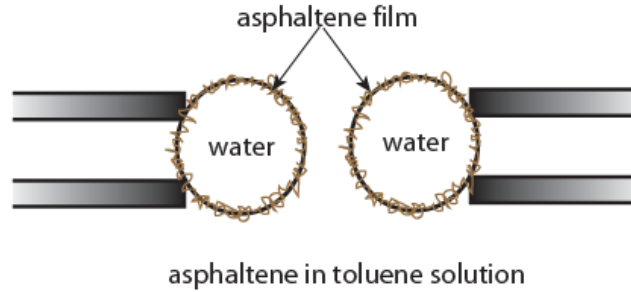
Figure 2.9 Two water droplets interacting in asphaltenes-toluene solution.

2.5.3 Computer-controlled 4-roll mill technique

The computer-controlled 4-roll mill can be applied to study a broad range of problems of (steady or time-dependent) flow-induced deformation, breakup, and coalescence of droplets or particles suspensions. In this research, a computer-controlled 4-roll mill was used to analyze the stability and coalescence of water-in-oil droplets, mainly the interaction of water-in-toluene droplets stabilized by asphaltene at the interface. Figure 2.10 (left) shows the schematic of experiment setup for a computer-controlled 4-roll mill based on Prof Gary Leal's design, which normally consists of a container with four equal size cylinders (called rollers) arranged at the vertices of a square.[33-36] Rumschel F. *et al*. have also used a similar technique called four-roller apparatus to study the drop behaviour.[37] The 4-roll mill designed and applied in this study is much advanced. Each roller is connected or geared to a stepping motor driven by a motor controller which is interfaced with the computer for the control. By controlling the step motor, the rollers rotate and thus generate a flow in the surrounding fluid. The fluid motion is lit by the light source above and imaged with a CCD camera connected to a magnifying lens. Depending on the rotation direction and speed of the cylinders, a variety of two-dimensional

linear flows can be easily realized ranging from purely rotational to a pure straining

to mimic real industrial flow processes.
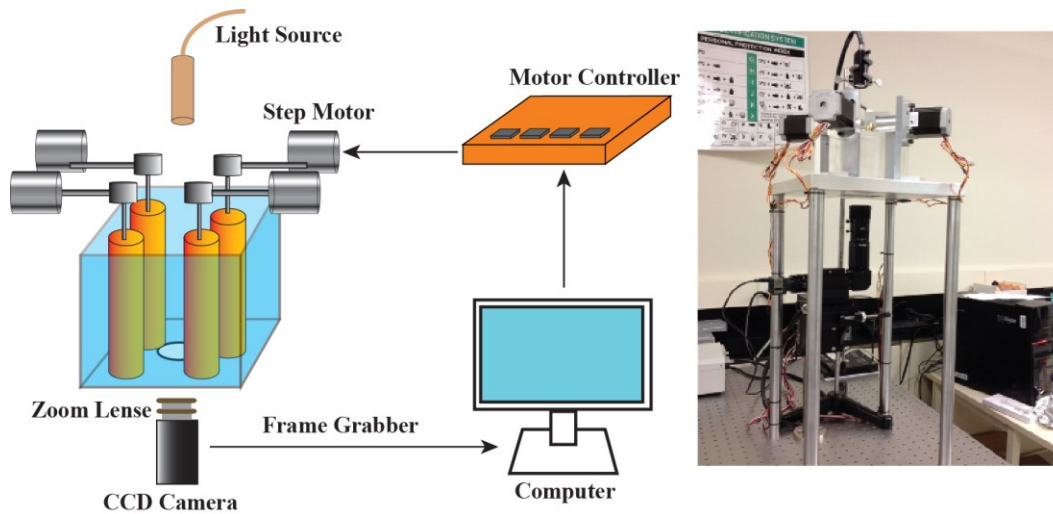
Figure 2.10 Schematic and picture of the assembled computer-controlled 4-roll mill

device for investigating droplet-droplet interactions under flow conditions.[38]

References

(1) Zhang, L. Y.; Lawrence, S.; Xu, Z. H.; Masliyah, J. H. *J Colloid Interf Sci* **2003**, *264*, 128-140.

(2) Tabor, D.; Winterto.Rh *Proc R Soc Lon Ser-A* **1969**, *312*, 435-&.

(3) Israelachvili, J.; Tabor, D. *Nature* **1972**, *236*, 106-106.

(4) Israelachvili, J.; Tabor, D. In *Proceedings of the Royal Society of London A: Mathematical, Physical and Engineering Sciences*; The Royal Society, 1972; Vol. 331; pp 19-38.

(5) Israelachvili, J. N.; Adams, G. E. *Nature* **1976**, *262*, 773-776.

(6) Israelachvili, J. N. *Faraday Discuss* **1978**, *65*, 20-24.

(7) Israelachvili, J. N.; Mcguiggan, P. M. *J Mater Res* **1990**, *5*, 2223-2231.

(8) Israelachvili, J.; Min, Y.; Akbulut, M.; Alig, A.; Carver, G.; Greene, W.; Kristiansen, K.; Meyer, E.; Pesika, N.; Rosenberg, K.; Zeng, H. *Rep Prog Phys* **2010**, *73*.

(9) Mcguiggan, P. M.; Israelachvili, J. N. *J Mater Res* **1990**, *5*, 2232-2243.

(10) Zeng, H.; Tian, Y.; Anderson, T. H.; Tirrell, M.; Israelachvili, J. N. *Langmuir* **2008**, *24*, 1173-1182.

(11) Teng, F. C.; Zeng, H. B.; Liu, Q. X. *J Phys Chem C* **2011**, *115*, 17485-17494.

(12) Natarajan, A.; Xie, J. G.; Wang, S. Q.; Liu, Q. X.; Masliyah, J.; Zeng, H. B.; Xu, Z. H. *J Phys Chem C* **2011**, *115*, 16043-16051.

(13) Natarajan, A.; Kuznicki, N.; Harbottle, D.; Masliyah, J.; Zeng, H. B.; Xu, Z. H. *Langmuir* **2014**, *30*, 9370-9377.

(14) Faghihnejad, A.; Zeng, H. *Soft Matter* **2012**, *8*, 2746-2759.

(15) Israelac.Jn *J Colloid Interf Sci* **1973**, *44*, 259-272.

(16) Israelachvili, J. *Intermolecular and Surface Forces*; third ed.; Academic Press, 2011.

(17) Heuberger, M.; Zäch, M.; Spencer, N. *Science* **2001**, *292*, 905-908.

(18) Strausser, Y. E.; Heaton, M. G. *Am Lab* **1994**, *26*, 20-&.

(19) Giessibl, F. J. *Rev Mod Phys* **2003**, *75*, 949-983.

(20) Oliver, R. A. *Rep Prog Phys* **2008**, *71*.

(21) Alexander, J.; Magonov, S.; Moeller, M. *J Vac Sci Technol B* **2009**, *27*, 903-911.

(22) Binnig, G.; Rohrer, H. *Helv Phys Acta* **1982**, *55*, 726-735.

(23) Binnig, G.; Quate, C. F.; Gerber, C. *Phys Rev Lett* **1986**, *56*, 930-933.

(24) Zeng, H. *Polymer adhesion, friction, and lubrication*; John Wiley & Sons, 2013.

(25) Leckband, D.; Israelachvili, J. *Q Rev Biophys* **2001**, *34*, 105-267.

(26) Ekholm, P.; Blomberg, E.; Claesson, P.; Auflem, I. H.; Sjoblom, J.; Kornfeldt, A. *J Colloid Interf Sci* **2002**, *247*, 342-350.

(27) Dudasova, D.; Silset, A.; Sjoblom, J. *J Disper Sci Technol* **2008**, *29*, 139-146.

(28) Hannisdal, A.; Ese, M. H.; Hemmingsen, P. V.; Sjoblom, J. *Colloid Surface A* **2006**, *276*, 45-58.

(29) Binazadeh, M.; Zeng, H.; Unsworth, L. D. *Acta Biomater* **2014**, *10*, 56-66.

(30) Voinova, M. V.; Rodahl, M.; Jonson, M.; Kasemo, B. *Phys Scripta* **1999**, *59*, 391-396.

(31) Wang, S. S.; Zhang, L.; Yan, B.; Xu, H. L.; Liu, Q. X.; Zeng, H. B. *J Phys Chem C* **2015**, *119*, 7327-7339.

(32) Yeung, A.; Dabros, T.; Masliyah, J.; Czarnecki, J. *Colloid Surface A* **2000**, *174*, 169-181.

(33) Bentley, B. J.; Leal, L. G. *J Fluid Mech* **1986**, *167*, 219-240.

(34) Bentley, B. J.; Leal, L. G. *J Fluid Mech* **1986**, *167*, 241-283.

(35) Leal, L. G. *Phys Fluids* **2004**, *16*, 1833-1851.

(36) Borrell, M.; Leal, L. G. *Langmuir* **2007**, *23*, 12497-12502.

(37) Rumschel.F; Mason, S. G. *J Coll Sci Imp U Tok* **1961**, *16*, 238-&.

(38) Zhang, L.; Shi, C.; Lu, Q. G.; Liu, Q. X.; Zeng, H. B. *Langmuir* **2016**, *32*, 4886-4895.

CHAPTER 3 PROBING MOLECULAR INTERACTIONS OF ASPHALTENES IN HEPTOL USING A SURFACE FORCES APPARATUS: IMPLICATIONS ON STABILITY OF WATER-IN-OIL EMULSIONS

3.1 Introduction

Asphaltenes are present in crude oil and bitumen products, which are practically defined as a solubility class soluble in toluene but insoluble in n-alkanes such as n-heptane. Generally, asphaltenes are considered to consist of polycyclic rings and peripheral alkane side chains with heteroatoms (e.g. N, O, S) in the form of functional groups including acid and base.[1] The combination of hydrophobic hydrocarbon structures and the hydrophilic polar groups renders asphaltenes interface active. Therefore, asphaltenes can readily adsorb onto both oil/water and oil/solid interfaces and change the interfacial properties and behaviors, leading to many challenging issues in oil production. For example, the adsorbed asphaltenes on oil/water interface are reported to play a critical role in stabilizing the water-in-oil emulsions by forming a protective interfacial coating.[2-5] These emulsions are highly undesirable,[6-9] because the contained salt ions (e.g. Cl⁻) can induce corrosion of the downstream equipment and transportation devices. Moreover, phase separation and precipitation of asphaltenes can occur during transportation due to changes of environmental conditions (e.g. temperature and pressure change), resulting in serious problems like equipment fouling and pipeline/wellbore plugging. Over the past several decades, much effort has been made to study the properties and behaviors of

asphaltenes under different conditions in terms of their aggregation, precipitation, deposition and interfacial adsorption behaviors.[10-21]

Fundamentally, the properties and behaviors of asphaltenes in organic media are largely determined by the molecular interactions of asphaltenes. Generally, the attraction between asphaltene molecules will lead to asphaltenes aggregation and further precipitation, while intermolecular repulsion corresponds to a stable dispersion of asphaltenes. Aromaticity of the organic media, which determines the solubility of asphaltenes, is a significant factor impacting the molecular interactions of asphaltenes, thereby affecting their aggregation and precipitation behaviors. The stability and aggregation behaviors of asphaltenes in various organic solvents have been experimentally investigated and several aggregation models are also proposed.[11,12,22] Some researchers reported that the asphaltenes could aggregate in the same way as surfactants due to the amphiphilic nature.[10,23-25] Rogel *et al*. reported critical micelle concentration (CMC) in organic solvents for asphaltenes from surface tension measurement, which varied with solvent type. On the other hand, some other researchers showed that the aggregation behavior of asphaltenes was similar to polymer association process due to some polymer-like properties of asphaltene aggregates[26,27] and the high molecular weight of certain asphaltene compositions.[28] Despite many aggregation models proposed, there are still some debates regarding the molecular interaction mechanisms involved, and there is only limited work directly correlating the macroscopic aggregation behaviors of asphaltenes with their measured intermolecular interactions in different organic media. Wang et al. applied an atomic force microscopy (AFM) with asphaltenes

coated silica probe to measure the interaction forces between asphaltenes in organic solvents.[29,30] However, the swelling thickness of asphaltenes could not be directly measured using AFM. Surface forces apparatus (SFA) was applied to measure the intermolecular interaction of asphaltenes in pure toluene and n-heptane as well as probe the swelling behaviors of asphaltenes simultaneously.[31,32] No report is available on simultaneously probing interaction forces and swelling behaviors of asphaltenes in a mixture of good and poor solvents (i.e. heptol solvent with varying toluene/n-heptane ratio, mimicking commercial naphtha-based solvent for froth treatment in oil sands bitumen extraction) using nanomechanical tools such as SFA.

The molecular interaction of asphaltenes in organic media is also one of the determining factors for the stability of water-in-oil emulsions. Due to the interfacial activity, asphaltenes have been reported to adsorb onto oil/water interface in the form of monomer, aggregates and clusters.[16,33-36] The interfacial asphaltenes can form a protective coating around water droplets and induce repulsion against droplet coalescence.[37] The properties of the interfacial asphaltenes films were also characterized using different techniques and correlated to their aggregation state at interfaces, and the results showed that interfacial films of asphaltenes formed in a relatively "poor" solvent would be denser, thereby enhancing the stability of the water-in-oil emulsions.[38,39] Thus, understanding and correlating the behaviors of water-in-oil emulsion droplets with the interaction forces between asphaltene molecules in organic solvents is of both fundamental and practical importance to understand the stabilization mechanism of water-in-oil emulsions in the presence of asphaltenes.

In this work, the molecular interactions between asphaltene surfaces in heptol solvents of varying toluene/n-heptane weight ratio have been directly probed using an SFA, and the measured interaction results are further correlated to the stability of water-in-oil emulsions. A micropipette technique was applied to qualitatively evaluate the interaction and stability of two water-in-oil emulsion droplets attached to glass pipettes, and the impact of water chemistry (e.g. salts, salinity) was investigated. A computer controlled 4-roll mill fluidic device was built, and the interactions of free-suspending water-in-oil emulsions under dynamic flow condition were also monitored. The results provide insightful information on the basic molecular interaction mechanism of asphaltenes as well as the stabilization/destabilization of water-in-oil emulsions.

3.2 Materials and Experimental Methods

3.2.1 Materials and asphaltenes extraction

The detailed procedure of extracting asphaltenes from vacuum distillation feed Athabasca bitumen has been reported elsewhere.[40] Briefly, vacuum distillation feed bitumen was dissolved in toluene at a bitumen to toluene volume ratio of 1:5. Solids were removed by centrifuge and the toluene was allowed to evaporate in a well-ventilated fume hood to obtain the toluene-free bitumen. The toluene-free bitumen was then added to certified ACS grade n-heptane at a volume ratio of 1:40 (bitumen to n-heptane) for asphaltenes precipitation. The precipitated asphaltenes were washed using n-heptane until the supernatant of the solution was clear and colorless. High-performance liquid chromatography (HPLC) grade n-heptane was used for the

final two washes. The total mass of the dry asphaltenes solids obtained was ~12 wt% of the original bitumen. HPLC grade toluene, n-heptane and certified ACS grade n-heptane (99%) were all purchased from Fisher Scientific Canada and used as received. HCl, NaOH, NaCl and $CaCl_2 \cdot 2H_2O$ used in different tests were all purchased from Fisher Scientific Canada. Mica sheets were purchased from S & J Trading Inc. (Glen Oaks, NY). Heptol was prepared by mixing the HPLC grade toluene and n-heptane with different toluene weight fractions of $\omega = 0.8, 0.5, 0.2$.

3.2.2 Surface forces measurement using the SFA

SFA was used to measure the intermolecular interaction forces of asphaltenes in heptol. The detailed setup of the SFA experiments has been widely reported elsewhere.[41-46] The asphaltene films on mica surfaces were prepared by drop coating method. Several drops of 0.5 wt% asphaltenes toluene solution were placed on the freshly cleaved, back-silvered mica sheets (thickness of 1–5 μm) which were already glued on cylindrical silica disks (radius $R = 2$ cm). The surfaces were then thoroughly flushed with HPLC-grade toluene after 15 minutes, and the surfaces were kept under vacuum overnight to remove the residual solvent. The prepared asphaltene surfaces were then mounted in the SFA chamber in a crossed-cylinder configuration which was locally equivalent to a sphere of radius R against a flat surface when the surface separation $D \ll R$. The normal forces F between the curved surfaces were measured as a function of absolute surface separation distance D with force sensitivity and absolute separation distance accuracy down to <10 nN and 0.1 nm, respectively. The absolute surface separation can be monitored in real time and *in situ* using an optical technique called multiple beam interferometry (MBI) by

employing fringes of equal chromatic order (FECO).[47-50] Each measurement was repeated at least three times under a fixed experimental condition.

In this study, the interaction forces between asphaltene surfaces were measured in heptol using the SFA in a configuration shown in Figure 3.1. The reference distance ($D = 0$) was determined at the adhesive contact between two bare mica surfaces in air. The thickness of two dry asphaltenes films was measured at their adhesive contact in the air and determined to be ~5 nm per film.

(a)

0.4 nm	2.9 nm
-0.4 nm	-2.9 nm
(b)	(c)
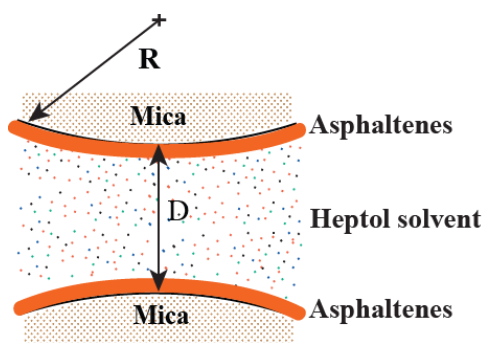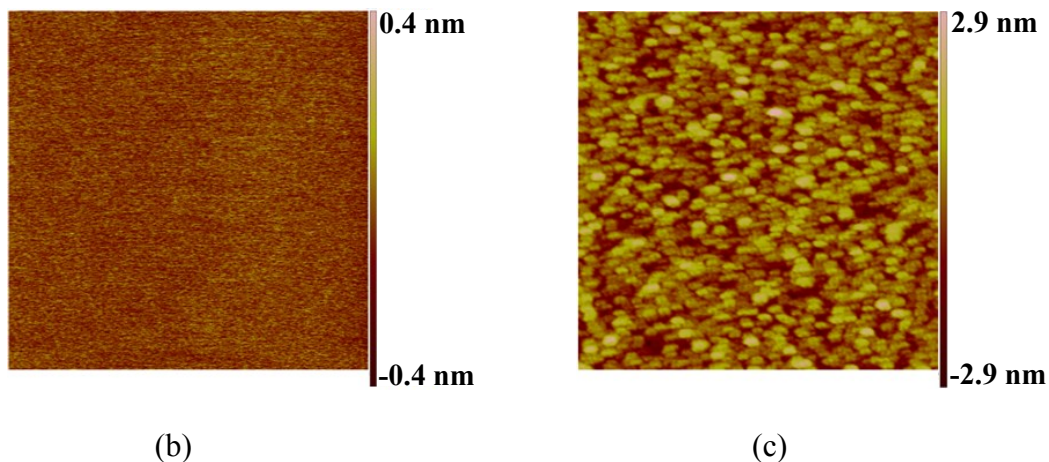
Figure 3.1 (a) The experimental configuration of surface forces measurement between two asphaltene surfaces with solvent injected in between. AFM images of (b) a bare mica surface and (c) the drop-coated asphaltene film on mica. The scan size of the images was 1 μm×1 μm.

3.2.3 The morphology characterization of asphaltene films using AFM

The morphology of the asphaltene films was characterized by AFM (Dimension ICON, Bruker, Santa Barbara, CA, USA) using tapping mode in air. The impacts of different solvents on the surface morphology of asphaltene films was investigated by treating asphaltene films in the different solvents for 2.5 hours, and then the treated surfaces were kept under vacuum overnight before imaging.

3.2.4 Micropipette tests

Micropipette technique was employed to test the stability of water-in-oil emulsion droplets with asphaltenes adsorbed at interfaces in toluene. In the micropipette experiment, two individual emulsion droplets were manipulated using two small suction pipettes. The experiments could be monitored in real time through

an inverted microscope and was recorded on videos for analysis. A detailed setup of micropipette was reported by A. Yeung *et al.*[51] Briefly, about 50 µl emulsions was placed in a sample cell. Two micron-sized droplets were found and manipulated by two small pipettes which were inserted into the sample cell from two opposite sides. Adjustable suction pressures were applied at the pipette tips to grasp individual droplets by connecting the other ends of the pipettes to the syringes through flexible tubings. The applied compression was controlled by a micromanipulator connected to the pipettes which allowed continuous motion. Maximum one-minute contact time was applied unless coalescence occurred in less than a minute.

Here the water-in-oil emulsions with asphaltenes were prepared as follows. 10 wt% of Milli-Q water or salt solutions were added into asphaltenes in toluene solutions with asphaltenes concentrations of 0.3 wt% and 1.0 wt%. The mixture was shaken by hand for about 5 seconds to obtain the water-in-oil emulsion, which was then used for micropipette test. Thirty pairs of emulsion droplets with approximately equal size were studied for every single test condition. The pH of Milli-Q water was adjusted by adding HCl and NaOH. NaCl and $CaCl_2$ solutions were prepared by dissolving the desired amount of NaCl and $CaCl_2 \cdot 2H_2O$ in Milli-Q water respectively.

3.2.5 Computer-controlled 4-roll mill fluidic device for the study of droplet interactions under dynamic flow condition

A computer-controlled 4-roll mill fluidic device was in-house built (Figure S 3.1) and used to investigate the interaction and coalescence behavior of multiple

free-suspending water-in-oil (toluene) emulsion droplets with asphaltenes under flowing conditions. The modified computer-controlled 4-roll mill was built based on a design reported by L.G. Leal and co-workers,[52,53] which consists the main chamber with four equal size cylindrical rollers arranged at the vertices of a square. By controlling the rotation speed and direction of the 4 rollers of the 4-roll mill, four kinds of flow type can be obtained. The detailed setup of the computer-controlled 4-roll mill can be found in the Supporting Information.

For the 4-roll mill experiment, water-in-oil emulsions were prepared by dissolving desired amounts of asphaltenes into toluene, and then introducing a desired amount of water into the asphaltenes solution and dispersing the mixture using a homogenizer. Selected water-in-oil emulsion concentrate was collected, injected and suspended into toluene in the 4-roll mill chamber.

3.3 Results and Discussion

3.3.1 The morphology of drop-coated asphaltene film on mica

AFM was applied to characterize the morphology and roughness of asphaltene films drop-coated on the freshly cleaved mica. The bare mica surface was flat and featureless as shown in Figure 3.1b, whereas the drop-coated asphaltene film showed a uniform layer of asphaltene aggregates as shown in Figure 3.1c. The root-mean-square (RMS) roughness of the asphaltene film was about 0.5 nm.

3.3.2 Interactions between asphaltene surfaces in pure toluene

Toluene is a well-known good solvent for asphaltenes. SFA force measurement between two asphaltene films in toluene was performed to understand the interaction

mechanisms between asphaltenes in a good solvent. During a typical force measurement cycle (approach and separation), the two surfaces were moved to approach each other and kept in contact for a selected time, and then the surfaces were separated. The hard wall thickness was defined as the confined film thickness which did not significantly change with increasing the normal load or pressure. A typical force-distance profile is shown in Figure 3.2. The finite hard wall thickness D ~35 nm in toluene measured by the SFA (Figure 3.2) indicated that asphaltenes strongly adhered to the mica surfaces, and toluene was not able to dissolve or wash away the adsorbed asphaltene layers, which could be likely due to the strong van der Waals attraction between the polar groups of the asphaltenes and the mica surface.[31]

As shown in Figure 3.2, pure repulsion was detected during both approaching (denoted as "in") and separation ("out") between two asphaltene surfaces in toluene. As compared with the confined (dry) thickness ~10 nm of two asphaltene films, as indicated by the dashed line shown in Figure 3.2, the two asphaltene films swelled ~25 nm in toluene which corresponds to ~12.5 nm for each asphaltene film. The relatively long range repulsion measured during approaching suggested that the swollen asphaltene films were flexible and soft in the good solvent toluene. The measured repulsion between the asphaltene films was mainly attributed to the steric interaction between swollen asphaltenes chains in toluene.
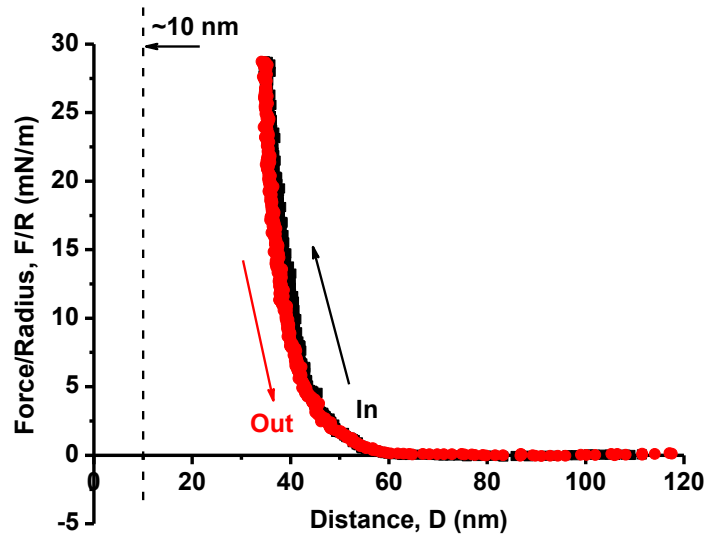
Figure 3.2 The force-distance profile between two asphaltene surfaces in pure toluene, i.e., ω = 1. The black and red curves are for approaching (in) and separation (out), respectively.

3.3.3 Interactions between asphaltene surfaces in heptol and pure n-heptane

The interaction of asphaltene surfaces in pure n-heptane and heptol solvents with different weight fraction (ω) of toluene were also investigated using SFA. Figure 3.3a, b and c present the typical force-distance profiles measured in heptol with toluene weight fraction of ω = 0.8, 0.5 and 0.2, respectively. For all the cases, pure repulsion was measured during approach. However, adhesion of $F_{ad}/R \sim$ -1.3 mN/m ($W_{ad} \sim 0.28$ mJ/m^2) was measured for ω = 0.8 during separation after the two asphaltene surfaces were kept in contact for 1 min. It is noted that the force-distance curves do not overlap during approach (in) and separation (out), which was mainly due to the interaction differences between the asphaltene surfaces during approach and separation, also known as adhesion hysteresis. [46, 50] As the weight fraction of toluene decreased to ω = 0.5 and ω = 0.2, the adhesion measured during the

51

separation increased to $F_{ad}/R \sim$ -2.5 mN/m ($W_{ad} \sim$ 0.53 mJ/m^2) and $F_{ad}/R \sim$ -3.0 mN/m ($W_{ad} \sim$ 0.64 mJ/m^2) respectively. The separation curves also showed stretching behaviors in heptol ($\omega = 0.8$, 0.5 and 0.2), suggesting that the asphaltenes were partially swollen in heptol. In pure n-heptane ($\omega = 0$), adhesion of $F_{ad}/R \sim$ -4.5 mN/m ($W_{ad} \sim$ 0.95 mJ/m^2) was detected (Figure 3.3d) during separation, indicating strong adhesion between asphaltenes in n-heptane. Figure 3.3e summarizes the normalized adhesive force (F_{ad}/R) and the adhesion energy (W_{ad}) as a function of the weight fraction of toluene in heptol, including pure n-heptane ($\omega = 0$) and toluene ($\omega = 1$). It can be clearly seen that the normalized adhesive force and adhesion energy between asphaltenes decreased as the weight fraction of toluene increased, and finally diminished in pure toluene.

The increased adhesion measured above between asphaltene surfaces with the addition of n-heptane plays a critical role in the increased tendency of asphaltene molecules to aggregate in heptol with higher content of n-heptane, a poor solvent for asphaltenes. Moreover, the range of repulsive forces during approach was observed to decrease slightly with increasing the weight fraction of n-heptane, and the thickness of the confined asphaltene films also appeared to be smaller as compared to that in pure toluene (Figure 3.2). All of these results indicate that the asphaltene molecules tend to adapt a more compressed conformation with the addition of n-heptane. Figure 3.4 shows a schematic of the conformational change of the asphaltene molecules in heptol with different weight fraction of toluene. In pure toluene (Figure 3.4a), a good solvent, the asphaltene molecules could swell and show fully extended conformation. In heptol, the asphaltene molecules became less

52

swollen and partially aggregated due to the presence of poor solvent n-heptane (Figure 3.4b). Eventually, in pure n-heptane, the asphaltene molecules strongly aggregated with each other and formed a much more compressed layer (Figure 3.4c).
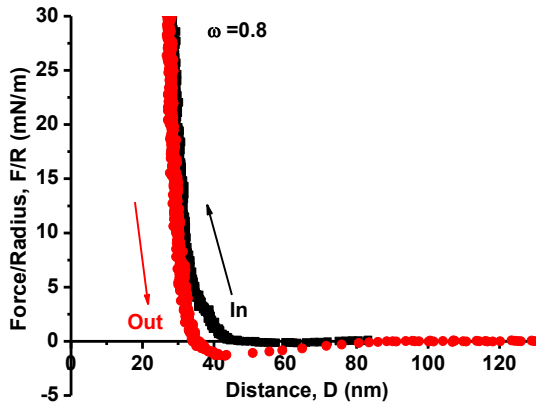
(a)
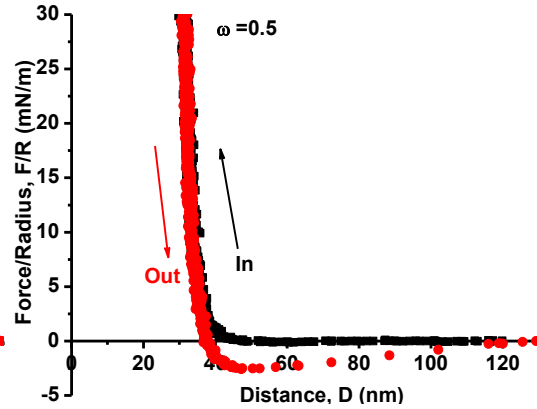
(b)
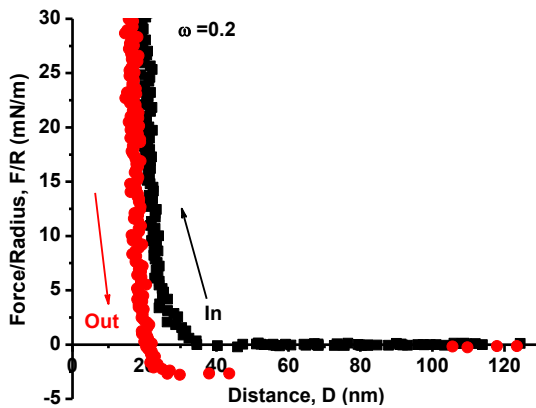
(c)
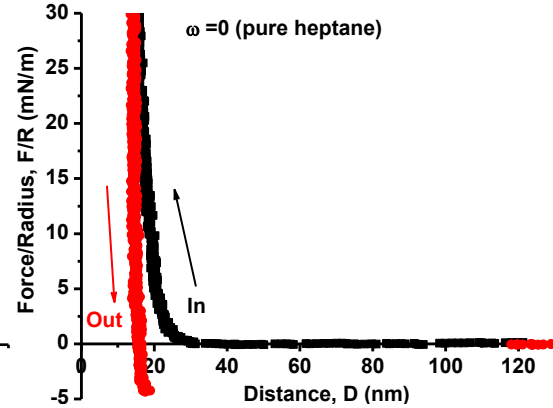
(d)
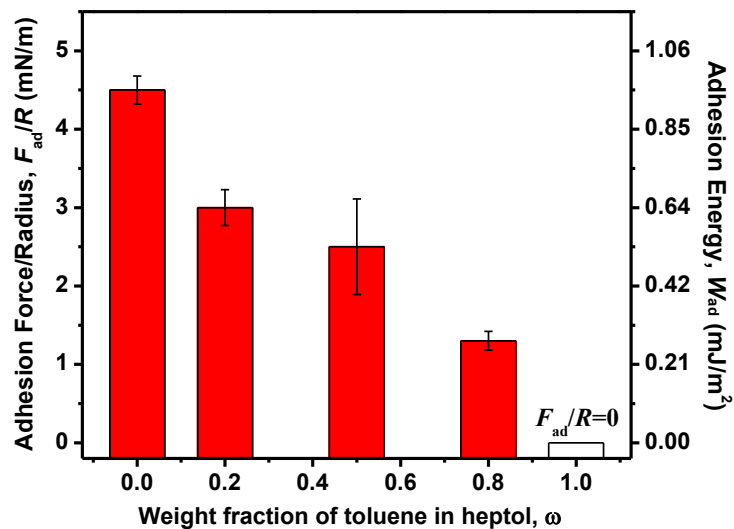
(e)

Figure 3.3 The force-distance profiles between two asphaltene surfaces interacting in heptol with different toluene weight fractions of (a) $\omega = 0.8$, (b) $\omega = 0.5$, (c) $\omega = 0.2$, and (d) in pure n-heptane, i.e. $\omega = 0$. The black and the red curves are for approaching (in) and separation (out), respectively. (e) The normalized adhesion forces (F_{ad}/R) and adhesion energy (W_{ad}) as a function of the weight fraction of toluene (ω) in heptol obtained from SFA measurements: $\omega = 0$, pure n-heptane; $\omega = 1$, pure toluene. The normalized adhesion forces, F_{ad}/R is on the left ordinate and the adhesion energy per unit area, W_{ad} ($W_{ad} = F_{ad}/1.5\pi R$) is on the right ordinate.

54

"fully extended"   "partially compressed"   "compressed"

(a)   (b)   (c)
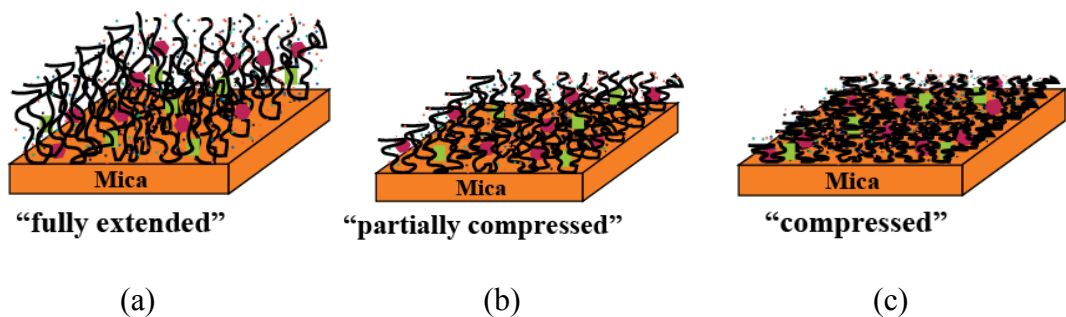
Figure 3.4 Schematic of the conformational change of asphaltene surfaces in different organic solvents: (a) toluene, (b) heptol, (c) n-heptane. Red and green symbol represent the aromatic ring structures of the asphaltene molecules. Small dots present the solvents.

3.3.4 The impact of solvent conditions on the surface morphology of asphaltene films

(a)   (b)   (c)
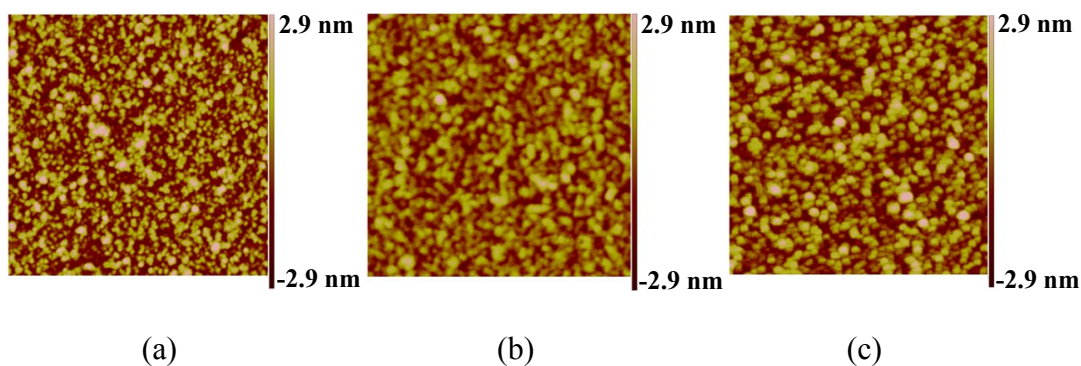
Figure 3.5 AFM images of the drop-coated asphaltene films on mica after incubation in (a) toluene ($\omega = 1.0$), heptol with toluene fraction of (b) $\omega = 0.5$ and (c) n-heptane ($\omega = 0$) for 2.5 hours. The images were taken after films were dried under reduced pressure overnight. The scan size of the images was 1 μm×1 μm.

In order to further understand the impact of solvents on the conformational changes of asphaltenes, the morphology of asphaltene films after treating with heptol solvents was characterized. Figure 3.5a, b and c show AFM images of asphaltene films after incubation in different solvents, i.e. toluene, heptol, and n-heptane, respectively. Comparing to the morphology of dry asphaltene film (after treated with poor solvent, n-heptane) shown in Figure 3.1c, larger aggregates/domains formed after incubation in toluene as shown in Figure 3.5a. Figure 3.5 also shows that the RMS roughness of the dry asphaltene film gradually increased from ~0.5 nm to ~1 nm and the peak-peak value increased from ~6 nm to ~8 nm, as the solvent conditions changed from good solvent toluene to heptol and then to poor solvent n-heptane. The formation of relatively larger aggregates/domains after incubation in toluene suggests that the asphaltene molecules can swell to have extended conformation in the good solvent. According to previous studies, asphaltenes could adsorb onto mica surface through most of the polar functional groups, leaving the aromatic rings and peripheral aliphatic chains extending in toluene. The opposing swollen asphaltene aggregates/chains could repel each other when brought together, inconsistency with the repulsive forces detected by the SFA. The finite hard wall distance ($D \sim 15$ nm) measured in pure n-heptane (Figure 3.3d) as compared with $D \sim 25$ nm in pure toluene (Figure 3.2) indicates that asphaltene films have the much less swelling capability in poor solvent n-heptane than that in the good solvent toluene.

3.3.5 The nature of interaction forces between asphaltene surfaces in heptol

The repulsive forces detected during approaching in the SFA experiments above were most likely attributed to the steric forces between the opposing asphaltene molecules of the two surfaces. The aromatic rings structures (also some flexible secondary chains) would swell in good solvent toluene whereas the aliphatic chains would show affinity to n-heptane. Since the swollen aromatic ring structures and/or the aliphatic chains of the asphaltene molecules may bear some similar behaviors in steric interactions as swollen polymer brushes, Alexander–de Gennes (AdG) scaling model was applied here to fit the approach force curves. The AdG model describes the steric forces between surfaces covered with end-tethered, monodisperse and neutral polymer brushes in good solvents.[54-56] When two polymer brush layers approach and overlap with each other, the local density of the polymer segments will increase, resulting in an increase of the osmotic pressure and repulsive interaction energy. The repulsive pressure between two planar brush layers according to the AdG model is described in Eq. 3.1

$$P(D) \approx \frac{kT}{s^3}\left[(\frac{2L}{D})^{9/4} - (\frac{D}{2L})^{3/4} \right] \qquad \text{for } D < 2L, \qquad (3.1)$$

where k denotes the Boltzmann constant and T is temperature, s is the mean distance between two grafting points on the surface, L is the brush layer thickness on one surface.[54] The surface forces between two asphaltene surfaces in the configuration of SFA measurement can be given by Eq. 3.2 according to the Derjaguin approximation[55] which correlates $F(D)$ between two curved surfaces to the

interaction free energy between two planar surfaces. R is the radius of local curvature for the surface forces measurement using SFA.

$$\frac{F(D)}{R} = 2\pi \int P(D)dD = \frac{16\pi kTL}{35s^3}\left[7(\frac{2L}{D})^{5/4} + 5(\frac{D}{2L})^{7/4} - 12\right] \qquad (3.2)$$

Figure 3.6 shows the fitting curves of measured repulsive forces between two asphaltene surfaces in heptol using the AdG model. It was found that the AdG model could well fit all the measured repulsive force curves at short separation distance under high compression (shown as dash lines), while deviation was found at longer separation distance under relatively low compression. The weak repulsive forces measured at relatively long separation distance might originate from some protruding polydispersed aliphatic chains on asphaltene aggregates and/or could be due to the complexity and polydispersity of secondary chains of the asphaltene molecules.[31] The additional weak repulsive force originated from the polydispersed chains is not considered in the AdG theory which is for monodisperse brushes. Therefore, AdG model with another independent set of fitting parameters was applied to fit the force curves in the lower compression regime, shown as solid lines in Figure 3.6.
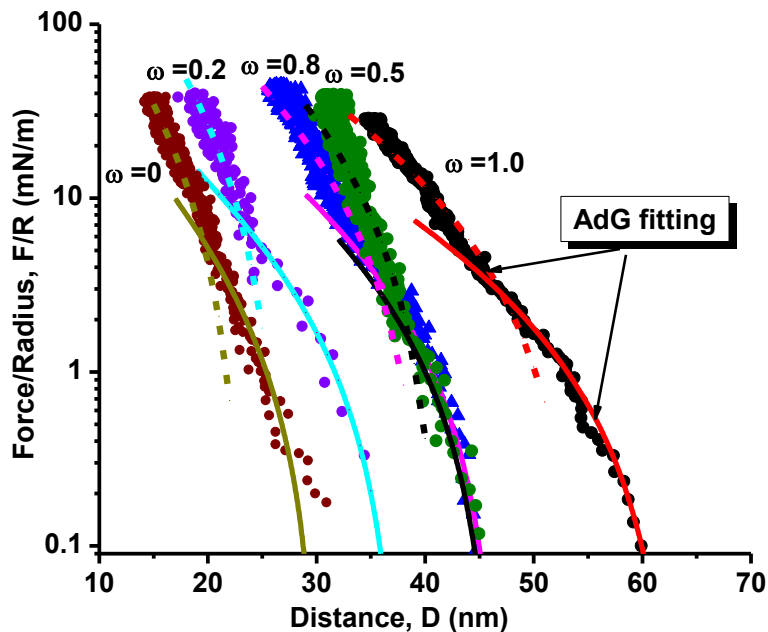
Figure 3.6 The experimentally measured force-distance profiles (dot curves) and theoretically fitted curves using the Alexander-de Gennes (AdG) model for two interacting asphaltene surfaces in pure toluene (ω = 1), heptol with different toluene weight fractions (ω) and n-heptane (ω = 0). The dash and solid lines are the fitting curves under higher and lower compression regime, respectively.

Table 3.1 summarizes the fitting parameters *L* and *s* using the AdG model in both high and relatively lower compression regimes. The *L* represents the thickness of the asphaltene aggregates under higher compression and the length of the polydispersed aliphatic side chains protruding from the asphaltene aggregates or molecules under lower compression, respectively. In good solvent toluene, due to the formation of large swollen aggregates and extension of flexible secondary chains, the *L* value was the largest in both lower and higher compression regimes. In heptol with

toluene fractions of 0.8 and 0.5, the *L* values were very close to each other but smaller than that in pure toluene. With toluene fraction of 0.2, *L* was even smaller, and in pure n-heptane, *L* value reached the smallest. For the toluene fraction of 0.8, 0.5, 0.2 and 0, the *s* values did not show significant differences. Whereas the *s* value in toluene case was relatively larger as compared to other four cases, which might be due to the most extended conformation of asphaltenes in the good solvent toluene.

Table 3.1 The fitting parameters (*L* and *s*) using the Alexander-de Gennes model for the experimentally measured force-distance profiles under both high and low compression regimes according to Figure 3.6. Low: low compression regime. High: high compression regime.

	$\omega = 1$		$\omega = 0.8$		$\omega = 0.5$		$\omega = 0.2$		$\omega = 0$	
	Low	High	Low	High	Low	High	Low	High	Low	High
L (nm)	31.7	27.5	23.6	20.3	23.4	20.8	19.0	13.5	15.3	11.7
s (nm)	4.2	2.6	3.4	2.0	3.5	1.8	3.6	1.5	3.4	1.7

3.3.6 The stability of water-in-oil emulsion droplets with asphaltenes

Asphaltenes have been believed to play a role in the stabilization of water-in-oil emulsions during oil production. As discussed above, asphaltenes can swell and sterically repel each other in a good solvent like toluene, while attracting each other

in a poor solvent like n-heptane. Here, the interaction of water-in-oil (toluene) droplets in the presence of asphaltenes was investigated by using the micropipette technique to better understand their stabilization and interaction mechanisms in good solvent toluene. The impacts of water chemistry (e.g. pH, salts type and salinity) and asphaltenes concentrations were also investigated.

Figure 3.7 shows some typical sequential images captured during the interaction of two emulsion droplets: non-coalescence case (series a1-a3) and coalescence case (series b1-b3). In Figure 3.7a and b, images (1), (2) and (3) represent the three stages of interaction: approaching/in contact, in contact under compression or coalescence (if occurred) and separation. For one case (a1-a3), the two droplets were brought into contact for 1 min under compression, and no coalescence was observed. For another separate case (b1-b3), larger deformation was caused by slightly higher compression, and the two droplets were observed to coalesce into one single droplet after several trials of collision. The real-time interaction processes can be found in the Supporting Information (Movie S 3.1 and Movie S 3.2). It is noted that in the micropipette tests, the two emulsion drops were carefully aligned for "head-on" collision so the effects of interfacial sliding could be minimized. However, interfacial shearing could still play a role in the interaction if the two drops were compressed under high load that led to interfacial displacement/shift of the drops, which could contribute to the coalescence observed in Figure 3.7b and Movie S 3.2.

61

(a1)   (a2)   (a3)

(b1)   (b2)   (b3)
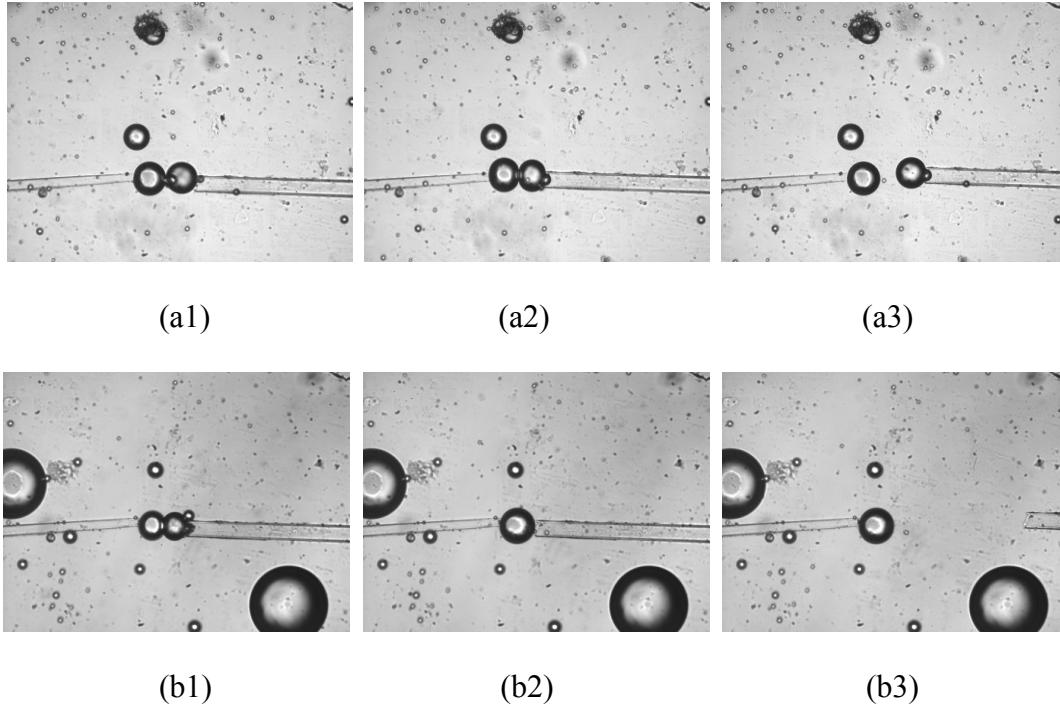
Figure 3.7 (a) and (b) show the sequential images (image size: 400 μm×300 μm) of the interaction of two water (with 0.01 M $CaCl_2$)-in-oil emulsion droplets with 0.3 wt% asphaltenes in toluene visualized by the micropipette technique: series (a) and (b) is the non-coalescence case and coalescence case, respectively; (1), (2) and (3) represent the three stages respectively: approaching/in contact, in contact under compression or coalescence (if occurred) and separation.
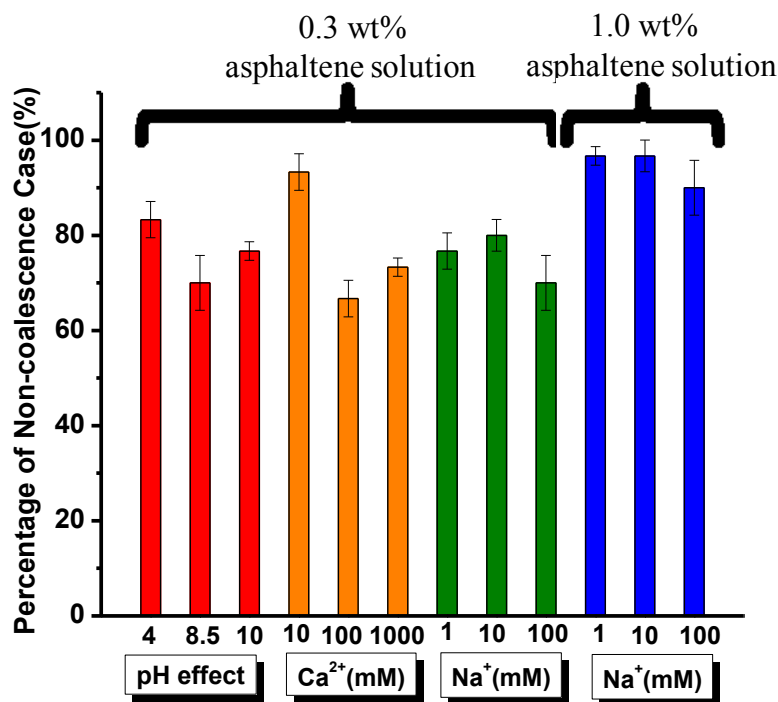
Figure 3.8 The percentage of non-coalescence pairs of emulsion droplets in thirty pairs as a function of water pH (4, 8.5, 10), concentration of $CaCl_2$ (10, 100, 1000 mM), concentration of NaCl (1, 10, 100 mM), concentration of asphaltenes in toluene (0.3 wt%, 1.0 wt%). Red bar: Milli-Q water with different pH of 4, 8.5 and 10 in 0.3 wt% of asphaltenes in toluene solution. Orange bar: 10, 100, 1000 mM $CaCl_2$ solutions in 0.3 wt% of asphaltenes in toluene solution. Green bar: 1, 10, 100 mM NaCl solutions in 0.3 wt% of asphaltenes in toluene solution. Blue bar: 1, 10, 100 mM NaCl solutions in 1.0 wt% of asphaltenes in toluene solution. Coalescence tests for each set of condition were repeated independently for at least three times.

Figure 3.8 summarizes the percentage of non-coalescence case of water-in-oil emulsion droplets under different solution conditions in toluene, which include

various pH (4, 8.5, 10), Ca^{2+} concentration (10, 100, 1000 mM) and Na^+ concentration in water (1, 10, 100 mM), and asphaltenes concentration in toluene (0.3 wt%, 1.0 wt%). With asphaltenes concentration of 0.3 wt%, 83% of emulsion droplets did not coalesce at pH=4, and increasing water pH only slightly facilitated coalescence of the emulsion droplets. The addition of Ca^{2+} slightly enhanced the coalescence which was most likely because Ca^{2+} could "bridge" two interfacial asphaltene layers through the interactions with carboxyl groups (-COOH) on the asphaltene molecules. Coalescence of the emulsion droplets was significantly inhibited when the asphaltenes concentration increased to 1.0 wt%, indicating more asphaltenes adsorbed to the water/oil interfaces could provide a stronger steric barrier for preventing the coalescence of the emulsion drops. The results in Figure 3.8 suggest that (1) solution pH and presence of monovalent ions (e.g. Na^+) do not significantly affect the coalescence of water drops in asphaltene-toluene solution, (2) the presence of Ca^{2+} can slightly enhance the coalescence through bridging interaction with carboxyl groups on the asphaltene molecules, and (3) the asphaltenes adsorbed at water/oil interface provide strong steric hindrance to prevent the coalescence of the emulsion drops and the amount of asphaltenes at the water/oil interface plays a significant role. It should be also noted that even for the coalescence cases, certain compression and contact time were needed, and no coalescence occurred immediately when the two droplets were brought into contact. Therefore, generally, the emulsion droplets could not easily coalesce for all the conditions which is consistent with the repulsive forces measured between asphaltene surfaces in toluene by SFA.

Asphaltene molecules are believed to adsorb onto the water/oil (toluene) interfaces which could help stabilize the emulsion droplets by forming a protecting coating and inducing repulsive forces between emulsion droplets. Figure 3.9a shows that a crinkled "skin" could form around the water droplet when the water droplet was contracted in asphaltenes-in-toluene solution, which indicates the presence of an interfacial asphaltene layer. The asphaltene molecules in this interfacial layer can swell and stretch into the toluene phase resulting in steric repulsion between two emulsion droplets which acts as a protective layer to inhibit drop coalescence, as shown in the schematic in Figure 3.9b. Therefore, droplet coalescence could hardly occur, while sufficient contact time and relatively high compression would be generally required to overcome the repulsion due to the protective asphaltenes coatings of the two emulsion droplets. Long contact time would increase the possibility of the interpenetration of the interfacial asphaltene molecules which might allow direct contact of water molecules of the two drops to facilitate coalescence. High compression could lead to larger deformation of the droplets and induce rearrangement or displacement of the interfacial asphaltene molecules, also facilitating droplet coalescence. Nevertheless, the micropipette tests show that even increasing contact time and compression load would not efficiently induce droplet coalesce of water-in-oil emulsion in the presence of asphaltenes.

(a) (b)
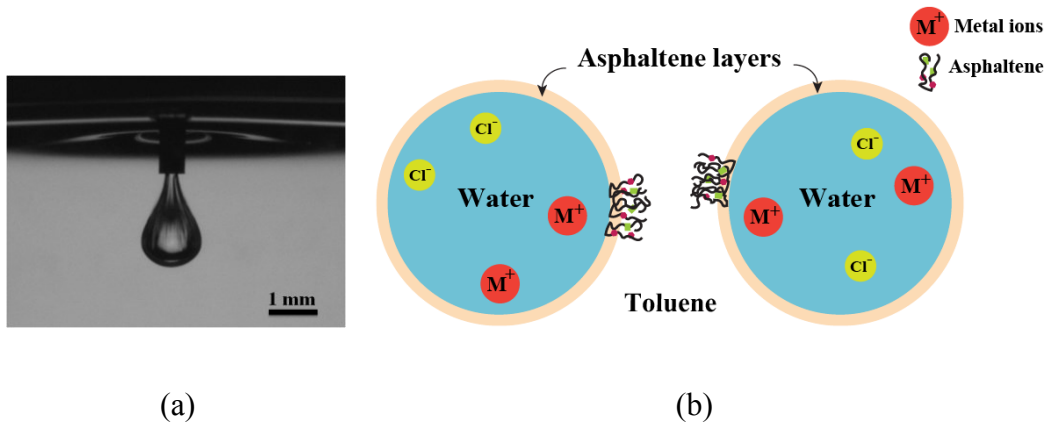
Figure 3.9 (a) Microscopic image showing a crinkled "skin" around the water droplet in asphaltenes-in-toluene solution when the water droplet was contracted to a smaller size indicating the adsorption of asphaltenes onto the water/toluene interface. (b) Schematic of two water-in-oil emulsion droplets interacting in toluene with asphaltenes at interfaces.

To better understand the interaction of water-in-oil emulsion drops with asphaltenes under dynamic flow condition (in contrast to static droplets in micropipette tests), a computer-controlled 4-roll mill was built and applied to explore the impact of external flow conditions. Here, only the interaction of multiple drops and effect of interfacial shearing on the drop coalescence are reported. A more detailed study on head-on collision of one pair of emulsion drops under different flow conditions will be reported separately.

Figure 3.10 shows the captured microscopic images of the interaction of one droplet (indicated as A drop with diameter ~131 μm) with multiple neighboring droplets, particularly against the B drop with diameter ~164 μm, under extensional

66

flow condition with a shear rate of 0.16 s^{-1} (Figure S 3.2). The interaction process can be found in Movie S 3.3 in the Supporting Information. Initially (t=0 s), the drop A and drop B were not in contact (Figure 3.10a). At t= 0.58 s, drop A was brought into contact with drop B and then started sliding along the drop B under the external extensional flow. Coalescence occurred within ~0.7 s as shown in Figure 3.10b, c, d and e. The above results indicate that interfacial sliding or shearing between the contacting water-in-oil drops under external flow could induce drop coalescence, which was most likely attributed to the conformation change and displacement of interfacial asphaltene molecules and/or aggregates caused by the sliding thus allowing direct contact of water of the two drops for coalescence.

Both micropipette tests on static emulsion drops and 4-roll mill tests on drops under dynamic flow have demonstrated that (1) the interfacial asphaltenes play a critical role in stabilizing the water-in-oil emulsions and inhibiting their coalescence, and (2) proper collision angles and compression are required to cause interfacial sliding or shearing between the contacted emulsion drops due to the crowding of the multiple drops under external flow, which locally destabilizes the protective interfacial asphaltene layers and thus enhances the coalescence probability of the water-in-oil emulsion drops; otherwise, the emulsion droplets would tend to be separated under the external flow and coalescence could not occur.

(a) Before contact at t=0 s (b) Just contact at t=0.58 s

(c) Shearing and sliding at t=1.09 s (d) Coalescing at t=1.25 s

(e) Just coalesced at t=1.28 s (f) After coalescence at t=2.47s
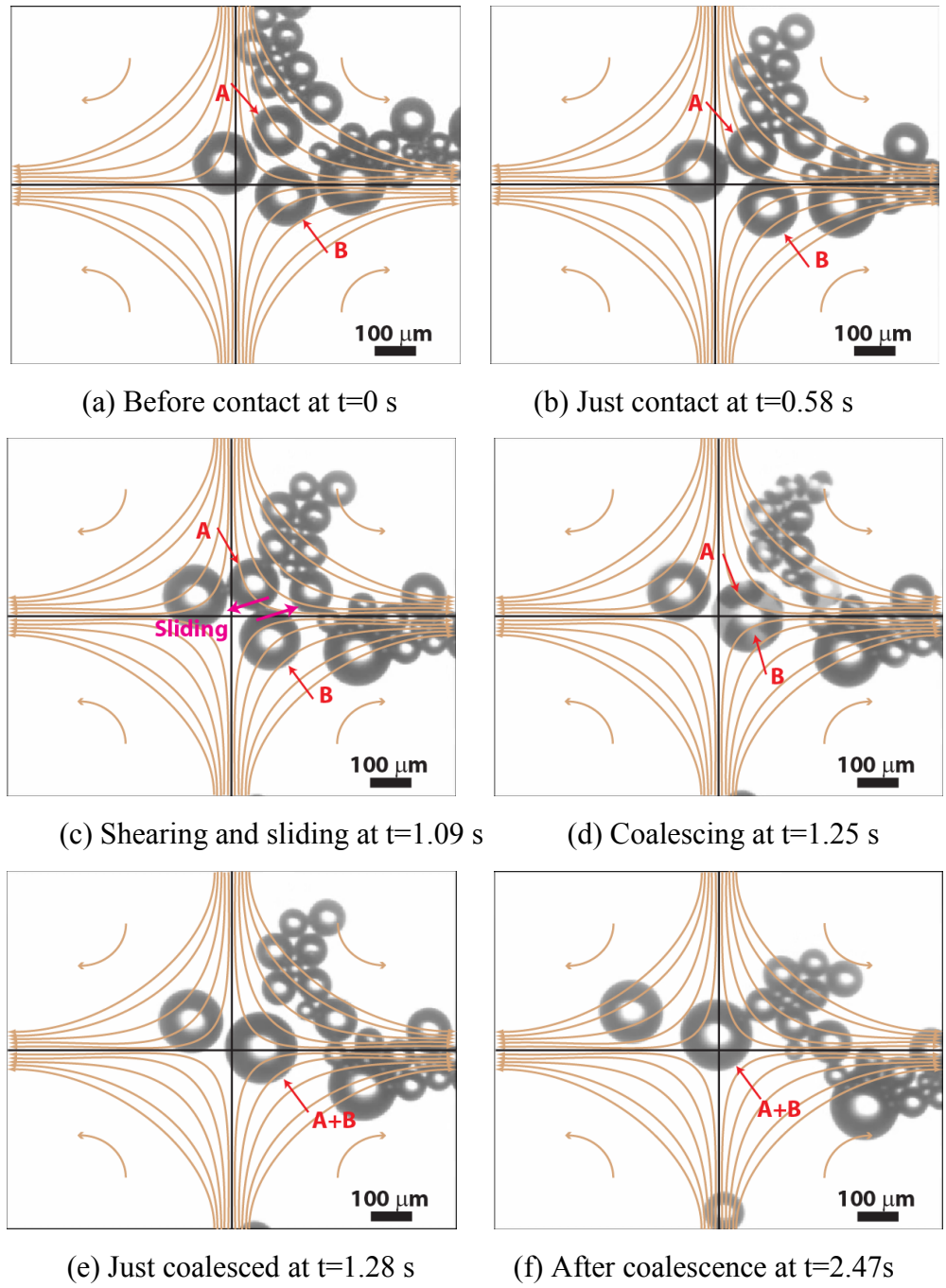
Figure 3.10 Microscopic images of a coalescence case for the interaction of multiple water-in-oil (toluene) emulsion droplets in the presence of asphaltenes under extensional flow field probed using a computer-controlled 4-roll mill fluidic device.

3.4 Conclusions

The molecular interactions of asphaltenes in organic solvents are related to challenging issues such as asphaltene aggregation, precipitation as well as undesirable water-in-oil emulsions in many oil production processes. In this work, using surface forces apparatus, micropipette and 4-roll mill fluidic device, the molecular interaction mechanisms of asphaltenes were directly probed in heptol with different toluene/n-heptane ratio. It was found that the solvent condition could significant impact on the interactions between asphaltenes. As the weight ratio of toluene (ω) in heptol decreased from 1 to 0 (i.e., 1, 0.8, 0.5, 0.2, 0), the interaction between asphaltene surfaces gradually changed from pure repulsion to weak attraction. The repulsive forces measured were mainly due to the steric interaction between the swelling asphaltene molecules and/or aggregates on the opposing surfaces. In good solvent toluene, the measured repulsion also well agreed with the results from micropipette tests and 4-roll mill tests, which demonstrate that asphaltenes can adsorb to the water/oil interfaces and inhibit the coalescence of the emulsions. The results from 4-roll mill tests suggest that proper collision angles and compression are required to cause interfacial sliding or shearing which locally destabilizes the protective interfacial asphaltene layers and thus enhances the coalescence probability of the water-in-oil emulsion drops. The results provide insights into the fundamental understanding of the stability mechanism of water-in-oil emulsions and their destabilization behaviours under flow condition. The methodologies used in this study can be extended to many other emulsion systems.

Supporting information

Computer-controlled 4-roll mill setup

The modified computer-controlled 4-roll mill fluidic device was in-house built and modified based on a design reported by Professor L.G. Leal and co-workers,[52,53] which consists the main chamber with four equal size cylindrical rollers arranged at the vertices of a square. Figure S 3.1a shows the schematic of the in-house built computer-controlled 4-roll mill. Each roller is coupled or geared to a stepping motor driven by the motor controller which is connected to a computer for automatic control. By controlling the step motor, the rollers can rotate and thus generate a flow in the surrounding fluid. The fluid motion is lit by the light source above and imaged with a CCD camera connected to a magnifying lens from the bottom. Depending on the rotation direction and speed of the cylinders, a variety of two-dimensional linear flows can be easily visualized ranging from purely rotational to purely straining to mimic real industrial flow processes. Figure S 3.1b shows the picture of the whole assembled 4-roll mill system, which mainly consists of a 4-roll mill chamber, the lighting source, an imaging system, step motors and motion control system. By controlling the rotation speed and direction of the 4 rollers of the 4-roll mill, four kinds of flow type can be created in the centre of the 4-roll mill, i.e., extensional flow, mixed type flow, rotational flow, and simple shear flow as shown in Figure S 3.2. The parameter α is defined as the flow type and generated by fixing the ratio of the sum of the speeds of diagonally opposed rollers ($\alpha = - (\omega_2 + \omega_4)/(\omega_1 + \omega_3)$). The obtainable accurate shear rate in the current system ranges from 0.00075 to 143.64 s^{-1}. The typical roller speed used in this study was 0.47 – 10 rpm, corresponding to

shear rate of $0.038 - 0.8$ s^{-1}. The imaged droplets can range from several millimeters to several microns.

(a)   (b)
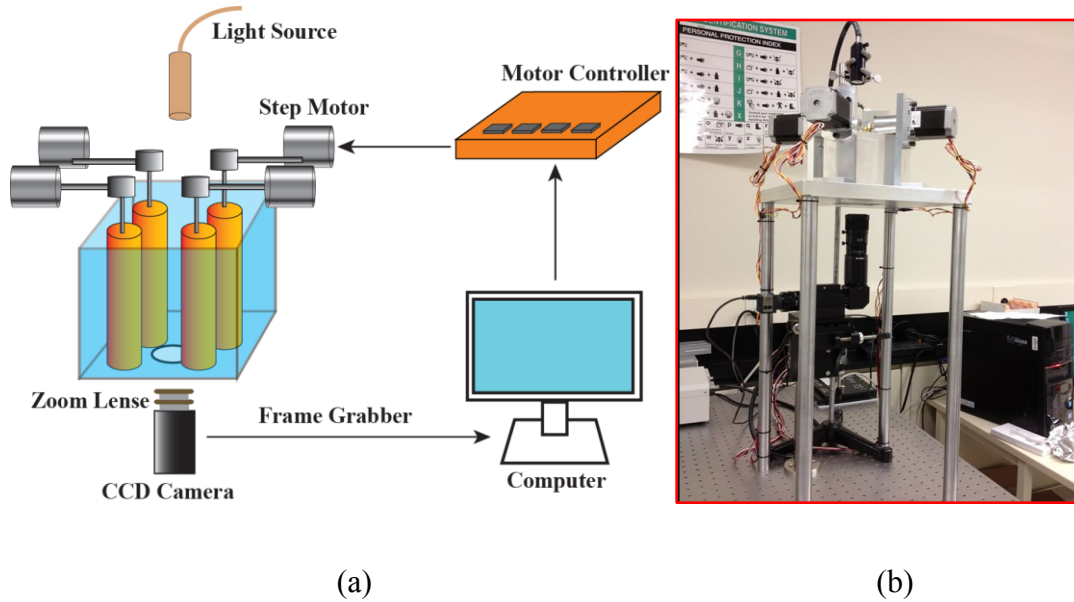
Figure S 3.1 The schematic (a) and picture (b) of the computer-controlled 4-roll mill device in-house built for studying the interactions between suspended emulsion droplets under flow conditions.

(a) Extensional flow   (b) Mixed-type flpw

(c) Rotational flow   (d) Simple shear flow
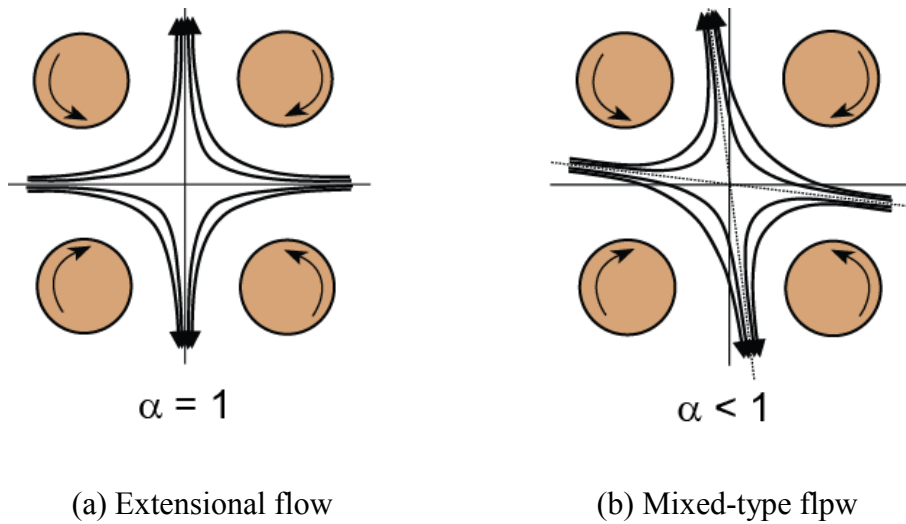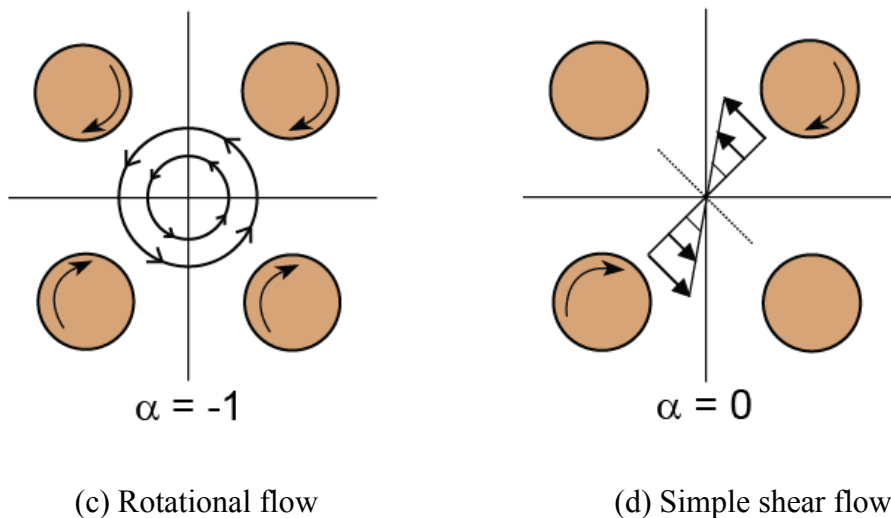
Figure S 3.2 Four types of flow patterns that can be generated in the centre of the 4-roll mill device, i.e., (a) extensional flow, (b) mixed type flow, (c) rotational flow, and (d) simple shear flow.

Movie S 3.1 The non-coalescence case of two interacting water (with 0.01 M $CaCl_2$)-in-oil emulsion droplets with 0.3 wt% asphaltenes in toluene visualized by the micropipette technique according to the sequential images shown in Figure 3.7a.

Movie S 3.2 The coalescence case of two interacting water (with 0.01 M $CaCl_2$)-in-oil emulsion droplets with 0.3 wt% asphaltenes in toluene visualized by the micropipette technique according to the sequential images shown in Figure 3.7b.

Movie S 3.3 A coalescence case for the interaction of multiple water-in-oil (toluene) emulsion droplets in the presence of asphaltenes under extensional flow field probed using a computer-controlled 4-roll mill fluidic device according to the pictures shown in Figure 3.10 (0.25×original speed).

Link for the videos: http://pubs.acs.org/doi/suppl/10.1021/acs.langmuir.6b01000

References

(1) Sheremata, J. M.; Gray, M. R.; Dettman, H. D.; McCaffrey, W. C. *Energ Fuel* **2004**, *18*, 1377-1384.

(2) Gu, G.; Zhang, L.; Xu, Z.; Mashyah, J. *Energ Fuel* **2007**, *21*, 3462-3468.

(3) Yarranton, H. W.; Hussein, H.; Masliyah, J. H. *J Colloid Interf Sci* **2000**, *228*, 52-63.

(4) Pekdemir, T.; Akay, G.; Dogru, M.; Merrells, R. E.; Schleicher, B. *Separ Sci Technol* **2003**, *38*, 1161-1183.

(5) Feng, X. H.; Mussone, P.; Gao, S.; Wang, S. Q.; Wu, S. Y.; Masliyah, J. H.; Xu, Z. H. *Langmuir* **2010**, *26*, 3050-3057.

(6) Kumar, K.; Nikolov, A. D.; Wasan, D. T. *Ind Eng Chem Res* **2001**, *40*, 3009-3014.

(7) *Kilpatrick, P. K.; Spiecker, P. M. Asphaltene emulsions. In Encyclopedic Handbook of Emulsion Technology*; Sjoblom, J., Ed.; Marcel Dekker: New York, 2001, pp 707-730.

(8) McLean, J. D.; Kilpatrick, P. K. *J Colloid Interf Sci* **1997**, *189*, 242-253.

(9) Angle, C. W.; Dabros, T.; Hamza, H. A. *Energ Fuel* **2007**, *21*, 912-919.

(10) Rogel, E.; Leon, O.; Torres, G.; Espidel, J. *Fuel* **2000**, *79*, 1389-1394.

(11) Pazuki, G. R.; Nikookar, M. *Fuel* **2006**, *85*, 1083-1086.

(12) Buckley, J. S.; Hirasaki, G. J.; Liu, Y.; Von Drasek, S.; Wang, J. X.; Gil, B. S. *Petrol Sci Technol* **1998**, *16*, 251-285.

(13) Mullins, O. C. *Spe J* **2008**, *13*, 48-57.

(14) Porte, G.; Zhou, H. G.; Lazzeri, V. *Langmuir* **2003**, *19*, 40-47.

(15) Stachowiak, C.; Viguie, J. R.; Grolier, J. P. E.; Rogalski, M. *Langmuir* **2005**, *21*, 4824-4829.

(16) Verruto, V. J.; Kilpatrick, P. K. *Langmuir* **2008**, *24*, 12807-12822.

(17) Jestin, J.; Simon, S.; Zupancic, L.; Barre, L. *Langmuir* **2007**, *23*, 10471-10478.

(18) Alvarez, G.; Jestin, J.; Argillier, J. F.; Langevin, D. *Langmuir* **2009**, *25*, 3985-3990.

(19) Wu, X. *Energ Fuel* **2003**, *17*, 179-190.

(20) Czarnecki, J.; Moran, K. *Energ Fuel* **2005**, *19*, 2074-2079.

(21) Czarnecki, J. *Energ Fuel* **2009**, *23*, 1253-1257.

(22) Chang, C.-L.; Fogler, H. S. *Langmuir* **1994**, *10*, 1749-1757.

(23) Roux, J. N.; Broseta, D.; Deme, B. *Langmuir* **2001**, *17*, 5085-5092.

(24) Andersen, S. I.; Christensen, S. D. *Energ Fuel* **2000**, *14*, 38-42.

(25) Sheu, E. Y.; Detar, M. M.; Storm, D. A.; Decanio, S. J. *Fuel* **1992**, *71*, 299-302.

(26) Agrawala, M.; Yarranton, H. W. *Ind Eng Chem Res* **2001**, *40*, 4664-4672.

(27) Long, J.; Xu, Z. H.; Masliyah, J. H. *Langmuir* **2007**, *23*, 6182-6190.

(28) Mitchell, D. L.; Speight, J. G. *Fuel* **1973**, *52*, 149-152.

(29) Wang, S. Q.; Liu, J. J.; Zhang, L. Y.; Masliyah, J.; Xu, Z. H. *Langmuir* **2010**, *26*, 183-190.

(30) Wang, S. Q.; Liu, J. J.; Zhang, L. Y.; Xu, Z. H.; Masliyah, J. *Energ Fuel* **2009**, *23*, 862-869.

(31) Natarajan, A.; Xie, J. G.; Wang, S. Q.; Liu, Q. X.; Masliyah, J.; Zeng, H. B.; Xu, Z. H. *J Phys Chem C* **2011**, *115*, 16043-16051.

(32) Natarajan, A.; Kuznicki, N.; Harbottle, D.; Masliyah, J.; Zeng, H. B.; Xu, Z. H. *Langmuir* **2014**, *30*, 9370-9377.

(33) Mullins, O. C.; Sabbah, H.; Eyssautier, J.; Pomerantz, A. E.; Barre, L.; Andrews, A. B.; Ruiz-Morales, Y.; Mostowfi, F.; McFarlane, R.; Goual, L.; Lepkowicz, R.; Cooper, T.; Orbulescu, J.; Leblanc, R. M.; Edwards, J.; Zare, R. N. *Energ Fuel* **2012**, *26*, 3986-4003.

(34) Rane, J. P.; Harbottle, D.; Pauchard, V.; Couzis, A.; Banerjee, S. *Langmuir* **2012**, *28*, 9986-9995.

(35) Pauchard, V.; Rane, J. P.; Zarkar, S.; Couzis, A.; Banerjee, S. *Langmuir* **2014**, *30*, 8381-8390.

(36) Sjöblom, J.; Aske, N.; Auflem, I. H.; Brandal, Ø.; Havre, T. E.; Sæther, Ø.; Westvik, A.; Johnsen, E. E.; Kallevik, H. *Advances in Colloid and Interface Science* **2003**, *100*, 399-473.

(37) Shi, C.; Zhang, L.; Xie, L.; Lu, X.; Liu, Q.; Mantilla, C.; van den Berg, F. G.; Zeng, H. *Langmuir* **2016**.

(38) McLean, J. D.; Kilpatrick, P. K. *J Colloid Interf Sci* **1997**, *196*, 23-34.

(39) Spiecker, P. M.; Kilpatrick, P. K. *Langmuir* **2004**, *20*, 4022-4032.

(40) Zhang, L. Y.; Lawrence, S.; Xu, Z. H.; Masliyah, J. H. *J Colloid Interf Sci* **2003**, *264*, 128-140.

(41) Zhang, L.; Zeng, H. B.; Liu, Q. X. *J Phys Chem C* **2012**, *116*, 17554-17562.

(42) Lu, Q. Y.; Wang, J.; Faghihnejad, A.; Zeng, H. B.; Liu, Y. *Soft Matter* **2011**, *7*, 9366-9379.

(43) Zeng, H. B.; Kristiansen, K.; Wang, P.; Bergli, J.; Israelachvili, J. *Langmuir* **2011**, *27*, 7163-7167.

(44) Zeng, H. B.; Hwang, D. S.; Israelachvili, J. N.; Waite, J. H. *P Natl Acad Sci USA* **2010**, *107*, 12850-12853.

(45) Wang, J.; Opedal, N. V.; Lu, Q. Y.; Xu, Z. H.; Zeng, H. B.; Sjoblom, J. *Energ Fuel* **2012**, *26*, 2591-2599.

(46) Israelachvili, J.; Min, Y.; Akbulut, M.; Alig, A.; Carver, G.; Greene, W.; Kristiansen, K.; Meyer, E.; Pesika, N.; Rosenberg, K. *Rep Prog Phys* **2010**, *73*, 036601.

(47) Israelac.Jn *J Colloid Interf Sci* **1973**, *44*, 259-272.

(48) Israelachvili, J. N.; Adams, G. E. *Nature* **1976**, *262*, 773-776.

(49) Zeng, H.; Tian, Y.; Anderson, T. H.; Tirrell, M.; Israelachvili, J. N. *Langmuir* **2008**, *24*, 1173-1182.

(50) Zeng, H. B.; Maeda, N.; Chen, N. H.; Tirrell, M.; Israelachvili, J. *Macromolecules* **2006**, *39*, 2350-2363.

(51) Yeung, A.; Dabros, T.; Masliyah, J.; Czarnecki, J. *Colloid Surface A* **2000**, *174*, 169-181.

(52) Leal, L. G. *Phys Fluids* **2004**, *16*, 1833-1851.

(53) Borrell, M.; Leal, L. G. *Langmuir* **2007**, *23*, 12497-12502.

(54) Degennes, P. G. *Adv Colloid Interfac* **1987**, *27*, 189-209.

(55) Lowrey, D. D.; Tasaka, K.; Kindt, J. H.; Banquy, X.; Belman, N.; Min, Y.; Pesika, N. S.; Mordukhovich, G.; Israelachvili, J. N. *Tribol Lett* **2011**, *42*, 117-127.

(56) Akbulut, M.; Alig, A. R. G.; Min, Y.; Belman, N.; Reynolds, M.; Golan, Y.; Israelachvili, J. *Langmuir* **2007**, *23*, 3961-3969.

CHAPTER 4   UNDERSTANDING THE ADSORPTION OF ASPHALTENES ON SILICA SURFACES IN TOLUENE USING QUARTZ CRYSTAL MICROBALANCE WITH DISSIPATION AND SURFACE FORCES APPARATUS

4.1 Introduction

As the heaviest component in crude oil and bitumen products, asphaltenes tend to deposit onto various surfaces during many oil production processes. The reservoir solids wettability change resulted from deposition of asphaltenes brings recovery and quality problems, and can also enhance the formation of emulsions leading to difficulties in water treatment. Asphaltenes are defined as a solubility class, which is soluble in aromatic solvents, such as toluene and benzene, and insoluble in alkanes such as n-pentane and n-heptane. Therefore, asphaltenes tend to form asphaltene aggregates in the presence of n-heptane while in toluene, asphaltenes are reported to be stable below the concentration of 100 mg/L.[1] The presence of the heteroatoms and metals may confer to them the affinity to various solid surfaces.[2-5] However, the mechanism of asphaltenes adsorption on surfaces remains not well understood because asphaltenes adsorption is an extremely complex process depending on lots of variables such as sources of asphaltenes, types of solvents, types of solid surfaces and etc.[6-10]

Many studies have been done on the adsorption of asphaltenes on various solid surfaces. Most of the adsorption experiments were carried out using asphaltenes in

76

model oil solutions by using techniques, such as UV-visible spectrometry,[11-14] quartz crystal microbalance (QCM),[15-20] ellipsometry,[21] photothermal surface deformation spectrometry[22], etc. Depending on the sources of the asphaltenes, different solvents used and asphaltene concentrations, the adsorption capacity of asphaltene on different surfaces could vary in a wide range from 0.2 mg/m^2 [23] to 100 mg/m^2.[24] It is commonly believed that decreasing the aromaticity of the solvent would normally increase the adsorbed amount of asphaltenes. Most of the studies showed that the adsorption capacity was larger in heptol (toluene and n-heptane mixture) solvent than that in toluene.[17]

Besides the quantification of adsorbed amount, the adsorption kinetics also varied from literature. Xie et al., reported the asphaltenes adsorption on metal surface did not reach the equilibrium even after 700 min under flow conditions.[25] Goual used asphaltenes from five different sources and found equilibrium adsorption for four of them whereas one of them could not reach the steady state within the experiment time in 0.1 wt% asphaltenes toluene solution.[26] Moreover adsorption isotherm was also analysed. Both monolayer and multilayer adsorption were reported throughout the related literature. A lot of researchers reported the adsorption might follow the behaviour described by the Langmuir isotherm.[14,18,23,27-30] Multilayers were also found in lots of cases, especially in high concentration of asphaltenes solutions, or with longer adsorption time or in alkane solutions.[31-33] Overall, the QCM data often showed multilayer formation compared to other methods. Since most of the QCM studies were under flow conditions, the adsorption

77

of asphaltene was continuous and the adsorption capacity was mostly much higher than that using other techniques.[18,34,35]

Therefore, to date, a consensus on the asphaltenes adsorption mechanisms has not been achieved and many more issues remain to be resolved. In this study, a QCM-D was employed to quantify the adsorbed kinetics and adsorbed amount of two types of asphaltenes on silica surfaces in both toluene and 1:1 heptol solvents. The morphology of the adsorbed asphaltene surfaces was imaged using AFM. Interactions measured between solid surfaces in asphaltenes solutions by surface force measurement can provide more valuable information on mechanisms of asphaltenes adsorption. Therefore, surface force apparatus (SFA) was applied to measure the asphaltenes adsorption kinetics as well as the interaction force between model surfaces (mica) in asphaltenes solutions to further understand the adsorption mechanisms of asphaltenes on the silica surface. The results provide insightful information on the interactions of different types of asphaltenes on surfaces and the mechanisms of asphaltenes adsorption on silica surfaces were proposed.

4.2 Materials and Experimental Methods

4.2.1 Extraction of asphaltenes

Asphaltenes were extracted from two different sources, crude oil and bitumen, using the same following procedure: n-heptane was firstly added into the crude oil or bitumen at n-heptane/crude oil or n-heptane/bitumen ratio of 30/1 (vol/wt) and the mixture was stirred and refluxed for 1 hour. The mixture was then stored in the refrigerator for 2.5 hours before the filtration. The mixture was filtered using filter

papers and the precipitated asphaltenes were obtained. The filter papers with precipitated asphaltenes were then placed in a Soxhlet extractor and extracted by n-heptane for 1 hour to remove the remaining n-heptane-soluble contents. Methylene chloride was then used to extract the asphaltenes on the filter papers using another Soxhlet extractor. The asphaltenes in methylene chloride solution were then concentrated and fully dried under nitrogen flow. The asphaltenes extracted from crude oil and bitumen is indicated as asphaltenes A and asphaltenes B, respectively, in the later sections.

4.2.2 Materials and samples preparation

Asphaltenes stock solutions (2000 mg/L) were prepared for both asphaltenes A and asphaltenes B by dissolving the desired amount of asphaltene solids in toluene and sonicated for 30 min before diluted to other concentrations. Before every single QCM-D test or surface force measurement, the asphaltene solution was also sonicated for 30 min. Toluene, n-heptane and methylene chloride and were all purchased from Fisher Scientific Canada and used as received. The mica used in the surface force measurement was purchased from S & J Trading Inc. (Glen Oaks, NY).

4.2.3 Characterization of asphaltenes

Elemental analysis was applied to determine the content of C, H, N, S and O in both asphaltenes A and asphaltenes B. X-ray photoelectron spectroscopy (XPS) was also applied to detect the possible elements besides C, H, N, S and O for both asphaltenes. Asphaltenes A was further characterized by inductively-coupled-plasma mass spectrometry (ICP-MS) to determine the content of possible metal elements

due to the missing of a significant amount of elements besides C, H, N, S and O. The silica surface after adsorption of asphaltenes A was also characterized using XPS.

4.2.4 Adsorption tests using QCM-D

QCM-D E1 system (Q-sense, Sweden) was used to investigate the adsorption kinetics of both asphaltenes A and asphaltenes B on silica sensor surface in toluene. QCM-D is able to monitor the frequency change (Δf) and dissipation change (ΔD) at the same time when mass is adsorbed on the sensor surface. In most of the studies, Sauerbrey equation was used to determine the mass adsorbed on the surface; however, the Sauerbrey equation is only valid when the following three conditions are satisfied: 1) the mass adsorbed is evenly distributed; 2) the Δm is much smaller than that of quartz crystal itself and 3) the adsorbed layer is rigidly attached to the crystal surface. The third condition can be satisfied only when there is no energy dissipation (dissipation factor D) observed.[17,18,36] In this study, the adsorption layer was treated as a soft layer as long as the dissipation change was above zero. For most cases in this study, the liquid association with the adsorbed asphaltene layers was very substantial which gave a significant rise to the dissipation factor. Therefore, the Sauerbrey equation is no longer valid under this condition and Voigt viscoelastic model embedded in Q-sense Qtools was used to obtain the mass of the adsorbed asphaltene layers related to the changes in both frequency and dissipation.[37,38] The Voigt model can be expressed as follows by correlating the oscillation frequency f, dissipation factor D, thickness h, density ρ, viscosity η, shear modulus μ and circular frequency ω for a viscoelastic layer (index 1) on quartz crystal (index 0) immersed in a bulk Newtonian fluid (index 2) as well as the penetration depth δ of this fluid.

80

$$\Delta f \approx -\frac{1}{2\pi\rho_0 h_0}\left\{\frac{\eta_2}{\delta_2}+\left[h_1\rho_1\omega-2h_1\left(\frac{\eta_2}{\delta_2}\right)^2\frac{\eta_1\omega^2}{\mu_1^2+\eta_1\omega^2}\right]\right\} \tag{4.1}$$

$$\Delta D \approx -\frac{1}{2\pi f\rho_0 h_0}\left\{\frac{\eta_2}{\delta_2}+\left[2h_1\left(\frac{\eta_2}{\delta_2}\right)^2\frac{\eta_1\omega^2}{\mu_1^2+\eta_1\omega^2}\right]\right\} \tag{4.2}$$

$$\delta_2 = \sqrt{\frac{2\eta_2}{\rho_2\omega}} \tag{4.3}$$

A detailed operational procedure of QCM-D experiment has been reported elsewhere.[38,39] Firstly, sensor surface should be thoroughly cleaned following the standard cleaning procedure for silica sensor surface which required a 10-min UV/Ozone clean, 30-min soaking in 2 wt% of sodium dodecyl sulfate (SDS) solution and another 10-min UV/Ozone clean. After the clean sensor was carefully placed in the flow module, a baseline was then established first by injecting the background solvents (toluene) where the frequency and dissipation changes were defined as zero. After a steady baseline was reached, the asphaltene solution was injected into the flow module at a flow rate of 100 µL/min. The background solvent (toluene) was injected again after asphaltenes adsorption to rinse off the unbounded or loosely bounded asphaltenes.

4.2.5 Surface forces measurement

SFA was employed here to study the adsorption of asphaltenes as well as the interactions between adsorbed asphaltene layers by injecting the asphaltenes-in-toluene solution between two mica surfaces (mimicking silica surfaces). The building up of the asphaltenes on mica surfaces due to the asphaltenes adsorption can

be monitored *in-situ* and in real time by multiple interferometry beam (MIB) employing the fringes of equal chromatic order (FECO).[40] The detailed principle and setup of the SFA experiment have been reported elsewhere.[41-45] After injecting the asphaltene solution between two mica surfaces, a typical force measurement cycle was completed by approaching the two surfaces to a "hard wall" (refers to the confined gap distance which hardly changed with the increased normal load or pressure) and then separating the two surfaces. In this study, the reference distance D=0 was determined at the adhesive contact between two bare mica surfaces in air.

4.2.6 AFM imaging

An AFM (MFP-3D, Asylum, Santa Barbara, CA, USA) was used to image the silica sensor surfaces in the air after QCM-D adsorption tests to obtain the morphology of the adsorbed asphaltene layers. The tapping mode was applied to avoid possible surface damage.

4.3 Results and Discussion

4.3.1 Asphaltenes characterization

Table 4.1 shows that the total amount of C, H, N, S and O is 87.33 wt% and 97.28 wt% in asphaltenes A and asphaltenes B, respectively. The elemental analysis results showed that a significant amount of other elements (besides C, H, N, S and O) should be present in asphaltenes A. Figure 4.1 shows the survey spectrum of asphaltenes A and asphaltenes B obtained by XPS where chlorine (Cl) and calcium (Ca) was found in asphaltenes A. Therefore, ICP-MS was then applied to obtain the content of other elements in asphaltenes A and the results are shown in Table 4.2

(only elements with amount above 100 ppm are shown here). Significant amounts of calcium (Ca) and sodium (Na) as well as small amounts of potassium (K), magnesium (Mg), metal iron (Fe), vanadium (V) and nickel (Ni) were detected. Assuming the most possible form of Ca, Na, Mg and K was originally chlorides, so the amount of the chlorides was calculated to be ~8.86 wt% based on the amount of Ca, Na, Mg and K. Hence, ~8.99 wt% of chlorides and trace metals (i.e., Fe, V and Ni) in total are in asphaltenes A which almost compensates the rest of the elements besides C, H, N, S and O.

Table 4.1 Elemental analysis of asphaltenes A and asphaltenes B.

	wt% C	wt% H	wt% N	wt% S	wt% O	Aromaticity (molar ratio C/H)
Asphaltenes A	67.80	7.08	0.95	5.64	5.86	0.798
Asphaltenes B	76.99	7.94	1.03	8.63	2.69	0.808
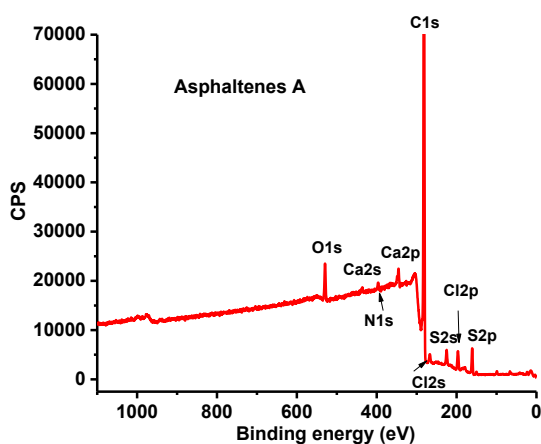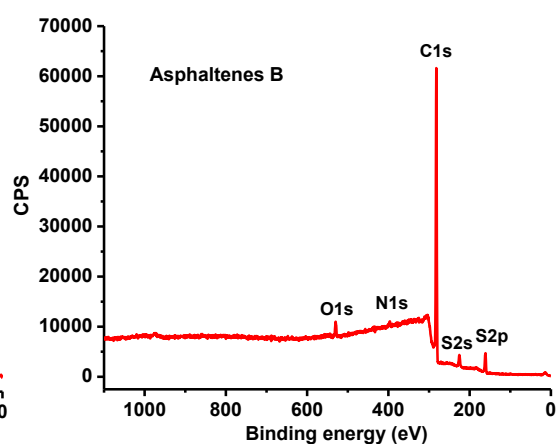
(a)   (b)

Figure 4.1 The XPS survey spectrum of (a) asphaltenes A and (b) asphaltenes B.

Table 4.2 ICP-MS analysis of asphaltenes A (only elements with content above 100 ppm are shown here).

Element	Ca	Na	K	Mg	Fe	V	Ni
Content (ppm)	28271	2930	235	232	549	523	174
Content (wt%)	2.83	0.29	0.024	0.023	0.055	0.052	0.017

4.3.2 QCM-D study on adsorption of asphaltenes in toluene

Adsorption of asphaltenes A on silica sensor surface

Figure 4.2 shows the adsorption of asphaltenes A on silica sensor surfaces in toluene under different asphaltene concentrations. Overall, the frequency first dropped very sharply after injection of asphaltene solution and then kept decreasing slowly with time indicating that the asphaltenes A kept adsorbing on the silica surface. The frequency change reached -41 Hz in 50 mg/L asphaltene-in-toluene solution in 200 min as shown in Figure 4.2a. Figure 4.2b, c and d show the frequency decreased to -93 Hz, -126 Hz and -142 Hz under asphaltene concentrations of 200 mg/L, 500 mg/L and 1000 mg/L, respectively. The dissipation factor D increased under all the concentrations and the dissipation change ΔD was more significant under higher asphaltene concentrations. The change of the dissipation suggested that the adsorbed asphaltenes were soft due to the association of toluene solvent. It has been reported that the absolute value of $\Delta D/\Delta f$ could indicate the structure of the materials adsorbed on the sensor surface.[38,46] A higher absolute value of $\Delta D/\Delta f$ could

suggest a relatively softer and looser layer adsorbed. As the asphaltene concentration increased from 50 mg/L to 1000 mg/L, the absolute value of $\Delta D/\Delta f$ increased from 0.17 Hz^{-1} to almost 1 Hz^{-1} indicating much softer and looser structure formed on the silica surface with increasing the asphaltene concentration. The adsorption of asphaltenes A on silica surface in toluene was irreversible based on the amount of mass loss from the silica surface after rinsed with toluene. The mass loss was not significant under asphaltene concentration of 50, 200, 500 mg/L, which were less than 5%. The mass loss was ~20% at the concentration of 1000 mg/L also showing that the most loosely adsorbed asphaltenes formed on the silica surface under the highest asphaltene concentration tested.

Since dissipation changes were not negligible at all the concentrations tested, the Voigt viscoelastic model was used to obtain the mass (mg/m^2) adsorbed on the silica surface as a function of time shown in Figure 4.4a. The calculated amount of asphaltenes adsorbed on the silica surfaces in toluene was substantially higher than the reported values which might be attributed to the following two reasons: (1) the model used for mass calculation is different in this study. In literature, the solvent association was usually not considered and the Sauerbrey equation was used leading to a much less amount calculated.[15,17,18] (2) asphaltenes A showed continuous adsorption behaviour on silica surface in toluene which is normally observed in a poor solvent, such as heptol (toluene and n-heptane mixture).[25] The adsorbed amount *vs*. time curves under all the concentrations did not level off within the experimental time indicating that asphaltenes A could keep adsorbing on silica surface and further suggesting a possible multilayer coverage of asphaltenes on the silica surface. It has

been reported that for multilayer adsorption when asphaltenes adsorbed on silica in toluene, it could create new adsorption site for other asphaltenes to adsorb. It is similar to the process of forming asphaltene aggregates in the solutions due to the asphaltenes-asphaltenes interaction.[31] Therefore the continuous adsorption of asphaltenes A found in toluene was more likely the asphaltenes kept adsorbing on the asphaltenes on the silica surface. At first, the sharp frequency drop should be attributed to the adsorption of asphaltenes on the silica sensor surface. With increasing the adsorption time, the adsorption of asphaltenes A might happen between asphaltenes and asphaltenes which had a lower adsorption rate resulting in a continuous adsorption of asphaltenes A on silica sensor surface in toluene. From the AFM images of the silica sensor surface after asphaltenes A adsorption, it can be clearly seen that asphaltene A could aggregate even at a very low concentration (50 mg/L) in toluene and the adsorbed of asphaltenes was very heterogeneous on the silica surface as shown in Figure 4.5a. Even larger aggregated domains were found under asphaltenes concentration of 1000 mg/L. Figure 4.5b shows a "network" of asphaltenes formed on the silica surface under asphaltenes A concentration of 1000 mg/L and the aggregates connected to each other and formed like swollen islands which could be due to the significant toluene association in asphaltenes aggregates evident from the large dissipation observed in the QCM-D test.
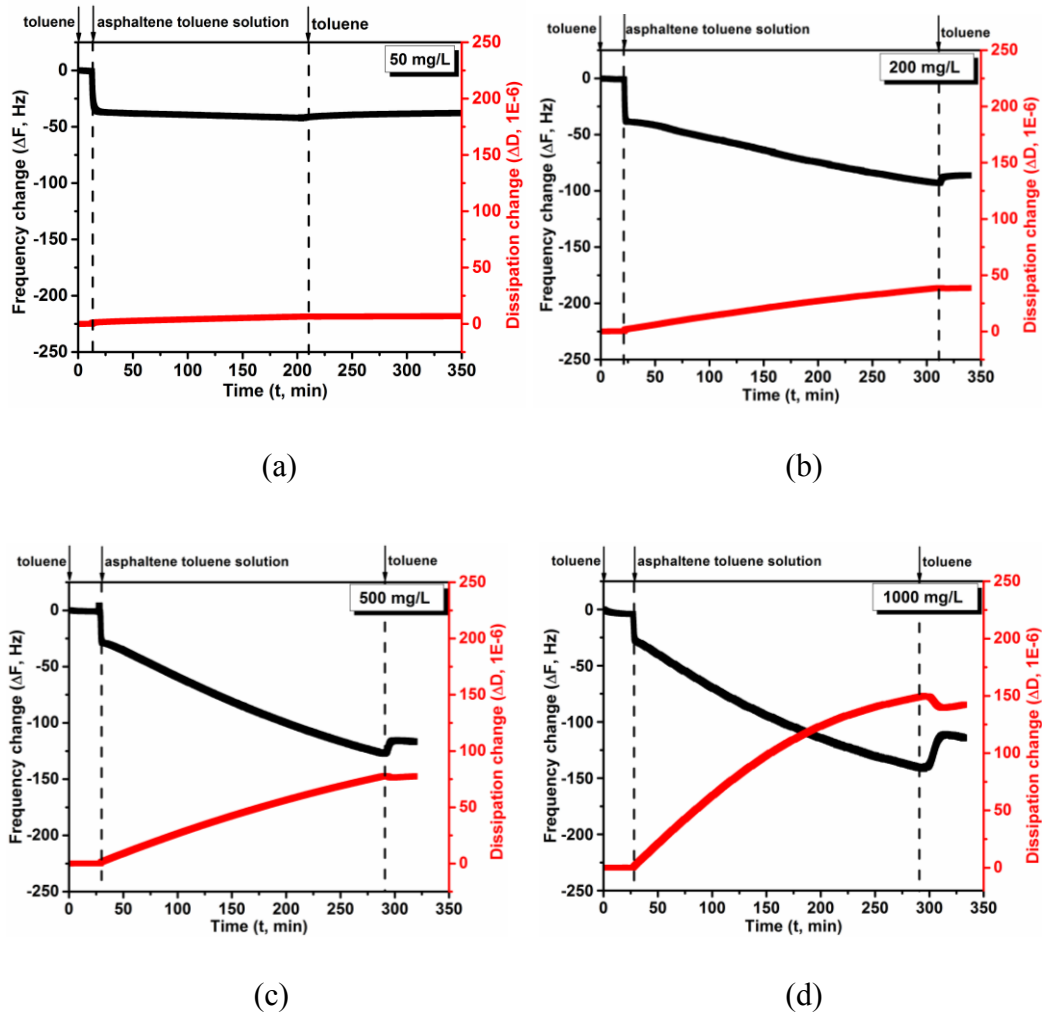
Figure 4.2 Change in frequency Δf and dissipation ΔD associated with the adsorption of asphaltenes A on silica sensor surface in toluene solvent under asphaltene concentrations of (a) 50 mg/L, (b) 200 mg/L, (c) 500 mg/L and (d) 1000 mg/L.

Adsorption of asphaltenes B on silica sensor surface

The asphaltenes B showed very different adsorption behaviour on silica surface in toluene as shown in Figure 4.3. In 50 mg/L asphaltenes in toluene solution, the frequency dropped to about -40 Hz and reached the equilibrium state

shortly after injection as shown in Figure 4.3a. In 200, 500 and 1000 mg/L asphaltenes in toluene solution, the initial sharp changes of the frequency were almost the same and then the adsorbed asphaltenes seemed to be flushed away very slowly with time shown as the black curves of the frequency change in Figure 4.3b, c and d. The dissipation factor D was also above zero and the absolute value of $\Delta D/\Delta f$ increased very slightly (from 0.05 Hz^{-1} to 0.06 Hz^{-1}) as the concentration of asphaltene solution increased from 50 mg/L to 1000 mg/L and much smaller value of $\Delta D/\Delta f$ indicated that the adsorbed asphaltenes B on silica surface in toluene was relatively rigid compared to asphaltenes A. Similarly with asphaltenes A, desorption of asphaltenes after rinsed with toluene could be neglected under all the asphaltene concentrations tested. The mass of asphaltenes adsorbed on the silica surface was also obtained using Voigt model and plotted as a function of time shown in Figure 4.4b. The adsorbed amount of asphaltenes B increased as the asphaltene concentration increased to 500 mg/L and then had a slight decrease under 1000 mg/L. Compared to the typically adsorbed amount of asphaltenes on surfaces in toluene, the amount obtained for asphaltenes B was still slightly higher which should be due to the different calculation model used. Here, we still incorporate the effect of toluene association although the dissipation change was very small. From the AFM images of sensor surface after asphaltenes B adsorption, no obvious aggregates could be observed both under asphaltene concentrations of 50 mg/L and 1000 mg/L as shown in Figure 4.5c and d. The almost same topographic images could also reflect the similarly adsorbed amount obtained for asphaltenes B under different concentrations. The uniform layer of asphaltenes B adsorbed on silica surfaces under

both low and high asphaltene concentrations indicating the asphaltenes adsorbed on the silica surface might be in the form of asphaltene molecules or asphaltene nano-aggregates.
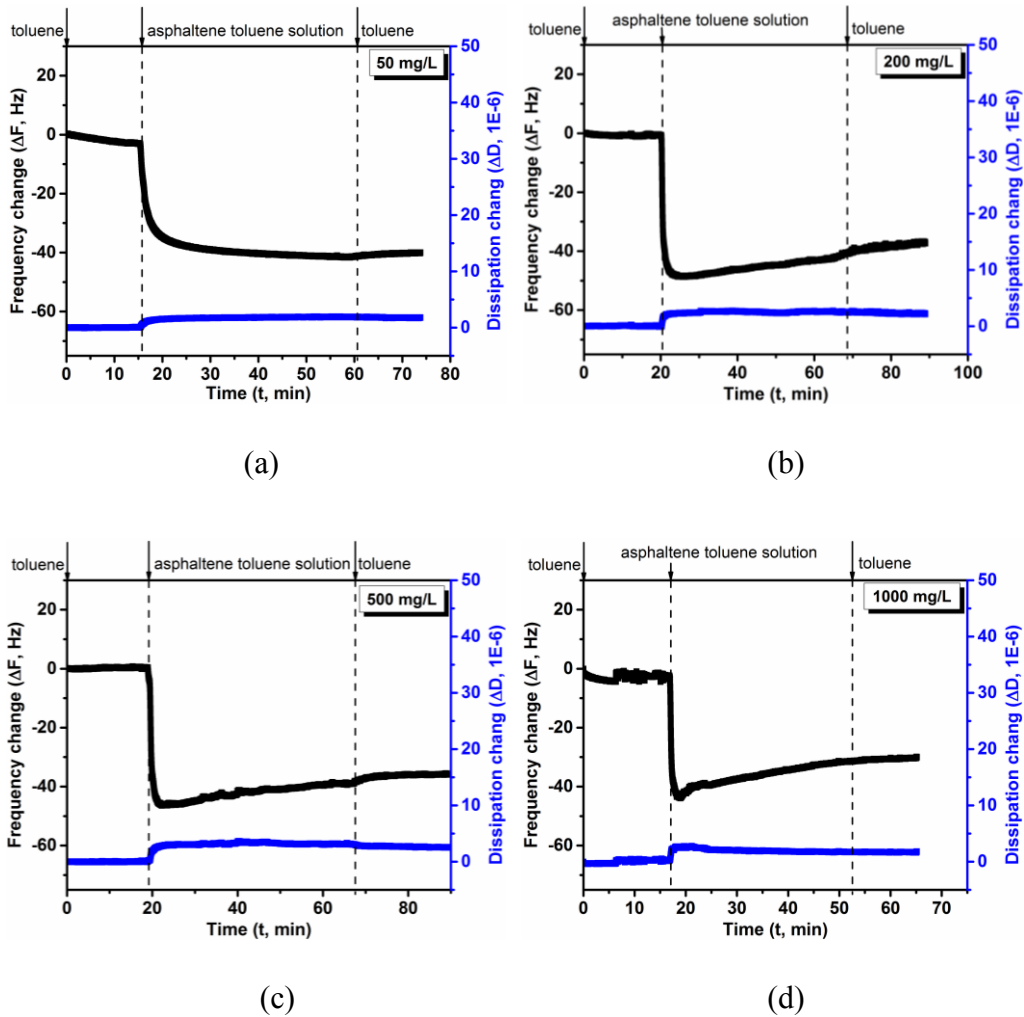
Figure 4.3 Change in frequency Δf and dissipation ΔD associated with the adsorption of asphaltenes B on silica sensor surface in toluene solvent under asphaltene concentrations of (a) 50 mg/L, (b) 200 mg/L, (c) 500 mg/L and (d) 1000 mg/L.
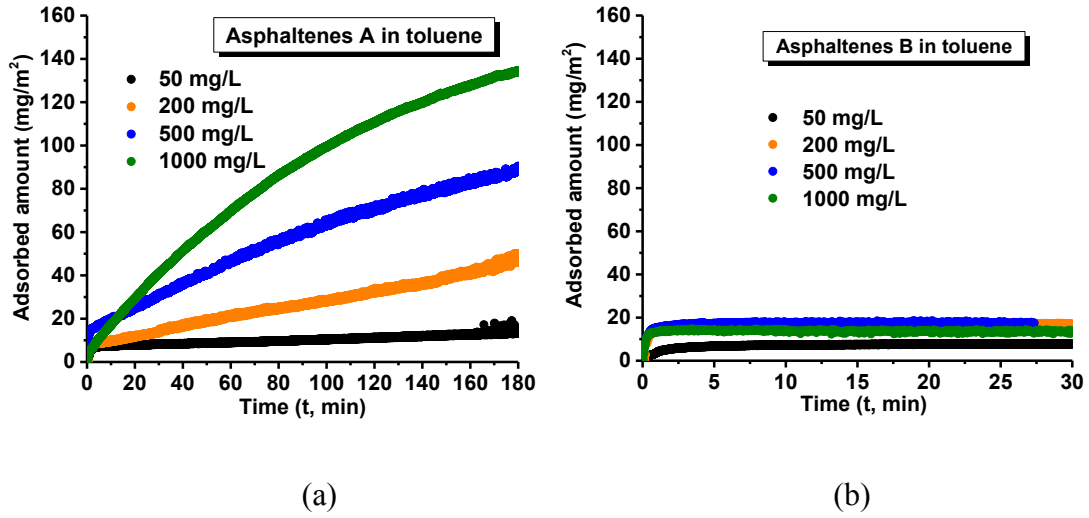
Figure 4.4 The mass of (a) asphaltenes A and (b) asphaltenes B adsorbed on the silica sensors as a function of time in toluene obtained using Voigt viscoelastic model.

(a)

(b)

(c)

(d)
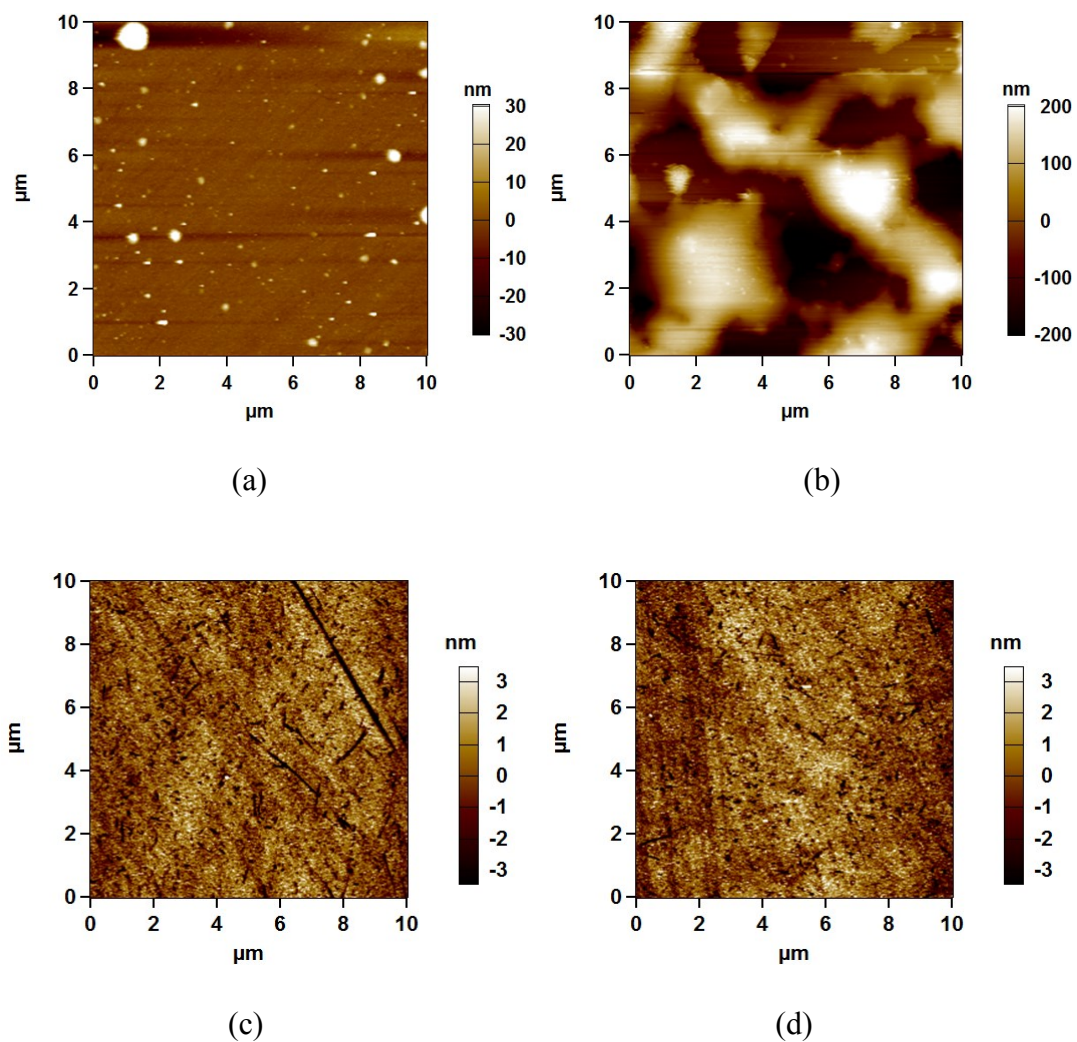
Figure 4.5 Morphology of the silica sensor surfaces after asphaltenes A adsorption in toluene under concentration of (a) 50 mg/L and (b) 1000 mg/L and after asphaltenes B adsorption in toluene under concentration of (c) 50 mg/L and (d) 1000 mg/L.

4.3.3 Adsorption of asphaltenes in toluene on mica surfaces using SFA

Based on the QCM-D results, completely different adsorption behaviour was observed for asphaltenes A and asphaltenes B in toluene. To better understand the

adsorption mechanisms of asphaltenes in toluene, SFA was applied to further investigate the adsorption and interactions of asphaltenes A and asphaltenes B in toluene. Measuring the surface forces between two mica surfaces in asphaltene solutions not only allows us to know the adsorption kinetics of asphaltenes on mica but also the interactions of adsorbed asphaltene layers.[43] The experimental configuration of the SFA measurement in this study is shown in Figure 4.6a. The 500 mg/L asphaltenes-in-toluene solution was injected between the mica surfaces and the interactions were measured as a function of time.

Asphaltenes A   Figure 4.6b shows the measured interaction force-distance profiles between two mica surfaces in 500 mg/L asphaltenes A in toluene solution. Approach and separation force curves are separately presented with adsorption time. The adsorption thickness of the asphaltenes on one mica surface was determined as the half of the hard wall distance between two mica surfaces. As shown in the approach curves, repulsion at ~20 nm was measured during approach at 25 min and the confined layer thickness was compressed to about 11 nm as the normal force increased which corresponded to the asphaltene thickness of ~5.5 nm (solvent excluded) on each mica surface and which also indicated the adsorbed asphaltene layer was soft. The thickness of the adsorbed asphaltenes on mica surface almost did not change as the adsorption time increased up to about 4 hours. During separation, adhesion was detected and hardly changed as the adsorption time increased. The adhesion measured might be attributed to the bridging interaction between adsorbed asphaltene layers because of the interpenetration of asphaltene chains/aggregates at the interface when the two surfaces were brought into contact.[43] In addition, the

92

adhesion measured here might also result from the attraction between asphaltenes A which drove asphaltenes A forming aggregates and keeping building up as seen from the QCM-D results.

The quick build-up of the asphaltenes A on mica surface manifests that the asphaltenes A had a strong affinity to the mica surface in toluene. Therefore, during the first stage in the QCM-D test, there was a sharp response to the frequency change which corresponded to the strong interactions between asphaltenes A and silica surface. Moreover, both QCM-D and SFA results showed that soft asphaltene layers formed on the surfaces. However, inconsistencies were also found between the adsorption behaviours of asphaltenes A obtained by the QCM-D and SFA. In toluene, the adsorption thickness of asphaltenes on mica surface was much smaller than that adsorbed on the silica sensor surface. Assuming the density of asphaltenes A is 1200 kg/m^3, the adsorbed thickness of the asphaltenes was ~70 nm on silica surface under 500 mg/L whereas the thickness of asphaltenes on mica surface was only ~10 nm even the solvent effect was considered (half of the distance where repulsion started). Moreover, the adsorbed asphaltene thickness hardly changed with time as shown in the forces curves, which was also different with the unsteady state observed in the QCM-D tests.
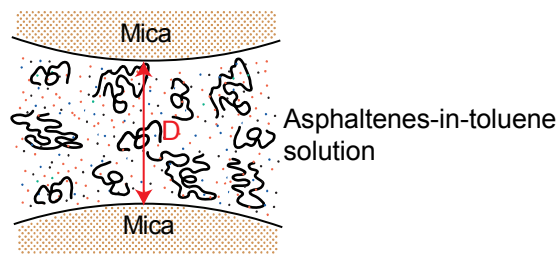
(a)
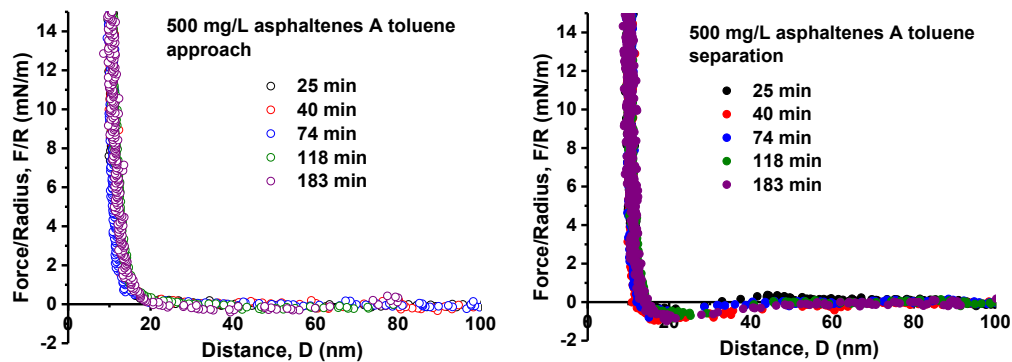
(b)
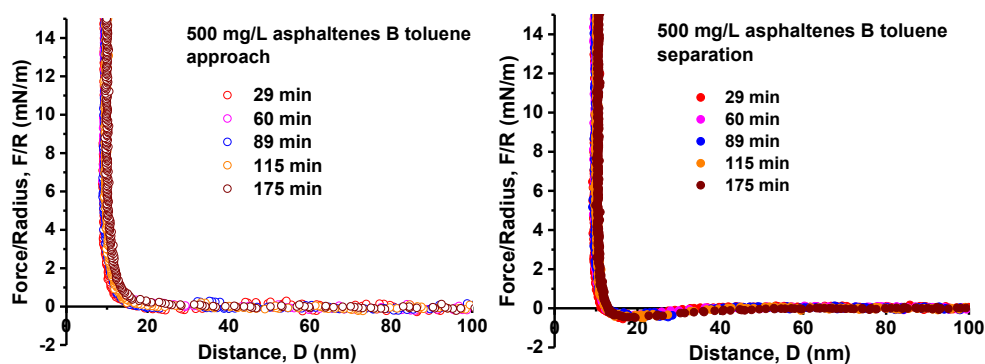
(c)

Figure 4.6 (a) The illustration of the experimental configuration of the SFA measurement in this study. (b-c) The approach and separation force-distance profiles between two mica surfaces in (b) asphaltenes A-in-toluene solution and in (c) asphaltenes B-in-toluene solution with asphaltene concentration of 500 mg/L.

Asphaltenes B Figure 4.6c shows the interactions between mica surfaces in asphaltenes B toluene solution with asphaltene concentration of 500 mg/L. The force curves obtained was very similar with asphaltenes A. The build-up of the asphaltenes B also reached the equilibrium very fast and the adsorbed thickness of the

94

asphaltenes was ~5 nm on each mica surface and hardly changed after about 4 hours. During separation, small adhesion was always measured with time which should also be due to the bridging interaction between adsorbed asphaltene layers in toluene upon contact. The asphaltene adsorbed thickness on silica sensor surface was calculated to be ~14 nm under 500 mg/L (assume the density of asphaltenes B is also 1200 kg/m^3) based on the QCM-D test result (Figure 4.4b). The repulsive range was ~20 nm before compression corresponding to the thickness of ~10 nm of asphaltenes adsorbed associated with toluene which was slightly smaller than the thickness measured in the QCM-D test.

4.3.4 Adsorption mechanism for asphaltenes in toluene

Asphaltenes A and asphaltenes B showed substantially different adsorption behaviours in toluene as seen from the QCM-D results. From the morphology of the silica sensor surfaces after asphaltenes adsorption in toluene, the differences can be also clearly seen aforementioned. By comparing the adsorption kinetics and adsorption thickness obtained from QCM-D and SFA measurement, only slight differences were found for asphaltenes B adsorption in toluene. However, the thickness determined in the QCM-D test was much larger than the thickness measured in the SFA measurement for asphaltenes A. The difference of these two techniques is that QCM-D adsorption test was conducted under flow condition, while SFA adsorption measurement was more like under static condition. Therefore, in order to further elucidate the effect of flow and static conditions on the adsorption process of asphaltenes in toluene, a QCM-D adsorption test under static condition was conducted for both asphaltenes A and asphaltenes B under 500 mg/L in toluene

solvent, which was as follows: after the background solvent baseline was established, asphaltenes-in-toluene solution was pumped into the flow module until the module was fully filled with asphaltene solution, and then the pump was stopped.

Figure 4.7 shows that the frequency change reached equilibrium shortly after the solution was pumped in for both asphaltenes A and asphaltenes B. Asphaltenes B showed similar frequency change (Figure 4.7b) compared to that under flow condition (Figure 4.3c) and the calculated thickness of asphaltenes B on silica surface was ~8 nm using Voigt model. However, the frequency change for asphaltenes A (Figure 4.7a) was much smaller compared to that under flow conditions (Figure 4.2c) and the thickness of asphaltenes A on silica surface was calculated to be ~10 nm which agreed well with the thickness obtained from the SFA measurement. The significant difference of asphaltenes A adsorption under flow and static conditions suggested that the continuous pumping in of the fresh asphaltenes A solution might assist the asphaltenes A to keep adsorbing on the surface. Therefore it is proposed that a fraction in asphaltenes A might have a strong affinity to each other which resulted in the aggregation of asphaltenes A even at 50 mg/L in toluene as evident from the AFM image shown in Figure 4.5a. Under the static condition, the limited amount of this fraction in the asphaltene solution would limit the continuous adsorption and hence the adsorption equilibrium could be reached. If the adsorbed asphaltenes A on silica surfaces were mainly from this fraction, the fraction could be more concentrated on the silica surface than that in the bulk asphaltenes A. Therefore, XPS was further conducted on asphaltenes A adsorbed on the silica surface to analyse the elements on the surface. The atomic ratio of Ca/C, O/C, S/C and N/C

were compared for bulk asphaltenes A and asphaltenes A adsorbed on the surface. Table 4.3 shows the atomic ratio of Ca/C and O/C increased substantially after the asphaltenes adsorbed onto the silica surface suggesting that the fractions containing Ca and O preferred adsorbing onto the surface. However, the ratio of S/C decreased and the ratio of N/C was not even detected after the asphaltenes adsorbed onto the silica surface indicating the heteroatoms S and N hardly influenced the asphaltenes A adsorption. The XPS results revealed that the element Ca and O might have significant contributions to the interactions between asphaltenes A leading to the aggregation of asphaltenes in toluene.

(a)   (b)
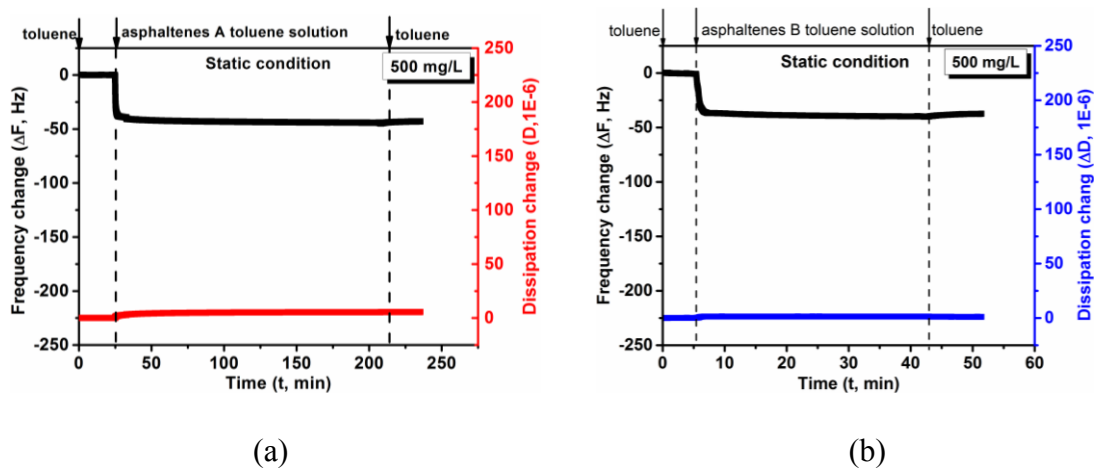
Figure 4.7 The static QCM-D test: change of frequency $\varDelta f$ and dissipation $\varDelta D$ associated with the adsorption of (a) asphaltenes A and (b) asphaltenes B on QCM-D silica sensors in toluene under asphaltenes concentration of 500 mg/L. The adsorbed thickness of asphaltenes A was ~10 nm and that of asphaltenes B was ~8 nm calculated based on the Voigt viscoelastic model.

Table 4.3 The atomic concentration comparison for bulk asphaltenes A and that adsorbed on the silica surface obtained by XPS.

Element (atomic ratio)	Ca/C	O/C	S/C	N/C
Asphaltenes A	0.0088	0.0375	0.0299	0.0116
Asphaltenes A adsorbed on silica surface	0.0456	0.0979	0.0194	N/A

4.4 Conclusions

In this study, the adsorption mechanisms of two types of asphaltenes were investigated using QCM-D and SFA. The QCM-D results showed that asphaltenes A could continuously adsorb on silica surface in toluene whereas asphaltenes B saturated the silica surfaces shortly in toluene. The AFM imaging of the adsorbed asphaltenes showed that asphaltenes A even formed large aggregates at the concentration of 50 mg/L in toluene while no obvious aggregates were found for asphaltenes B. The adsorption measurement using SFA showed that the adsorption behaviour of asphaltenes B in toluene agreed well with the results obtained from the QCM-D tests. However, a significant difference was observed for asphaltenes A adsorbed on the surface in toluene. More asphaltenes A could absorb on the surface under flow conditions (QCM-D) than that under static condition (SFA) which might be due to the specific interactions between some fractions in asphaltenes A. The XPS results also showed that the existence of Ca and O might contribute to the

interactions between the fractions in asphaltenes A leading to the continuous

adsorption under flow condition in toluene.

References

(1) Andreatta, G.; Bostrom, N.; Mullins, O. C. *Langmuir* **2005**, *21*, 2728-2736.

(2) Mullins, O. C. *Annu Rev Anal Chem* **2011**, *4*, 393-418.

(3) Sheremata, J. M.; Gray, M. R.; Dettman, H. D.; McCaffrey, W. C. *Energ Fuel* **2004**, *18*, 1377-1384.

(4) Wang, S. Q.; Liu, J. J.; Zhang, L. Y.; Masliyah, J.; Xu, Z. H. *Langmuir* **2010**, *26*, 183-190.

(5) Dechaine, G. P.; Gray, M. R. *Energ Fuel* **2010**, *24*, 2795-2808.

(6) Liu, J. J.; Xu, Z. H.; Masliyah, J. *Can J Chem Eng* **2004**, *82*, 655-666.

(7) Angle, C. W.; Dabros, T.; Hamza, H. A. *Energ Fuel* **2007**, *21*, 912-919.

(8) Saukowski, D. M.; Yarranton, H. W. *J Colloid Interf Sci* **2005**, *285*, 821-833.

(9) Jiang, T.; Hirasaki, G. J.; Miller, C. A.; Moran, K. *Energ Fuel* **2008**, *22*, 4158-4164.

(10) Alvarez, G.; Jestin, J.; Argillier, J. F.; Langevin, D. *Langmuir* **2009**, *25*, 3985-3990.

(11) Marchal, C.; Abdessalem, E.; Tayakout-Fayolle, M.; Uzio, D. *Energ Fuel* **2010**, *24*, 4290-4300.

(12) Nassar, N. N. *Energ Fuel* **2010**, *24*, 4116-4122.

(13) de la Cruz, J. L. M.; Castellanos-Ramirez, I. V.; Ortiz-Tapia, A.; Buenrostro-Gonzalez, E.; Duran-Valencia, C. D.; Lopez-Ramirez, S. *Colloid Surface A* **2009**, *340*, 149-154.

(14) Alboudwarej, H.; Pole, D.; Svrcek, W. Y.; Yarranton, H. W. *Ind Eng Chem Res* **2005**, *44*, 5585-5592.

(15) Rudrake, A.; Karan, K.; Horton, J. H. *J Colloid Interf Sci* **2009**, *332*, 22-31.

(16) Goual, L.; Horvath-Szabo, G.; Masliyah, J. H.; Xu, Z. H. *Langmuir* **2005**, *21*, 8278-8289.

(17) Ekholm, P.; Blomberg, E.; Claesson, P.; Auflem, I. H.; Sjoblom, J.; Kornfeldt, A. *J Colloid Interf Sci* **2002**, *247*, 342-350.

(18) Dudasova, D.; Silset, A.; Sjoblom, J. *J Disper Sci Technol* **2008**, *29*, 139-146.

(19) Abudu, A.; Goual, L. *Energ Fuel* **2009**, *23*, 1237-1248.

(20) Zahabi, A.; Gray, M. R. *Energ Fuel* **2012**, *26*, 1009-1018.

(21) Labrador, H.; Fernandez, Y.; Tovar, J.; Munoz, R.; Pereira, J. C. *Energ Fuel* **2007**, *21*, 1226-1230.

(22) Acevedo, S.; Castillo, J.; Fernandez, A.; Goncalves, S.; Ranaudo, M. A. *Energ Fuel* **1998**, *12*, 386-390.

(23) Kokal, S.; Tang, T.; Schramm, L.; Sayegh, S. *Colloid Surface A* **1995**, *94*, 253-265.

(24) Castro, M.; de la Cruz, J. L. M.; Buenrostro-Gonzalez, E.; Lopez-Ramirez, S.; Gil-Villegas, A. *Fluid Phase Equilibr* **2009**, *286*, 113-119.

(25) Xie, K.; Karan, K. *Energ Fuel* **2005**, *19*, 1252-1260.

(26) Goual, L.; Abudu, A. *Energ Fuel* **2010**, *24*, 469-474.

(27) Simon, S.; Jestin, J.; Palermo, T.; Barre, L. *Energ Fuel* **2009**, *23*, 306-313.

(28) Syunyaev, R. Z.; Balabin, R. M.; Akhatov, I. S.; Safieva, J. O. *Energ Fuel* **2009**, *23*, 1230-1236.

(29) Acevedo, S.; Ranaudo, M. A.; Garcia, C.; Castillo, J.; Fernandez, A. *Energ Fuel* **2003**, *17*, 257-261.

(30) Balabin, R. M.; Syunyaev, R. Z.; Schmid, T.; Stadler, J.; Lomakina, E. I.; Zenobi, R. *Energ Fuel* **2011**, *25*, 189-196.

(31) Acevedo, S.; Ranaudo, M. A.; Garcia, C.; Castillo, J.; Fernandez, A.; Caetano, M.; Goncalvez, S. *Colloid Surface A* **2000**, *166*, 145-152.

(32) Acevedo, S.; Ranaudo, M. A.; Escobar, G.; Gutierrez, L.; Ortega, P. *Fuel* **1995**, *74*, 595-598.

(33) Marczewski, A. W.; Szymula, M. *Colloid Surface A* **2002**, *208*, 259-266.

(34) Adams, J. J. *Energ Fuel* **2014**, *28*, 2831-2856.

(35) Piro, G.; Canonico, L. B.; Galbariggi, G.; Bertero, L.; Carniani, C. *Spe Prod Facil* **1996**, *11*, 156-160.

(36) Hannisdal, A.; Ese, M. H.; Hemmingsen, P. V.; Sjoblom, J. *Colloid Surface A* **2006**, *276*, 45-58.

(37) Voinova, M. V.; Rodahl, M.; Jonson, M.; Kasemo, B. *Phys Scripta* **1999**, *59*, 391-396.

(38) Binazadeh, M.; Zeng, H.; Unsworth, L. D. *Acta Biomater* **2014**, *10*, 56-66.

(39) Wang, S. S.; Zhang, L.; Yan, B.; Xu, H. L.; Liu, Q. X.; Zeng, H. B. *J Phys Chem C* **2015**, *119*, 7327-7339.

(40) Israelac.Jn *J Colloid Interf Sci* **1973**, *44*, 259-272.

(41) Israelachvili, J.; Min, Y.; Akbulut, M.; Alig, A.; Carver, G.; Greene, W.; Kristiansen, K.; Meyer, E.; Pesika, N.; Rosenberg, K.; Zeng, H. *Rep Prog Phys* **2010**, *73*.

(42) Zeng, H.; Tian, Y.; Anderson, T. H.; Tirrell, M.; Israelachvili, J. N. *Langmuir* **2008**, *24*, 1173-1182.

(43) Natarajan, A.; Kuznicki, N.; Harbottle, D.; Masliyah, J.; Zeng, H. B.; Xu, Z. H. *Langmuir* **2014**, *30*, 9370-9377.

(44) Wang, J.; Lu, Q. Y.; Harbottle, D.; Sjoblom, J.; Xu, Z. H.; Zeng, H. B. *J Phys Chem B* **2012**, *116*, 11187-11196.

(45) Faghihnejad, A.; Zeng, H. B. *Soft Matter* **2012**, *8*, 2746-2759.

(46) Dutta, A. K.; Belfort, G. *Langmuir* **2007**, *23*, 3088-3094.

CHAPTER 5   INTERACTION MECHANISMS BETWEEN

ASPHALTENE SURFACES IN AQUEOUS SOLUTIONS

STUDIED BY SURFACE FORCES APPARATUS AND

ATOMIC FORCE MICROSCOPE

5.1 Introduction

Water plays an important role in heavy oil and oil sands production processes such as bitumen extraction process of oil sands. The so-called Clark hot water extraction process and Steam-Assisted Gravity Drainage (SAGD) process are both complicated by the challenging issues of stable water-in-oil (W/O) and oil-in-water (O/W) emulsions which can be detrimental to the bitumen production from the reservoir to the downstream operations.[1-4] For instance, the adsorption of W/O emulsions can cause fouling and corrosion issues from wellbores to the surface facilities due to the interfacial materials adsorbed at W/O interfaces as well as high concentrations of salt contained in the water phase.[5-9] The formation of stable O/W emulsions (i.e. bitumen drops) during the bitumen extraction and flotation process generally leads to lower bitumen recovery.[6,10-14] In addition, stable oil droplets suspended in process water and waste water can also result in operational problems in water treatment.[15,16]

Asphaltenes, the heaviest component in crude oil and bitumen products, have been reported to be the vital factor in stabilizing W/O and O/W emulsions.[7,17-24] Asphaltenes are operationally defined as a solubility class which are soluble in

aromatic solvents, such as toluene, but insoluble in paraffinic solvents, such as n-pentane and n-heptane.[11,25,26] The hydrophobic hydrocarbon skeleton with hydrophilic polar groups (e.g. carboxyl groups and amino groups) renders asphaltenes interfacially active; hence asphaltenes are able to adsorb onto water/oil interfaces, forming an interfacial layer and in turn changing the interfacial properties of the emulsion drops.[11,21,27-31] The asphaltenes can also readily adsorb onto solid particles and render them partially oil-wet, which can in turn adsorb onto the water/oil interfaces and contribute to emulsion stabilization.[32,33] In previous studies, the interactions of asphaltenes, bitumen or asphaltenes model compounds were measured using nanomechanical techniques including atomic force microscope (AFM) and surface forces apparatus (SFA) to understand the stabilization mechanism of different emulsions. The interaction forces between asphaltene films in toluene and heptol solvents has been measured using SFA and AFM, and steric repulsion between asphaltenes in relatively good solvent was measured, resulting in the stabilization of the W/O emulsions in the presence of asphaltenes.[6,34-36] Recently, an AFM droplet probe technique was developed to measure the forces between two oil droplets in aqueous solutions with asphaltenes adsorbed at oil-water interfaces. Steric and electrical double layer repulsion that prevents O/W emulsions drops from coalescing were reported.[17] To date, most of previous studies on force measurements of asphaltenes and bitumen focused on oil media, and the understanding of interaction mechanisms of asphaltenes in aqueous solution of varying water chemistry still remain limited.

In this study, nanomechanical tools, i.e. SFA and AFM, have been employed to measure the interactions between asphaltene films in aqueous solutions, and the effects of solution pH, salinity and Ca^{2+} addition were investigated. SFA was applied to directly measure the surface forces between two asphaltene films. AFM imaging was applied to monitor the morphology of asphaltene films under various aqueous solution conditions which were further correlated to the SFA force measurements. The interactions between AFM tip and asphaltene film were also measured to provide more information on the interaction behaviours of asphaltenes at nanoscale. The results obtained by combining SFA and AFM show useful information regarding the interactions of asphaltenes in aqueous solutions from nanoscale to surface level, and also provide insights into the stabilization mechanisms of O/W emulsions and colloidal particles in the presence of asphaltenes.

5.2 Materials and Experimental Methods

5.2.1 Materials and sample preparation

The detailed procedure of extracting asphaltenes from vacuum distillation feed Athabasca bitumen has been reported elsewhere.[37] Briefly, the bitumen was firstly dissolved in toluene with toluene/bitumen ratio of 5/1 and the bitumen toluene solution was centrifuged to remove the undissolved solids. Toluene was allowed to evaporate to obtain the solvent-free bitumen. Then the asphaltenes were precipitated by adding n-heptane into the toluene-free bitumen at n-heptane/bitumen ratio at 40/1, and the precipitated asphaltenes were washed using n-heptane until the supernatant of the solution was clear and colourless. The obtained asphaltenes were dried under

nitrogen flow after the supernatant was carefully decanted. Toluene and n-heptane were purchased from Fisher Scientific Canada and used as received.

Mica was purchased from S & J Trading Inc. (Glen Oaks, NY). NaCl, $CaCl_2 \cdot H_2O$, HCl and NaOH were all purchased from Fisher Scientific Canada and used as received. For the preparation of asphaltene films, mica surfaces were first pre-treated under octadecyltrichlorosilane (OTS) vapour in an evaporation chamber for one hour following a procedure reported previously[38,39] in order to improve the stability of spin-coated asphaltene film in water. Briefly, a few drops of OTS were put in a small vial which was placed besides the mica surfaces in the evaporation chamber. After the OTS treatment, asphaltene surface was prepared by spin-coating 2-3 drops of 0.5 wt% of asphaltenes toluene solution on the OTS-treated mica surface. The spin-coated asphaltene surfaces were vacuum dried overnight to remove the residual solvent. The thickness of the asphaltene film was measured to be ~20 nm using SFA which was further confirmed using ellipsometry (on asphaltene films spin-coated under the same condition on silicon wafer). NaCl solutions with different concentrations were prepared by dissolving desired amount of NaCl in Milli-Q water. $CaCl_2 \cdot H_2O$ was used as the Ca^{2+} ions source by adding $CaCl_2 \cdot H_2O$ in the 1 mM NaCl solutions to the desired Ca^{2+} ion concentration. The solution pH was adjusted by addition of HCl or NaOH.

5.2.2 Surface forces measurement using SFA

The interaction forces between two asphaltene surfaces in aqueous solutions were directly measured using SFA. The detailed working principle and setup of the

SFA experiments have been reported elsewhere.[6,27,40-45] Briefly, a pair of silica discs glued with thin mica sheets (1-5 μm) that were coated with asphaltenes were mounted in the SFA chamber in a crossed-cylinder configuration. The interaction force was measured as a function of absolute separation distance. The absolute separation distance could be monitored in situ and in real time using multiple beam interferometry by employing fringes of equal chromatic order (FECO).[46] In the force measurements, the measured adhesion force F_{ad} could be related to the adhesion energy per unit area W_{ad} using $F_{ad}=1.5\pi R W_{ad}$.[47] The experimental configuration for the surface force measurement in this study is shown in Figure 5.1. The reference distance $D=0$ was determined at the adhesive contact between two asphaltene films in air.
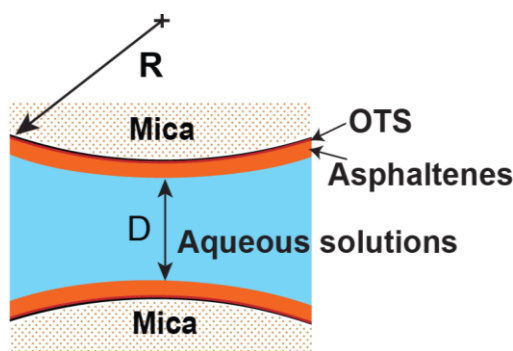
Figure 5.1 Experimental configuration for forces measurement between two asphaltene surfaces in aqueous solution using an SFA.

5.2.3 AFM imaging and force measurement

An AFM (MFP-3D, Asylum, Santa Barbara, CA, USA) was applied to characterize the morphology of the OTS-treated mica surface and asphaltene surfaces spin-coated on OTS-treated mica in air as well as the morphology of the

asphaltene surfaces in aqueous solutions. All the samples were imaged using tapping mode to avoid possible surface damage. The AFM was also applied to measure the interaction force between silicon nitride AFM tip and asphaltene surfaces in aqueous solutions. The samples for AFM imaging and force measurement were prepared on flat OTS-mica substrate following exactly the same procedure as that for SFA measurements. The asphaltene-coated surfaces were placed in a fluid cell filled with desired aqueous solutions for *in situ* imaging and force measurement.

5.2.4 Theoretical analysis of AFM force curves

To better understand the measured approach force-distance profiles between an AFM tip and asphaltene surface, theoretical analysis was conducted based on the classical Derjaguin–Landau–Verwey–Overbeek (DLVO) theory by reasonably assuming the pyramidal geometry of AFM tip to be conical with a spherical cap at the apex shown in Figure 5.2.[48] The total DLVO forces include van der Waals force and electrical double layer force as shown by equation (5.1).

$$F_{DLVO} = F_{vdW} + F_{EDL} \tag{5.1}$$

The van der Waals (VDW) force between an AFM tip and a flat substrate, F_{vdW} is given by equation (5.2).[49]

$$F_{vdW} = \frac{A_H}{6} \left[\frac{R+D-2L}{L^2} - \frac{R-D}{D^2} \right] - \frac{A_H}{3\tan^2\alpha} \left(\frac{1}{L} + \frac{R\sin\alpha\tan\alpha - D - R(1-\cos\alpha)}{2L^2} \right)$$

$$\tag{5.2}$$

where A_H is the non-retarded Hamaker constant, D is the distance between the end of the tip and the surface, $L = D + R(1-\cos\alpha)$ and R is the radius of the spherical cap at the end of the tip as shown in Figure 5.2. α and β are the geometrical angles for the

spherical cap at the tip apex and the conical tip, with $\alpha + \beta = 90°$. The electrical double layer (EDL) force between an AFM tip and a flat substrate, F_{EDL}, is given by equation (5.3) under the boundary condition of constant charge.[49]

$$
\begin{aligned}
F_{EDL} &= \frac{4\pi}{\varepsilon_0 \varepsilon \kappa^2} \sigma_T \sigma_S (a_0 e^{-\kappa D} - a_1 e^{-\kappa L_1}) \\
&+ \frac{2\pi}{\varepsilon_0 \varepsilon \kappa^2} (\sigma_T^2 + \sigma_S^2)(a_2 e^{-2\kappa D} - a_3 e^{-2\kappa L_2}) \\
&+ \frac{4\pi}{\varepsilon_0 \varepsilon \kappa^2 \tan\alpha} \left[b_1 \sigma_T \sigma_S e^{-\kappa L_1} + b_2 \frac{(\sigma_T^2 + \sigma_S^2)}{2} e^{-2\kappa L_1} \right]
\end{aligned}
\tag{5.3}
$$

where subscripts T and S represents the AFM tip and the surface, respectively and $a_0 = \kappa R - 1$, $a_1 = \kappa R \cos(\alpha - 1)$, $a_2 = a_0 + 0.5$ and $a_3 = a_1 + 0.5$. b_1 and b_2 are expressed as follows:

$$
b_1 = R\sin\alpha - \frac{D + R(1 - \cos\alpha)}{\tan\alpha} + \frac{1}{\tan\alpha}\left[L + \frac{1}{\kappa}\right]
$$

$$
b_2 = R\sin\alpha - \frac{D + R(1 - \cos\alpha)}{\tan\alpha} + \frac{1}{\tan\alpha}\left[L + \frac{1}{2\kappa}\right]
$$

The surface potential (ψ) and the surface charge density (σ) are correlated by the Grahame equation shown in equation (5.4).

$$
\sigma = \sqrt{8c_0 \varepsilon \varepsilon_0 k_B T} \sinh(\frac{e\psi}{2k_B T})
\tag{5.4}
$$

where e is the elementary charge, κ^{-1} is the Debye length, c_0 is the bulk ion-number concentration, k_B is the Boltzmann constant, and T is temperature. ε and ε_0 are the permittivity of solution and vacuum, respectively.
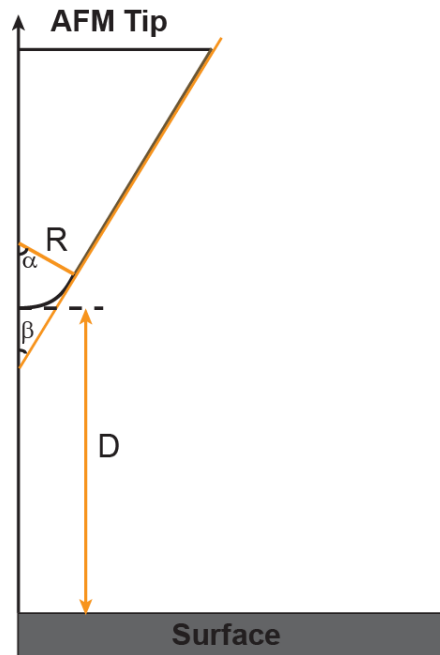
Figure 5.2 The schematic of the pyramidal geometry of an AFM tip which is conical with a spherical cap at the apex used for DLVO force calculations.

5.2.5 Contact angle measurement

Contact angles of water on OTS-treated mica surfaces and spin-coated asphaltene surface were characterized by the sessile drop method using a goniometer (Ramé-hart, USA). A water drop of ~3 µL was placed on the substrate surface, and the shape of the drop was fitted by image processing software to determine the contact angle.

5.2.6 Zeta potential measurement

Zeta potentials of asphaltenes coated on silica particles were measured using Zetasizer Nano (Malvern Instruments Ltd., UK). Silica particles (D_{80}~5 µm: 80 wt% of the particles with size below 5 µm) were first mixed with 2000 mg/L asphaltene-in-toluene solution at a weight ratio of 1/10 and the mixture was placed on a shaker

to allow asphaltene adsorption for 24 h. Concentrate of silica particles with adsorbed asphaltenes was obtained by centrifugation, and then the concentrate was completely dried in vacuum before dispersed into aqueous solutions with a concentration of 0.2 mg/ml. Ultrasonic treatment was applied to assist the dispersion of the silica particles with asphaltene coatings in aqueous solutions right before zeta potential measurements. The zeta potential was measured under the same solution conditions as used in the force measurement.

(a)   (b)
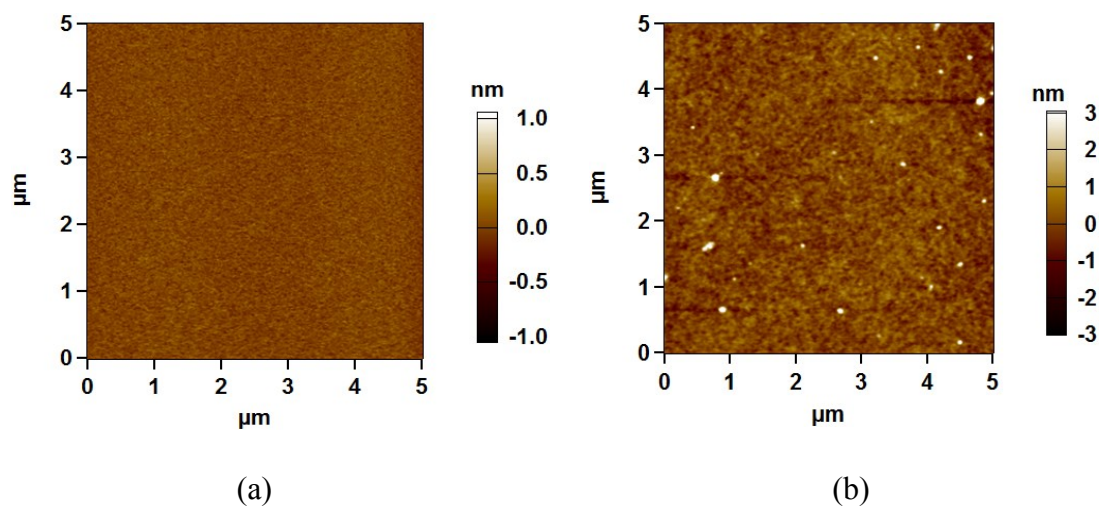
Figure 5.3 AFM topographic images of (a) OTS-treated mica surface and (b) spin-coated asphaltenes on OTS-treated mica in air.

5.3 Results and Discussion

5.3.1 Characterization of the OTS-treated mica and spin-coated asphaltene surface

It was found that asphaltene films spin-coated on freshly cleaved mica surface were easy to rupture upon contact with a water drop or immersion in aqueous solution. To improve the stability of the asphaltene film on mica surface, freshly cleaved mica surface was gently treated under OTS vapour for 1 hour leading to a water contact angle of about 40-50°. Figure 5.3 shows the AFM images of OTS-treated mica and asphaltene-coated surface (coated on OTS-treated mica) in air. The OTS-treated mica surface shows a smooth and featureless morphology (Figure 5.3a) with root-mean-square (RMS) roughness of less than 0.5 nm. Figure 5.3b shows that asphaltenes were uniformly coated on the OTS-treated mica with RMS roughness of ~1 nm. The contact angle measurement showed that water drop was very stable on the asphaltene surface with a contact angle of ~90°.

5.3.2 Surface interactions between asphaltene surfaces in aqueous solutions measured by SFA

Effect of solution pH

SFA was applied to measure the interaction forces between asphaltene surfaces during approach and separation in aqueous solutions. The "hard wall" distance here refers to the confined gap distance that hardly changed with increasing normal force or pressure. Figure 5.4 shows the measured interaction force-distance curves between asphaltene surfaces in 1 mM NaCl solutions with different pH. As shown in

Figure 5.4, repulsive forces were measured during approach and adhesion was observed when the two asphaltene surfaces were separated for all the pH conditions investigated. At pH 8.5 as shown in Figure 5.4a, a hard wall distance of ~19 nm was measured based on the reference distance (D=0) of asphaltenes-asphaltenes contact in air, which indicated that the thickness of each asphaltene film increased by about 9.5 nm (half of the "hard wall" thickness). Repulsion was detected starting at a distance D~80 nm, suggesting the asphaltene films were compressible under this solution condition. It has been reported that asphaltenes carry negative charges at alkaline pH, and hence the repulsive force measured during approach might originate from electrical repulsion at pH 8.5.[50,51] The approach force curve is also shown in semi-log plots in Figure S 5.1a (supporting information). If the DLVO model applies, the long range electric double layer force should show a linear relation with distance in the semi-log plots. However, such linear relation is absent in Figure S 5.1a, thus the approach force profile could not be well described by the DLVO model.

As the solution pH was decreased to 4.0, the hard wall distance did not change significantly, and repulsion was also measured during approach, whereas the starting distance of repulsion decreased to ~65 nm. As the solution pH was further decreased to 2.2, the hard wall distance decreased to ~5 nm, and the range of repulsion became even smaller as ~40 nm. It is also evident from Figure S 5.1a that the approach force profiles for both pH 4.0 and 2.2 could not be directly described by the DLVO model. The reason for the disagreement between the measured forces and the DLVO model was investigated and discussed in a later section.

113

Figure 5.4 shows that under all the three solution pH conditions, adhesion was measured during separation. At pH 8.5, an adhesion of $F_{ad}/R \sim$ -1.3 mN/m ($W_{ad} \sim$ 0.28 mJ/m^2) was measured, and the separation curve also showed a stretching behaviour before detachment, which might due to the stretching of bridged asphaltene molecules/aggregates at the contact interface in 1 mM NaCl solution. As the solution pH was decreased to 4.0 and 2.2, the measured adhesion changed to $F_{ad}/R \sim$ -4.4 mN/m ($W_{ad} \sim$ 0.93 mJ/m^2) and $F_{ad}/R \sim$ -1.1 mN/m ($W_{ad} \sim$ 0.23 mJ/m^2), respectively. Stretching behaviours were also observed at both pH 4.0 and pH 2.2 in 1 mM NaCl solutions. Figure 5.6 shows that the normalized adhesion and adhesion energy between asphaltene surfaces first increased as the solution pH decreased from pH 8.5 to pH 4.0 and then decreased as the solution pH further decreased to pH 2.2. The change of adhesion under different pH conditions might be due to several factors: surface charges, surface hydrophobicity and roughness. The water contact angle on asphaltene surface was ~90°, and attraction would be expected between the contacting hydrophobic asphaltene surfaces, as confirmed by the adhesion measured. It has been reported that the point of zero charge (PZC) of asphaltenes is around pH 3.0 to 4.0.[51] Asphaltene surface was close to the PZC and almost neutral at pH 4.0, so the electrical repulsion would be minimal among the three pH conditions and strongest attraction was measured. For comparison, asphaltene surface would carry negative charge and slightly positive charge at pH 8.5 and 2.2, respectively, which could cause electrical repulsion between asphaltene surfaces and lead to a weakened adhesion. Surface topography and roughness might also play a role, which has been investigated and will be discussed in a later section.
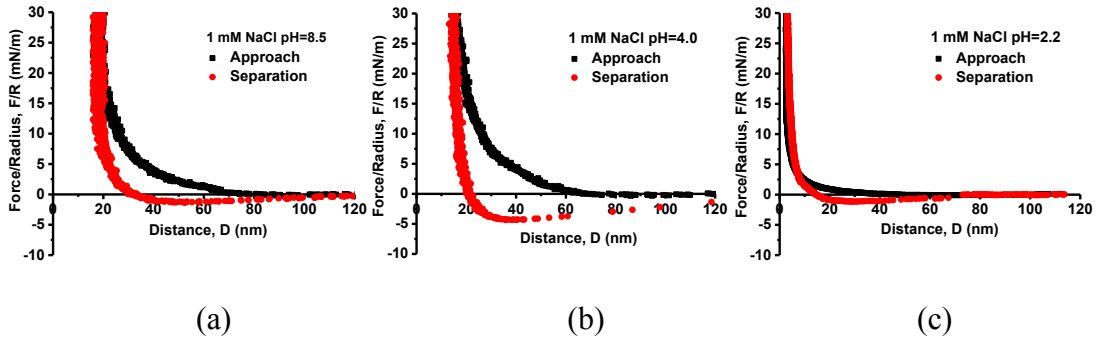
Figure 5.4 Force-distance profiles between two asphaltene surfaces interacting in 1 mM NaCl solution at (a) pH 8.5, (c) pH 4.0 and (d) pH 2.2.

Effect of solution salinity and Ca^{2+} ions

Figure 5.5 shows the interactions between asphaltene surfaces in solutions with different salt types and salt concentrations at pH 8.5 investigated using SFA. Figure 5.5a and b show the force-distance profiles in 10 mM NaCl and 100 mM NaCl solutions at pH 8.5, respectively, which have very similar feature as that measured in 1 mM NaCl shown in Figure 5.4a. Basically, repulsive forces of almost the same range were measured during approach, while adhesion was detected during separation, showing similar hard wall distance. DLVO model predicts that the electrical Debye length decreases from 9.6 nm in 1 mM NaCl to ~1 nm in 100 mM NaCl. Therefore, the interaction force profiles under different NaCl concentration could not be directly described by the DLVO model, as more visible in semi-log plots shown in Figure S 5.1b.

The adhesion F_{ad}/R measured in 1, 10 and 100 mM NaCl solutions does not show significant difference, and was measured to be F_{ad}/R ~-1.35±0.15 mN/m

(corresponding to $W_{ad} \sim 0.28$ mJ/m^2) as shown in Figure 5.6. The possible reason for this phenomenon was further discussed in a later section.

The effect of the addition of Ca^{2+} on the interactions between asphaltene surfaces were also measured by SFA. Figure 5.5c and d show the force-distance profiles between two asphaltene surfaces in 1 mM NaCl solutions at pH 8.5 with addition of 1 mM and 100 mM of CaCl$_2$, respectively. Similarly, repulsion was measured during approach while adhesion was measured during retraction. However, the repulsion measured during approach was much shorter ranged as compared to that without Ca^{2+} addition (Figure 5.4a). With addition of 1 mM Ca^{2+}, the repulsion range decreased to ~40 nm which was also not likely due to the change of electrical double layer force (with semi-log force profile shown in Figure S 5.1c). The addition of 100 mM Ca^{2+} resulted in even shorter range of force starting at ~20 nm and weaker repulsion was still measured between asphaltene surfaces. It is noted that based on the DLVO theory, for interactions of two charged surfaces in aqueous solution, the Debye length of EDL interaction in 100 mM Ca^{2+} is less than 1 nm and the EDL force would be significantly compressed.

The normalized adhesion and adhesion energy between asphaltene surfaces with the additional of Ca^{2+} are summarized in Figure 5.6c. A much higher adhesion of $F_{ad}/R \sim -13.5$ mN/m ($W_{ad} \sim 2.87$ mJ/m^2) was measured by introducing 1 mM Ca^{2+} in 1 mM NaCl solution as compared to the case with only 1 mM NaCl ($F_{ad}/R \sim -1.35\pm0.15$ mN/m). The adhesion decreased to $F_{ad}/R \sim -4.8$ mN/m ($W_{ad} \sim 1.02$ mJ/m^2) with further increasing Ca^{2+} to 100 mM. Figure 5.5c and d also show that the contacted asphaltene films were stretched before detachment. The enhanced

adhesion with the addition of 1 mM Ca^{2+} should be mainly attributed to the "bridging" effect of Ca^{2+}. Ca^{2+} has been reported to be able to interact with carboxyl groups in asphaltenes, thus bridging the opposing asphaltene surfaces.[52] In 100 mM Ca^{2+}, most of the carboxyl groups on asphaltene surfaces were occupied by the excess amount of Ca^{2+} before approach, which significantly weakened the bridging effect and reduced the adhesion. The effects of pH, salinity and Ca^{2+} ions on the adhesion between two asphaltene surfaces discussed above are summarized in Figure 5.6a, b and c, respectively.

(a)

(b)

117

(c)   (d)
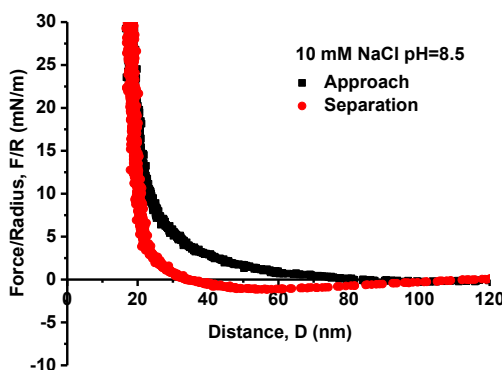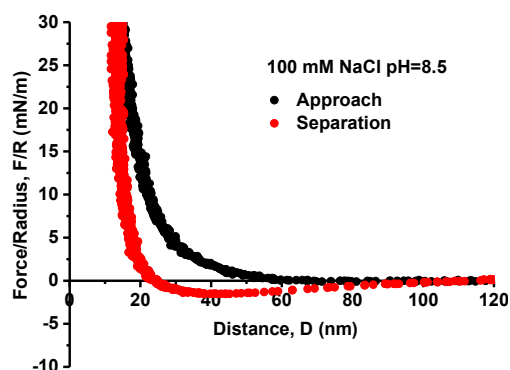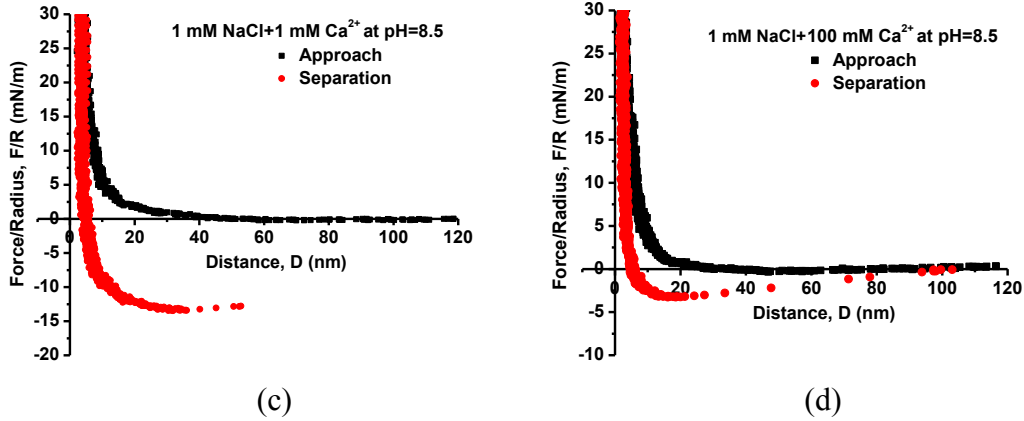
Figure 5.5 Force-distance profiles between two asphaltene surfaces interacting in NaCl solutions with concentrations of (a) 10 mM and (b) 100 mM at pH 8.5 and in 1 mM NaCl solution with addition of (c) 1mM Ca^{2+} and (d) 100 mM Ca^{2+} at pH 8.5.

(a)   (b)   (c)
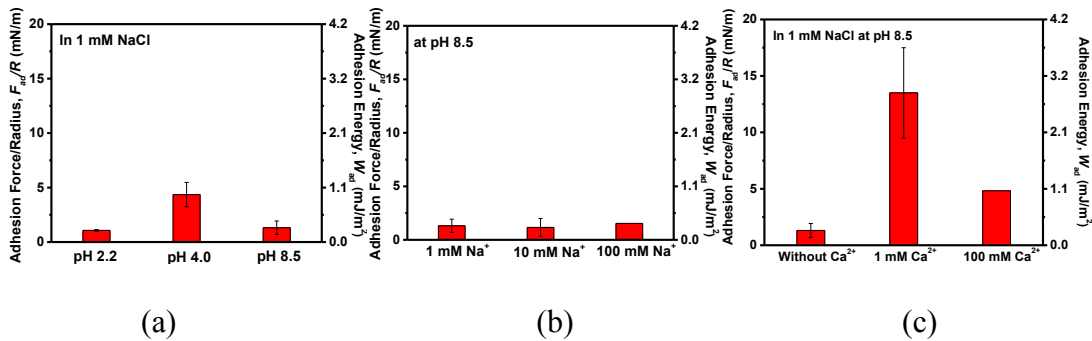
Figure 5.6 Normalized adhesion forces F_{ad}/R (left y-axis) and corresponding adhesion energy W_{ad} (D) (right y-axis) as a function of (a) pH, (b) NaCl concentrations and (c) Ca^{2+} concentrations in 1 mM NaCl solution.

The morphology of asphaltene surfaces in aqueous solutions

Figure 5.4, Figure 5.5 and Figure S 5.1 show that relatively long-range repulsion measured between asphaltene surfaces under various pH and salinity conditions could not be described by the DLVO theory, which implies that the surface morphology may play a role. The morphology of asphaltene surfaces was

118

imaged using AFM under the same aqueous solution conditions as in the SFA measurements. The typical topographic images are shown in Figure 5.7. Interestingly, the morphology of the asphaltene surfaces underwent significant changes in aqueous solutions. At pH 8.5 and pH 4.0, formation of pancake-like domains was observed and the height of the "pancakes" was higher at pH 8.5 (Figure 5.7a) than that at pH 4.0 (Figure 5.7b). Therefore, it is evident that the long range repulsion measured at pH 8.5 and pH 4.0 should be mainly attributed to formation of the pancake domains and the increased surface roughness. At pH 2.2, no obvious pancake-like domain was observed as shown in Figure 5.7c whereas a small increase of hard wall distance (about 2.7 nm shown in Figure 5.4c) was still measured in the SFA measurement suggesting there were still some slight (yet uniform) morphology changes over the asphaltene surface at pH 2.2. Figure 5.7d shows the morphology of the asphaltene surface in 100 mM NaCl at pH 8.5. No significant morphology change was observed as compared to that in 1 mM NaCl which agrees with SFA measurements that the interaction forces did not change significantly with varying the NaCl concentration. Figure 5.7e shows that the addition of 1 mM Ca^{2+} significantly decreased both the number and size of the pancake-like domains on the asphaltene surface, which was almost not visible in 100 mM Ca^{2+} (Figure 5.7f). The morphology changes of asphaltene surfaces support the significantly reduced repulsion range and hard wall distance in the presence of Ca^{2+}.

The long-range "stretching" behaviour observed during separation in the force-distance profiles could be also attributed to the formation of the pancake domains in NaCl solutions, interpenetration of the asphaltene chains at the contact interface, or

Ca^{2+} induced bridging when Ca^{2+} ions were added. As discussed in force measurements, the asphaltene surfaces were compressible during approach (Figure 5.4 and Figure 5.5) especially under the conditions where the asphaltene surfaces showed significant morphology change (Figure 5.7), suggesting that the pancake-like domains were soft and compressible. The formation of pancake-like domains of asphaltene thin films coated on mica was mainly due to interactions of asphaltene molecules (particularly the polar groups), water, and likely the supporting solid substrate, and water could diffuse into the asphaltene thin film interacting with polar groups, and further led to the morphology change, which will be reported in more details in a separate work.

(a)　　　　　　　　(b)　　　　　　　　(c)

(d)　　　　　　　　(e)　　　　　　　　(f)
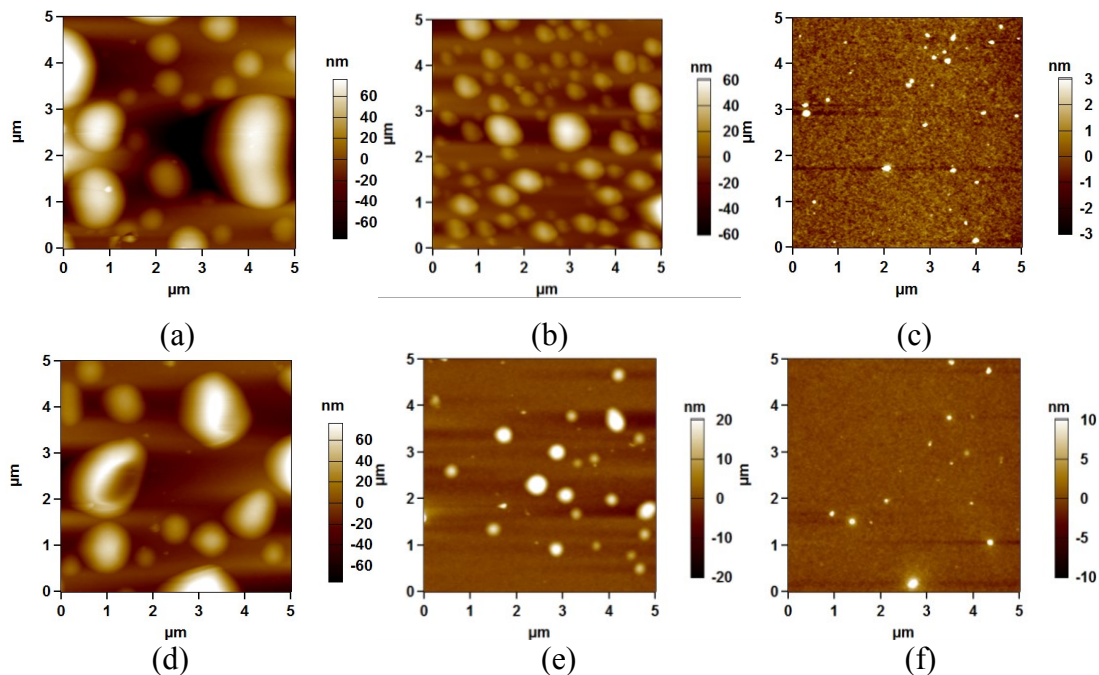
Figure 5.7 The *in-situ* AFM images of asphaltene surfaces in 1 mM NaCl solutions at (a) pH 8.5, (b) pH 4.0 and (c) pH 2.2. (d-f) The *in-situ* AFM images of asphaltene surfaces in (d) 100 mM NaCl solutions at pH 8.5, and in 1mM NaCl solutions with addition of (e) 1 mM Ca^{2+} and (f) 100 mM Ca^{2+} at pH 8.5.

120

5.3.3 Interaction force between silicon nitride tip and asphaltene surface using AFM

To better understand the surface properties and interactions of asphaltene surfaces at nanoscale, a silicon nitride AFM tip was used to measure its interaction force with asphaltene surface under the same conditions as in the SFA measurements. The theoretical calculation using zeta potentials of asphaltene surfaces were used to analyze the measured force-distance curves.

Effect of solution pH

Figure 5.8 shows the approach force-distance profiles between silicon nitride AFM tip and asphaltene surfaces interacting in 1 mM NaCl solution at different pH. Under each pH condition, at least three representative force curves are shown as different open symbols in the same figure. Figure 5.8a shows the measured force during approach was almost zero at distance larger than 2 nm at pH 2.2, indicating the existence of weak EDL repulsion that balanced the attractive VDW interaction. With solution pH increasing to 4.0, a weak attractive force was detected at distance of 5 nm shown in Figure 5.8b, which was consistent with the magnitude and range of a typical VDW attraction, suggesting that EDL interaction was almost negligible in this case. Further increase of pH to 8.5 (Figure 5.8c) resulted in a strong repulsion at distance up to ~30 nm, indicating the EDL repulsion dominated the tip-asphaltene interaction. Therefore, it is evident from the above results that both VDW and EDL interactions play an important role in the tip-asphaltene interactions.

Theoretical calculation based on the classical DLVO theory (red curve) was conducted to interpret the tip-asphaltene interactions shown in Figure 5.8. The Hamaker constant was calculated to be 1.52×10^{-20} J for Si_3N_4-water-asphaltenes.[42,52,53] The surface potential of the silicon nitride tip was calibrated by measuring and fitting the force-distance profile between the same tip and silica wafer under each solution conditions. Figure S 5.2 shows that the surface potential of silicon nitride tip was pH dependent and the PZC was around pH 4.0, which agreed well with the reported values shown in Table S 5.1.[54] The zeta potential of asphaltenes coated on silica particles was measured to be 14±1 mV at pH 2.2, -8±5 mV at pH 4.0 and -61±1 mV at pH 8.5, which was used to predict the tip-asphaltene interactions in 1 mM NaCl. The red curves in Figure 5.8 show that the theoretical calculations agreed well with the measured approach force-distance profiles (open symbols) under all the pH conditions. The discrepancy at distance below 2 nm might originate from the effect of surface roughness as well as exclusion of hydration interaction from theoretical consideration.[50,55,56] The PZC of asphaltene was measured roughly between 2.2 and 4, which coincided with the literature values shown in Table S 5.2.[50,52] The observed pH-dependent zeta potential of asphaltenes was most likely arising from the protonation and deprotonation of the polar groups such as carboxylic groups. Thus, the progressive deprotonation of carboxylic groups with increasing solution pH resulted in a more negatively charged asphaltene surface.

(a)   (b)   (c)
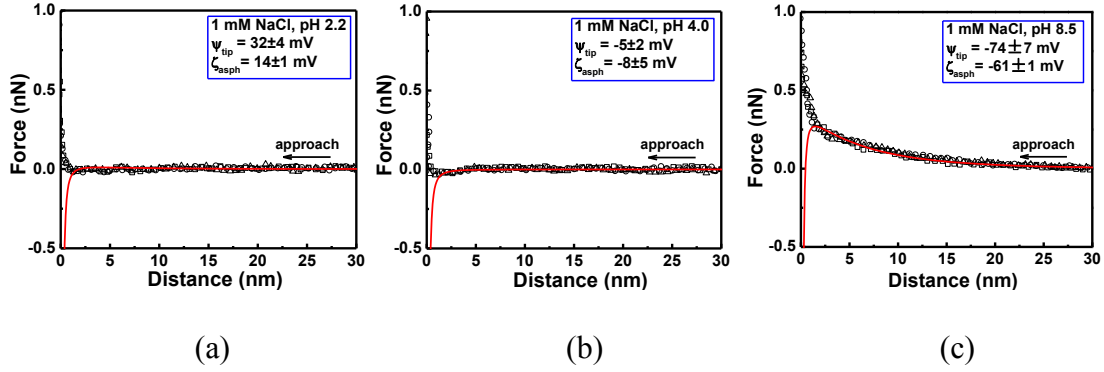
Figure 5.8 The measured force-distance profiles (open symbols, approach) between silicon nitride AFM tip and asphaltene surface in 1 mM NaCl at (a) pH 2.2 with ζ_{asph}= 14±1 mV, (b) pH 4.0 with ζ_{asph} = -8±5 mV and (c) pH 8.5 with ζ_{asph} = -61±1 mV. Red curves show theoretical calculation based on the DLVO theory.

Effect of solution salinity and Ca^{2+} ions

Figure 5.9 shows the measured force-distance profiles (open symbols) and theoretical calculation (red curve) between silicon nitride AFM tip and asphaltene surface in NaCl solution of different concentrations (10 mM and 100 mM in Figure 5.9a and b, respectively) as well as in 1 mM NaCl solution with different concentrations of CaCl$_2$ (1 mM and 100 mM in Figure 5.9c and d, respectively) at pH 8.5. As shown in Figure 5.9a and b, an increased NaCl concentration could screen the electrical double layer, thereby reducing the range of repulsive force to ~13 nm in 10 mM NaCl solution and to <5 nm in 100 mM NaCl solution. The zeta potential of asphaltenes was measured to be -49±4 mV in 10 mM NaCl and -32±3 mV in 100 mM NaCl, based on which the theoretical calculations agreed well with the measured approach force-distance profiles in Figure 5.9a and b. The above results further confirmed the electrostatic characteristics of the long-range repulsion.

The presence of calcium ions (Ca^{2+}) has a more significant influence on suppressing the electrical double layer as compared to sodium ions (Na^+) of the same ionic concentration, as evident from the reduced range of repulsive force in Figure 5.9c. The zeta potential of the asphaltene surface was measured to be -26±1 mV, the magnitude of which was much smaller than that in the 1 mM NaCl solution, indicating that Ca^{2+} could alter the electrostatic properties at asphaltene/water interface by suppressing the electrical double layer as well as interacting with the carboxyl groups of interface-active asphaltene molecules. With the addition of 100 mM $CaCl_2$, the measured force curve showed an attractive force (Figure 5.9d), where the EDL interaction was negligible whereas the VDW interaction dominated the interaction. Figure 5.9c and d also show that the theoretical calculation agreed very well with the experimental measurements. The zeta potentials of asphaltene surfaces coated on silica particles measured in this work are summarized in Table S 5.2, which coincided with the literature values. Based on all the AFM results above, the DLVO theory was found to successfully describe the interactions between charged silicon nitride tip and asphaltene surfaces, indicating the DLVO interaction origin of asphaltene surfaces in aqueous solutions at nanoscale.

(a)   (b)

124

_(c)_   _(d)_
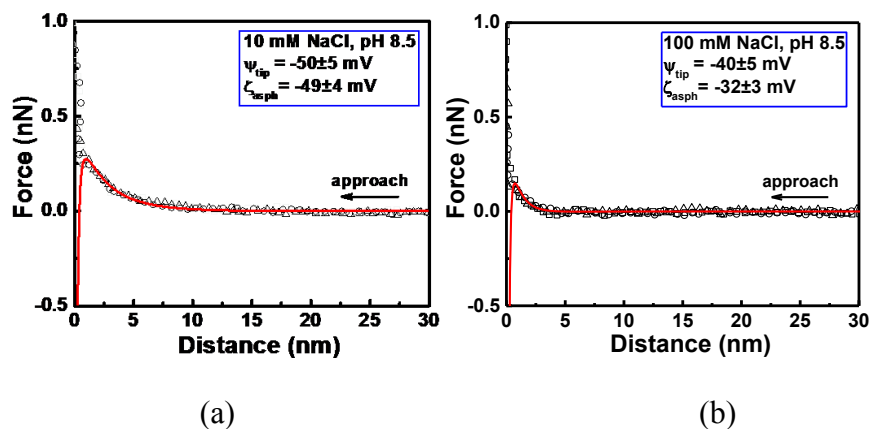
Figure 5.9 The measured force-distance profiles (open symbols, approach) between silicon nitride AFM tip and asphaltene surface in (a) 10 mM NaCl with ζ_{asph} = -49±4 mV, (b) 100 mM NaCl with ζ_{asph} = -32±3 mV and in 1 mM NaCl with addition of (c) 1 mM CaCl$_2$ with ζ_{asph} = -26±1 mV and (d) 100 mM CaCl$_2$ at pH 8.5, and theoretical calculations based on the DLVO theory (red curves).

5.4 Conclusions

The interactions between asphaltene surfaces in aqueous solutions play important roles in many interfacial processes and phenomena in oil production such as stability of oil-in-water emulsions and solid particles. In this work, SFA and AFM were applied to investigate the interaction mechanisms of asphaltenes in aqueous solutions of varying salinity and pH conditions. The SFA results showed that repulsion was measured during approach and adhesion was detected during separation between two asphaltene surfaces in solutions with 1 to 100 mM NaCl at pH 2.2 to 8.5 in the absence or presence of Ca^{2+}. The measured surface repulsion could be affected by the solution pH, salinity and addition of Ca^{2+} whereas the surface interactions measured could not be described by the DLVO theory, which

was due to the morphology change (i.e. pancake-like domains formation) and increased surface roughness of asphaltene surfaces in the aqueous solutions as evident from the AFM imaging. The adhesion measured during separation could be also influenced by the solution conditions, which was mainly attributed to the interpenetration of the asphaltene chains/aggregates at the contact interface and also due to the Ca^{2+} induced bridging effect when Ca^{2+} was added. For AFM force measurements, the theoretical calculations based on the DLVO theory and measured zeta potential of asphaltene surfaces agreed well with the interactions measured between the AFM tip and asphaltene surfaces. The AFM results revealed the DLVO characteristics for the interactions of asphaltenes at nanoscale in aqueous solutions. Our results have demonstrated the interaction behaviours of asphaltenes in aqueous media at nanoscale and submicron-scale can be described by colloidal interaction theory, while surface roughness and asphaltene aggregation can significantly influence their interactions at relatively large surface level. Our results provide useful information for an improved understanding of the interaction mechanisms between asphaltenes in aqueous solutions as well as the stabilization mechanism of oil-in-water emulsions and solid particles in the presence of asphaltenes.

The semi-log force-distance profiles between asphaltene surface in aqueous solutions

(a)   (b)   (c)
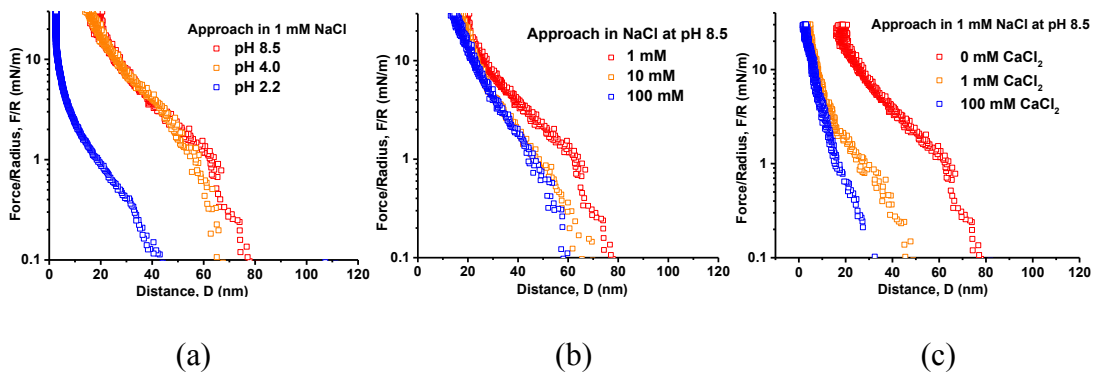
Figure S 5.1 Semi-log plots of force-distance profiles between asphaltene surfaces interacting in aqueous solutions: (a) pH effect, (b) NaCl effect and (c) $CaCl_2$ effect.

Calibration of the surface potential of silicon nitride AFM tip

Figure S 5.2 shows the force-distance profiles between silicon nitride tip and silica wafer in 1 mM NaCl solution at different pH. The surface potentials of the silicon nitride tip in 1 mM NaCl solution under different pH conditions were determined by fitting the measured force profiles (open symbols) with the theoretical calculations based on the DLVO theory (red curves), and the surface potentials of the silica wafer were adapted from the literature.[57,58] The values of the surface potentials of AFM tip and silica wafer are shown in the legend of each figure. Similarly, Figure S 5.3 shows the force-distance profiles (open symbols) and DLVO fittings (red curve) in NaCl solutions of different concentrations and in 1 mM NaCl solution with

addition of Ca^{2+} ions, and the fitted surface potentials of silicon nitride tip and the

adapted surface potentials of silica wafer are also shown in the legend of each figure.

(a)   (b)   (c)
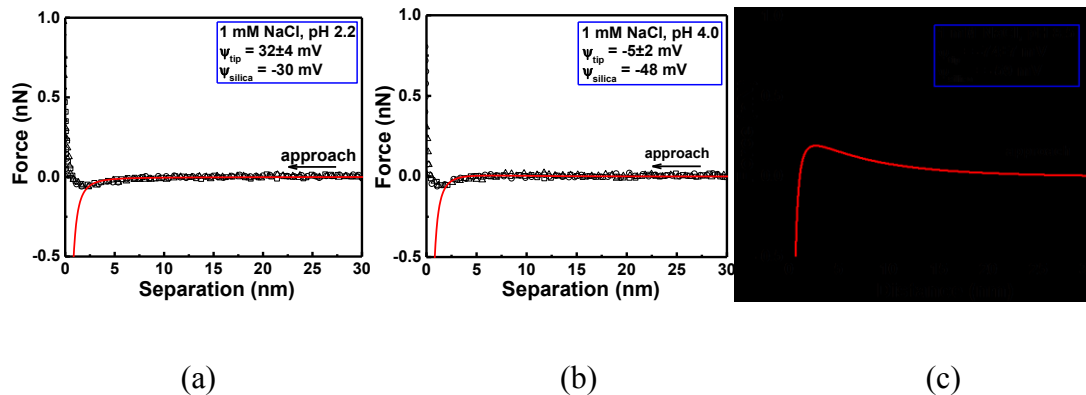
Figure S 5.2 The measured force-distance profiles (open symbols, approach) between silicon nitride tip and silica wafer in 1 mM NaCl solution at (a) pH 2.2, (b) pH 4.0 and (c) pH 8.5. Red curves show the theoretical fittings based on the DLVO theory.

(a)   (b)

(c)   (d)

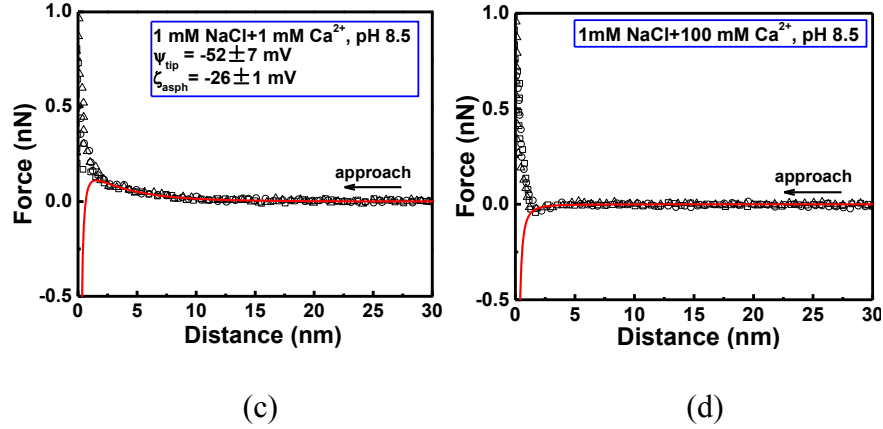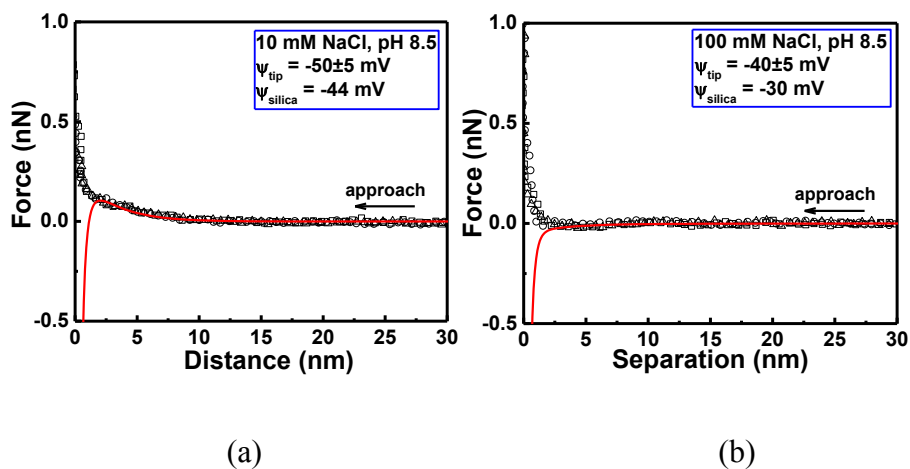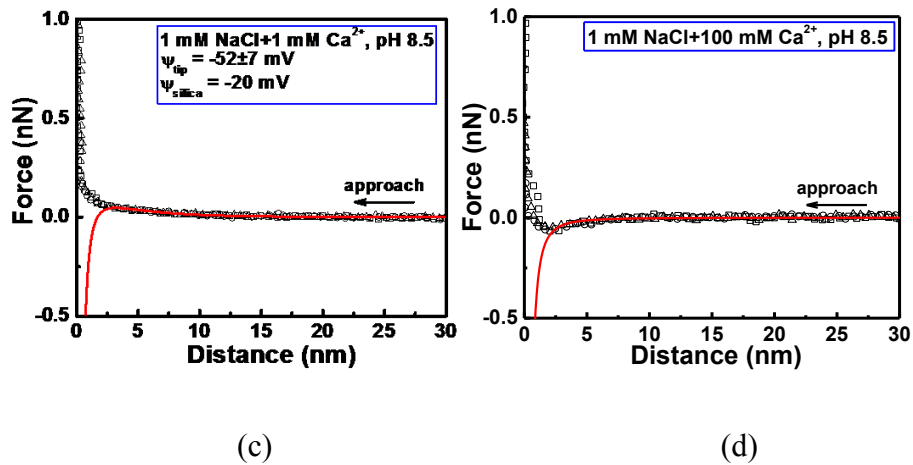**Figure S 5.3** The measured force-distance profiles (open symbols, approach) between silicon nitride tip and silica wafer in (a) 10 mM NaCl solution, (b) 100 mM NaCl solution and in 1 mM NaCl solution with addition of (c) 1mM $CaCl_2$ and (d) 100 mM $CaCl_2$ at pH 8.5. Red curves show the theoretical fittings based on the DLVO theory.

Table S 5.1 Comparison of theoretically fitted surface potential values of silicon nitride and the literature values[54,56]

Solution condition	Fitted value (mV)	Literature value (mV)
NaCl (1 mM), pH 2.2	32±4	35
NaCl (1 mM), pH 4.0	-5±2	0
NaCl (1 mM), pH 8.5	-74±7	-78
NaCl (10 mM), pH 8.5	-50±5	-62
NaCl (100 mM), pH 8.5	-40±5	N/A
CaCl$_2$ (1 mM) in 1 mM NaCl, pH 8.5	-52±7	N/A

Table S 5.2 Comparison of measured zeta potential values of asphaltenes and literature values[50,59]

Solution condition	Zeta potential (mV)	Literature value (mV)
NaCl (1 mM), pH 2.2	14±1	15
NaCl (1 mM), pH 4.0	-8±5	-5
NaCl (1 mM), pH 8.5	-61±1	-58
NaCl (10 mM), pH 8.5	-49±4	-45
NaCl (100 mM), pH 8.5	-32±3	-38
CaCl$_2$ (1 mM) in 1 mM NaCl, pH 8.5	-26±1	-32

References

(1)   Czarnecki, J.; Moran, K. *Energ Fuel* **2005**, *19*, 2074-2079.

(2)   Kwon, W. T.; Park, K.; Han, S. D.; Yoon, S. M.; Kim, J. Y.; Bae, W.; Rhee, Y. W. *J Ind Eng Chem* **2010**, *16*, 684-687.

(3)   Kallevik, H.; Kvalheim, O. M.; Sjöblom, J. *J Colloid Interf Sci* **2000**, *225*, 494-504.

(4)   Dai, Q.; Chung, K. H. *Fuel* **1996**, *75*, 220-226.

(5)   Kim, B.-Y.; Moon, J. H.; Sung, T.-H.; Yang, S.-M.; Kim, J.-D. *Separ Sci Technol* **2002**, *37*, 1307-1320.

(6)   Natarajan, A.; Xie, J. G.; Wang, S. Q.; Liu, Q. X.; Masliyah, J.; Zeng, H. B.; Xu, Z. H. *J Phys Chem C* **2011**, *115*, 16043-16051.

(7)   Kralova, I.; Sjoblom, J.; Oye, G.; Simon, S.; Grimes, B. A.; Paso, K. *Adv Colloid Interfac* **2011**, *169*, 106-127.

(8)   Kumar, K.; Nikolov, A.; Wasan, D. *Ind Eng Chem Res* **2001**, *40*, 3009-3014.

(9)   Pekdemir, T.; Akay, G.; Dogru, M.; Merrells, R.; Schleicher, B. *Separ Sci Technol* **2003**, *38*, 1161-1183.

(10) Tsamantakis, C.; Masliyah, J.; Yeung, A.; Gentzis, T. *J Colloid Interf Sci* **2005**, *284*, 176-183.

(11) Mullins, O. C. *Annu Rev Anal Chem* **2011**, *4*, 393-418.

(12) Angle, C. W.; Dabros, T.; Hamza, H. A. *Energ Fuel* **2007**, *21*, 912-919.

(13) Sparks, B. D.; Kotlyar, L. S.; O'Carroll, J. B.; Chung, K. H. *J Petrol Sci Eng* **2003**, *39*, 417-430.

(14) Kotlyar, L. S.; Sparks, B. D.; Woods, J. R.; Chung, K. H. *Energ Fuel* **1999**, *13*, 346-350.

(15) Yan, N. X.; Gray, M. R.; Masliyah, J. H. *Colloid Surface A* **2001**, *193*, 97-107.

(16) Zhang, W. B.; Shi, Z.; Zhang, F.; Liu, X.; Jin, J.; Jiang, L. *Adv Mater* **2013**, *25*, 2071-2076.

(17) Shi, C.; Zhang, L.; Xie, L.; Lu, X.; Liu, Q.; Mantilla, C.; van den Berg, F. G.; Zeng, H. *Langmuir* **2016**.

(18) Kilpatrick, P. K.; Spiecker, P. M.; Marcel Dekker: New York, 2001; Vol. 3; pp 707-730.

(19) Sjoblom, J. *Encyclopedic handbook of emulsion technology*; CRC Press, 2001.

(20) Gafonova, O. V.; Yarranton, H. W. *J Colloid Interf Sci* **2001**, *241*, 469-478.

(21) Yarranton, H. W.; Hussein, H.; Masliyah, J. H. *J Colloid Interf Sci* **2000**, *228*, 52-63.

(22) Pauchard, V.; Rane, J. P.; Zarkar, S.; Couzis, A.; Banerjee, S. *Langmuir* **2014**, *30*, 8381-8390.

(23) Czarnecki, J.; Tchoukov, P.; Dabros, T. *Energ Fuel* **2012**, *26*, 5782-5786.

(24) Jestin, J.; Simon, S.; Zupancic, L.; Barre, L. *Langmuir* **2007**, *23*, 10471-10478.

(25) Mullins, O. C. *Energ Fuel* **2010**, *24*, 2179-2207.

(26) Higaki, Y.; Hatae, K.; Ishikawa, T.; Takanohashi, T.; Hayashi, J.-i.; Takahara, A. *ACS applied materials & interfaces* **2014**, *6*, 20385-20389.

(27) Wang, J.; Lu, Q. Y.; Harbottle, D.; Sjoblom, J.; Xu, Z. H.; Zeng, H. B. *J Phys Chem B* **2012**, *116*, 11187-11196.

(28) Yarranton, H. W.; Alboudwarej, H.; Jakher, R. *Ind Eng Chem Res* **2000**, *39*, 2916-2924.

(29) Rane, J. P.; Pauchard, V.; Couzis, A.; Banerjee, S. *Langmuir* **2013**, *29*, 4750-4759.

(30) Kaminski, T. J.; Fogler, H. S.; Wolf, N.; Wattana, P.; Mairal, A. *Energ Fuel* **2000**, *14*, 25-30.

(31) Mullins, O. C.; Sabbah, H.; Eyssautier, J. l.; Pomerantz, A. E.; Barré, L.; Andrews, A. B.; Ruiz-Morales, Y.; Mostowfi, F.; McFarlane, R.; Goual, L. *Energ Fuel* **2012**, *26*, 3986-4003.

(32) Saukowski, D. M.; Yarranton, H. W. *J Colloid Interf Sci* **2005**, *285*, 821-833.

(33) Jiang, T.; Hirasaki, G. J.; Miller, C. A.; Ng, S. *Energ Fuel* **2011**, *25*, 2551-2558.

(34) Wang, S. Q.; Liu, J. J.; Zhang, L. Y.; Xu, Z. H.; Masliyah, J. *Energ Fuel* **2009**, *23*, 862-869.

(35) Wang, S. Q.; Liu, J. J.; Zhang, L. Y.; Masliyah, J.; Xu, Z. H. *Langmuir* **2010**, *26*, 183-190.

(36) Zhang, L.; Shi, C.; Lu, Q. G.; Liu, Q. X.; Zeng, H. B. *Langmuir* **2016**, *32*, 4886-4895.

(37) Zhang, L. Y.; Xu, Z. H.; Mashyah, J. H. *Langmuir* **2003**, *19*, 9730-9741.

(38) Shi, C.; Chan, D. Y. C.; Liu, Q. X.; Zeng, H. B. *J Phys Chem C* **2014**, *118*, 25000-25008.

(39) Shi, C.; Cui, X.; Xie, L.; Liu, Q. X.; Chan, D. Y. C.; Israelachvili, J. N.; Zeng, H. B. *Acs Nano* **2015**, *9*, 95-104.

(40) Israelachvili, J.; Min, Y.; Akbulut, M.; Alig, A.; Carver, G.; Greene, W.; Kristiansen, K.; Meyer, E.; Pesika, N.; Rosenberg, K.; Zeng, H. *Rep Prog Phys* **2010**, *73*.

(41) Li, L.; Yan, B.; Yang, J. Q.; Chen, L. Y.; Zeng, H. B. *Adv Mater* **2015**, *27*, 1294-1299.

(42) Israelachvili, J. N. *Intermolecular and surface forces: revised third edition*; Academic press, 2011.

(43) Alcantar, N. A.; Park, C.; Pan, J.-M.; Israelachvili, J. N. *Acta materialia* **2003**, *51*, 31-47.

(44) Alcantar, N.; Israelachvili, J.; Boles, J. *Geochimica et Cosmochimica Acta* **2003**, *67*, 1289-1304.

(45) Zeng, H.; Tian, Y.; Anderson, T. H.; Tirrell, M.; Israelachvili, J. N. *Langmuir* **2008**, *24*, 1173-1182.

(46) Israelac.Jn *J Colloid Interf Sci* **1973**, *44*, 259-272.

(47) Zeng, H. B.; Hwang, D. S.; Israelachvili, J. N.; Waite, J. H. *P Natl Acad Sci USA* **2010**, *107*, 12850-12853.

(48) Yang, D. Z.; Xie, L.; Bobicki, E.; Xu, Z. H.; Liu, Q. X.; Zeng, H. B. *Langmuir* **2014**, *30*, 10809-10817.

(49) Drelich, J.; Long, J.; Yeung, A. *The Canadian Journal of Chemical Engineering* **2007**, *85*, 625-634.

(50) Abraham, T.; Christendat, D.; Karan, K.; Xu, Z.; Masliyah, J. *Industrial & engineering chemistry research* **2002**, *41*, 2170-2177.

(51) Das, S.; Thundat, T.; Mitra, S. K. *Fuel* **2013**, *108*, 543-549.

(52) Liu, J. J.; Zhang, L. Y.; Xu, Z. H.; Masliyah, J. *Langmuir* **2006**, *22*, 1485-1492.

(53) Ducker, W. A.; Clarke, D. R. *Colloids and Surfaces A: Physicochemical and Engineering Aspects* **1994**, *93*, 275-292.

(54) Yan, L.; Englert, A. H.; Masliyah, J. H.; Xu, Z. *Langmuir* **2011**, *27*, 12996-13007.

(55) Zeng, H. B.; Kristiansen, K.; Wang, P.; Bergli, J.; Israelachvili, J. *Langmuir* **2011**, *27*, 7163-7167.

(56) Yang, D.; Xie, L.; Bobicki, E.; Xu, Z.; Liu, Q.; Zeng, H. *Langmuir* **2014**, *30*, 10809-10817.

(57) Ducker, W. A.; Senden, T. J.; Pashley, R. M. *Langmuir* **1992**, *8*, 1831-1836.

(58) Liu, J. J.; Xu, Z. H.; Masliyah, J. *Langmuir* **2003**, *19*, 3911-3920.

(59) Liu, J.; Zhang, L.; Xu, Z.; Masliyah, J. *Langmuir* **2006**, *22*, 1485-1492.

CHAPTER 6   **UNDERSTANDING THE STABILITY MECHANISMS OF ADSORBED ASPHALTENE THIN FILM: EFFECTS OF SUBSTRATE WETTABILITY AND WATER CHEMISTRY**

6.1 Introduction

In colloid and surface science, stability and properties of thin film adsorbed on different solid substrates have been an interesting topic attracting wide research interest. Understanding the stability and properties of thin film requires a solid knowledge of the interactions between the thin film and substrate under different ambient conditions. In the petroleum industry, adsorbed surface active components, e.g. asphaltenes, onto solid surfaces is a challenging issue which could lead to troublesome issues such as reservoir solids wettability alteration, instruments/devices fouling, pipelines/wellbore plugging and catalyst deactivation. Asphaltenes are operationally described as a solubility class, which are soluble in aromatic solvents such as toluene and benzene, but not soluble in n-alkanes, such as n-pentane and n-heptane. Asphaltenes are considered as complex mixtures which consist of polycyclic aromatic hydrocarbon skeleton and peripheral alkane chains, as well as the trace metal elements and polar groups (*e.g.* acid and base functional groups).[1-3] Hence, the hydrophobic carbon skeleton and the hydrophilic polar groups make the asphaltenes interface active thus adsorb to the water/oil interfaces and improve the stability of water-in-oil and oil-in-water emulsions.[4-7] The asphaltenes can also adsorb and even precipitate onto solid surfaces due to the temperature and pressure

change in the liquid media, which will lead to the problems such as fouling and clogging of pipelines and wellbores. The wettability change of the reservoir rock surface can also be due to the adsorption of asphaltenes on the solid surface which has negative impacts on the oil recovery efficiency during water injection processes as well as enhances the formation of "rag layers".[8-13]

Asphaltenes adsorption and the stability of the adsorbed layer involve the interactions between asphaltenes and solid surfaces in the surrounding liquid media and are highly sensitive to many variables such as the solid type, solvent type, the presence of water and water salinity and pH, etc. Therefore, the adsorption of asphaltenes and the stability of the adsorbed asphaltene film is an extremely complex problem which has defied many attempts of description or generalization. The mechanisms of asphaltenes adsorption on the solid surfaces in crude oil (or bitumen)/solids/water system has been studied by insightful work from different research groups by using techniques such as adsorption isotherms, interaction/surface force measurements and contact angle measurement.[4,14-25] It has been found the water or moisture would have a strong impact on the adsorption of asphaltenes on solid surfaces because water could compete with asphaltenes for the adsorption sites thus affecting the interactions between asphaltenes and the solid surfaces.[23,26] Therefore, the stability of the adsorbed asphaltenes will also be significantly impacted by the presence of water. Generally, strong attraction between the asphaltenes and the substrate will lead to enhanced stability whereas weak adhesion will lead to the rupture of the thin film. Atomic force microscope (AFM) has been applied to measure the asphaltenes-asphaltenes interaction, asphaltenes-

silica interaction and crude oil-solids interaction in aqueous solutions which showed that the molecular interactions of asphaltenes highly depended on the solution pH and salinity.[27-29] Drummond et al. reported the surface force measurement between asphaltene thin film and mica surface across brines using surface forces apparatus (SFA) and found that water could penetrate the asphaltene layer and cause it to swell and the surface forces were also strongly dependent on the brines composition and pH.[30,31] Therefore, the water chemistry is very important for understanding the interactions between asphaltenes and solid surfaces which has implications for the stability of the asphaltene film on the solid surface. In a real oil reservoir, there are various types of solids with different hydrophobicity which will substantially influence the competition adsorption of water and asphaltenes. It has been reported when exposed to the moisture, the adsorption capacity of asphaltenes on clay minerals with different hydrophobicity was significantly affected because water would be more affinity to more hydrophilic surfaces.[32] Hence it is also important to incorporate the effect of substrate hydrophobicity for studying the asphaltene film stability. In this work, we investigated the stability and morphology change of the thin asphaltene film on the substrate with different hydrophobicity in different aqueous solutions, which can not only contribute to the knowledge of reservoir wettability alteration but also the bitumen/crude oil liberation process ultimately improving the oil recovery for the oil industry.

In this study, mica was used as the substrate because it is atomically smooth which can eliminate the effects of surface roughness. The hydrophobicity of the mica was controlled by the chemical modification using octadecyltrichlorosilane (OTS).

Contact angle measurement and AFM imaging were applied as major techniques to obtain the morphology of the asphaltene film on the mica surface with variable wettability in both air and aqueous solutions. To better understand the mechanism of the asphaltene thin film properties on mica in aqueous solutions, the Hamaker constant of the asphaltene film was also determined and the model of van der Waals interaction was analysed. Finally, the water diffusion process was proposed.

6.2 Materials and experimental methods

6.2.1 Materials and sample preparation

The detailed procedure of extracting asphaltenes from the vacuum distillation feed Athabasca bitumen has been reported elsewhere.[33] Briefly, high-performance liquid chromatography (HPLC) grade toluene was used to dissolve the vacuum distillation feed bitumen at a bitumen/toluene volume ratio of 1:5. Solids were removed using a centrifuge and the toluene-free bitumen was then added to certified ACS grade n-heptane at a bitumen/heptane volume ratio of 1:40. The precipitated asphaltenes were washed using HPLC-grade n-heptane until the supernatant of the solution was clear and colourless. 1 mM NaCl solution was prepared by adding the desired amount of NaCl into Milli-Q water (18.2 MΩ·cm, Millipore system) and $CaCl_2 \cdot H_2O$ was used as a Ca^{2+} source by adding $CaCl_2 \cdot H_2O$ into 1 mM NaCl solutions to the desired concentration. NaOH and HCl solutions were added to adjust the pH of the salt solution to the desired level. HPLC grade toluene, n-heptane, certified ACS grade n-heptane (99%), NaCl, $CaCl_2 \cdot H_2O$, NaOH and HCl were all purchased from Fisher Scientific Canada and used as received.

138

Asphaltene thin films were prepared by spin coating 2-3 drops of asphaltenes toluene solution (0.5 wt%) on bare mica surfaces or hydrophobized mica surfaces and the coated asphaltene surfaces were kept under vacuum overnight to remove any residual solvent before use. Thicker asphaltene films were prepared by spin coating using 1.0 wt% of asphaltenes in toluene solution. Mica surfaces with variable wettability were obtained by treating mica surfaces under OTS vapour in an evaporation chamber for different periods of time.[34,35] The mica sheets were purchased from S & J Trading Inc. (Glen Oaks, NY, USA). OTS was also purchased from Fisher Scientific Canada and used as received.

6.2.2 Contact angle measurement

The water contact angles on hydrophobized mica surfaces and asphaltene films were characterized by a sessile drop method using a standard goniometer (Model 250, Ramé-hart, USA). A ~3 μL droplet of Milli-Q water or salt solution was placed on the surface and the contact angle was determined by fitting the shape of the drop by image processing software. Videos of the water drop evolution on the asphaltene films that were coated on the bare mica surface were recorded by the camera. To determine the Hamaker constant of the asphaltene surface, the contact angles of three different liquids were measured to obtain the surface energy component of the asphaltene surface using Good & Van Oss model.[36,37] Here, ethylene glyco, glycerol and diiodomethane were used as the three probe liquids and they were also purchased from Fisher Scientific Canada and used as received.

6.2.3 Characterization of the asphaltene films using AFM

An AFM (MFP-3D, Asylum, Santa Barbara, CA, USA) was applied to characterize the morphology of the coated asphaltene films both in the air and *in-situ* in aqueous solutions using tapping mode. The sample was placed in the fluid cell for imaging in the air and then imaging *in-situ* after injecting aqueous solutions. The morphology and roughness of the bare mica surface and OTS-treated mica surface were also imaged by the AFM in the air. Reproducibility was assured by imaging multiple sample surfaces at different locations.

6.3 Results and discussion

6.3.1 The stability of asphaltene films with thicknesses of 20 (+/- 5%) nm and 40 (+/- 5%) nm coated on bare mica surfaces in the presence of water

Asphaltene films with thickness of 20 (+/- 5%) nm and 40 (+/- 5%) nm (indicated as 20 nm and 40 nm below for simplicity) were obtained using different concentrations of asphaltene in toluene solutions, the thickness of which were determined by ellipsometry (on asphaltene films spin-coated under the same condition on silicon wafer). The evolution of water contact angle on the asphaltene film, which was spin-coated on a freshly cleaved bare mica surface, was recorded using the goniometer. Figure 6.1a shows the water contact angle as a function of time on the asphaltene films with both thickness of 20 nm and 40 nm. It was found that the water drop collapsed in about 13 s on the 20 nm-thick asphaltene film as shown in the Movie S 6.1 in the supporting information, whereas the water drop was quite stable on top of the asphaltene film with a thickness of 40 nm for within the

140

experiment time scale. The water drop collapsed on the thinner asphaltene film due to the rupture of the asphaltene film. Two different positions of the fractured asphaltene film were imaged by the confocal microscope and showed that the asphaltene film was crumpled and finally broke down into pieces of fractured sheets (Figure 6.1b and c). This observed instability of the asphaltene film due to the water indicated that water might have penetrated into the asphaltene thin film and led to the asphaltenes rupture on the bare mica surface.
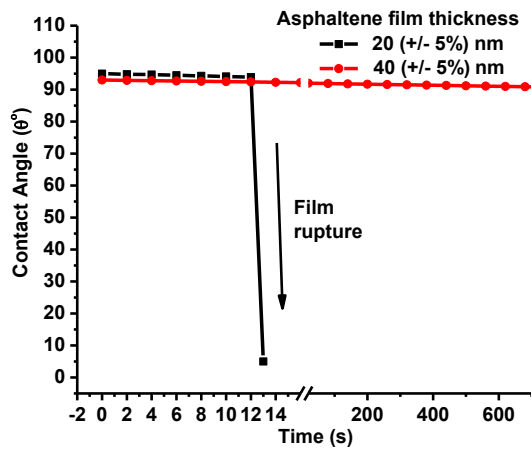
(a)
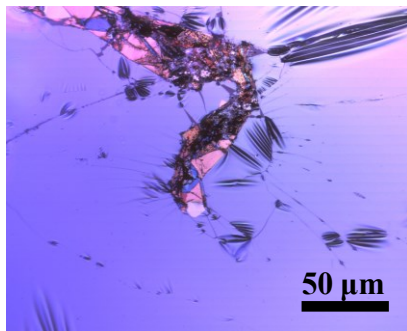
(b)
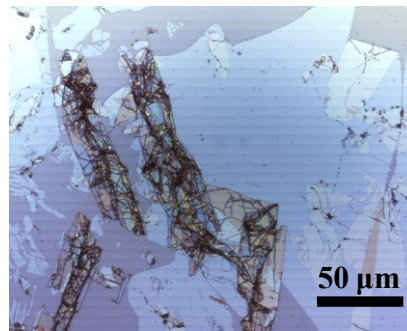
(c)

Figure 6.1 (a) The water contact angle as a function of time on the asphaltene films with a thickness of 20 nm and 40 nm. The confocal microscope images of fractured asphaltene film at two different locations of (b) and (c).

6.3.2 The stability of asphaltene thin film with thickness of 20 nm coated on the OTS-treated mica surface in the presence of water

20 nm-thick asphaltene films were prepared on hydrophobized mica surfaces in order to gain more insight into the stability of the asphaltene films in water. The mica surfaces were treated under OTS vapor with different periods of time to obtain different wettability. It was found a 1-hour treatment led to a water contact angle of 40° and 3 days treatment resulted in one of 85°. Both OTS-treated mica surfaces exhibited molecular smoothness (RMS roughness < 0.5 nm) as shown in Figure 6.2. By using the contact angle measurement as well as the AFM *in situ* imaging technique, the stability and behaviour of asphaltene films on mica surfaces with different hydrophobicity were investigated and the results are discussed in the following two sections.

(a)   (b)
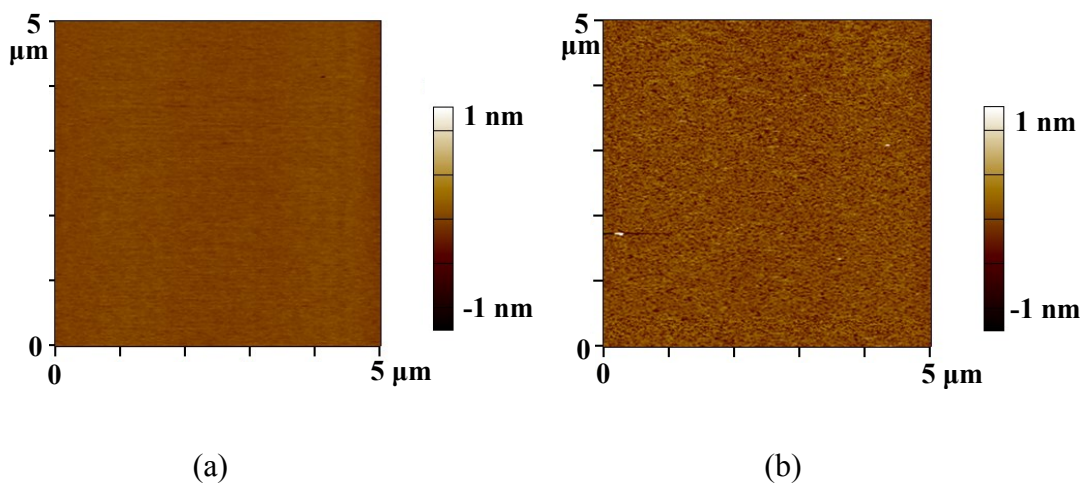
Figure 6.2 The morphology of the mica surfaces with OTS treatment for (a) 1 hour and (b) 3 days imaged in the air by the AFM.

***Asphaltene thin film (20 nm) coated on the OTS-treated mica with contact angle
θ=85°***

The uniformity and smoothness of the asphaltene film coated on the mica surface with contact angle of 85° were confirmed by the AFM topographic image as well as the height profile as shown in Figure 6.3a. A drop of 1 mM NaCl solution of pH 8.5 was used to probe the stability of the asphaltene film and it was found asphaltene film was very stable with the water contact angle of 93°. Figure 6.3b shows that the asphaltene film in 1 mM NaCl solution at pH 8.5 had similar morphology as that imaged in the air (Figure 6.3a). The enhanced stability of the asphaltene film against water could be possibly because of the inhibition of the water penetration through the asphaltene film and prevention of water touching the mica surface attributed to the increased hydrophobicity of the mica.
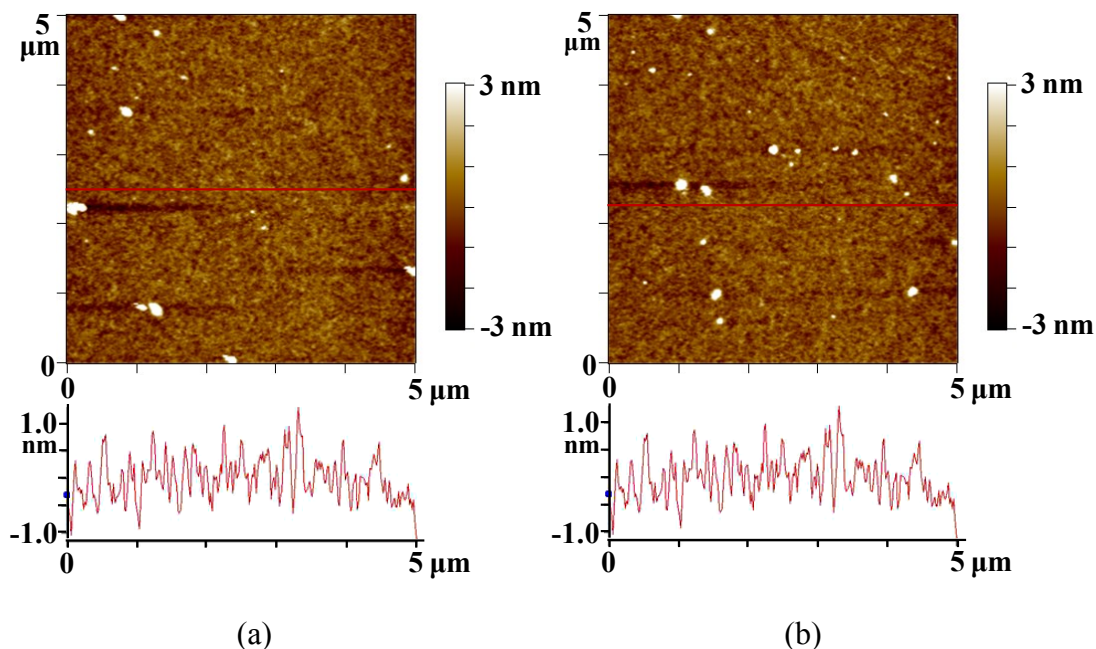
Figure 6.3 The morphology of (a) the asphaltene film spin-coated on the 3-day OTS-treated mica and (b) the same asphaltene film *in-situ* imaged in 1 mM NaCl solution at pH 8.5. The diagrams below the AFM images show the height profiles in red lines.

Asphaltene thin film (20 nm) coated on the OTS-treated mica with contact angle θ=40°

The contact angle measurement showed that the asphaltene thin film coated on the hydrophobized mica surface (with contact of 40°) was also stable with the water contact angle of 91°. Figure 6.4 shows the morphology of the asphaltene film imaged in the air and in 1 mM NaCl solution at pH 8.5. Figure 6.4a shows a uniform asphaltene film which was similar with that coated on the 3-day OTS-treated mica shown in Figure 6.3a. However, in 1 mM NaCl solution at pH 8.5, "pancake" domains with varying sizes were observed with the maximum height of ~100 nm,

which was even larger than the thickness of the asphaltene film (20 nm), as shown in Figure 6.4b. The possible explanation is that the asphaltenes attached to the partially hydrophobized mica surface at multiple points where the adhesion between asphaltenes and mica was relatively strong whereas there were still points where the adhesion between asphaltenes and mica was relatively weak. Therefore, small amounts of water could still penetrate through the asphaltene film to the mica surface, forcing the asphaltene film up and resulting in the formation of the "pancake" domains. However, the multiple-point attachment of the asphaltene film due to the strong adhesion could prevent the asphaltene from completely detaching from the mica surface. Similar pattern has been observed on the crude oil layer on the water wet mica surface that water was able to lift the sections of the organic layer off the substrate.[38]
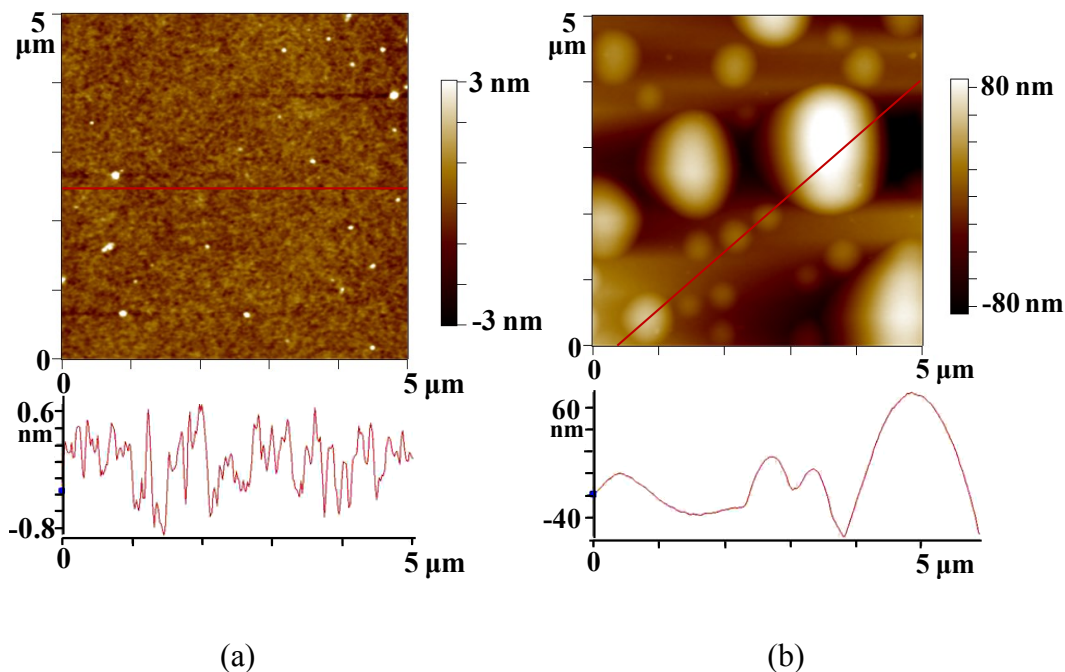
Figure 6.4 The morphology of (a) the asphaltene film spin coated on the hydrophobized mica surface with a contact angle of 40° and (b) the same asphaltene film *in-situ* imaged in 1 mM NaCl solution at pH 8.5. The diagrams below the AFM images show the height profiles in red lines.

6.3.3 The effect of water chemistry on the morphology of asphaltene thin film (20 nm) coated on OTS-treated mica with contact angle θ=40°

Effect of solution pH

As discussed above, the 20 nm-thick asphaltene thin films either fractured on the fresh bare mica surface or showed little change on the hydrophobized mica surface with a contact angle of 85° in NaCl solution at pH 8.5. The obvious "pancake" domains were observed *in-situ* only for the asphaltene film which was coated on the hydrophobized mica surface with contact of 40°. Thus, in order to

146

further explore the mechanisms of "pancake" domains formation, the impacts of various solution conditions were investigated. Solution pH and salinity were previously reported to have a significant impact on the interactions between asphaltenes and solid surfaces.[39] Based on the discussion above that the water penetration might induce the "pancake" domains formation, water chemistry should have a significant impact on the morphology of the asphaltene films. Therefore, in this section, the effect of solution pH was firstly investigated. Figure 6.5a and b show the *in-situ* AFM images of the asphaltene film in 1 mM NaCl solution at pH 2.2 and pH 4.0, respectively. At pH 2.2, the morphology of the asphaltene film hardly changed compared to the morphology of asphaltene film imaged in the air, showing no obvious "pancake" domains (Figure 6.4). However, with solution pH increased to 4.0, "pancake" domains was observed again, but the width and height of the "pancake" domains were much smaller compared to those observed at pH 8.5 (Figure 6.4b) as shown clearly in the height profiles in the diagrams below the AFM images.
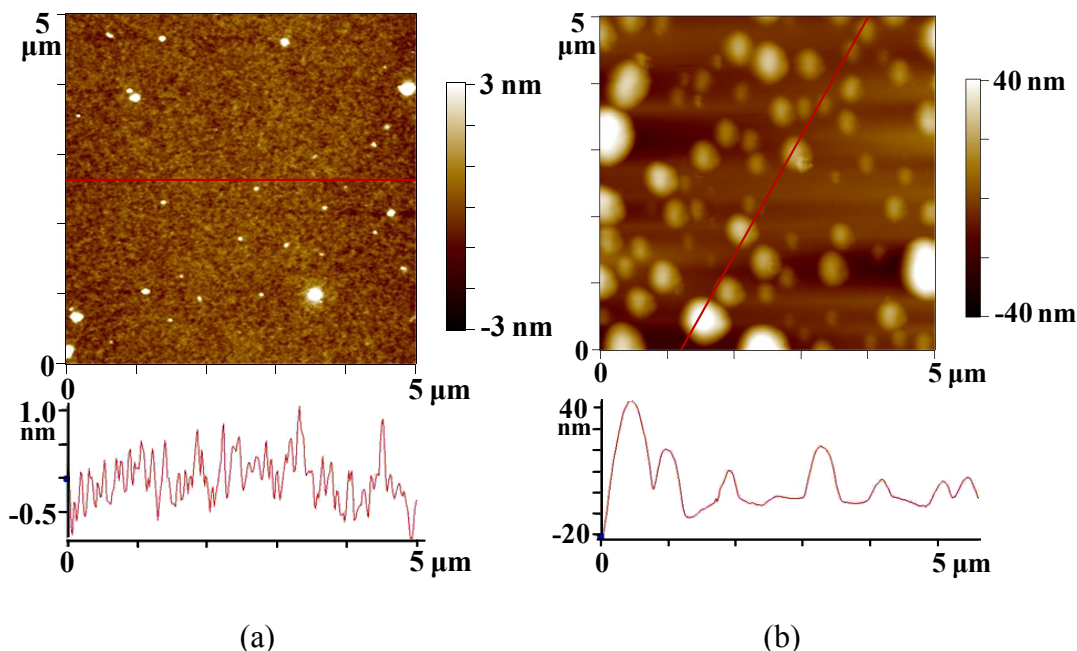
Figure 6.5 The morphology of the asphaltene thin film (20 nm) coated on hydrophobized mica with a contact angle of 40° and *in-situ* imaged in 1 mM NaCl solution at (a) pH 2.2 and (b) pH 4.0. The diagrams below the AFM images show the height profiles in red lines.

Effect of Ca^{2+} addition

The impact of the Ca^{2+} addition on the "pancake" pattern was explored as well. It was found that the number of the "pancake" domains became less in the presence of 1 mM Ca^{2+} as shown in Figure 6.6a and the size of the "pancake" decreased from about a hundred nanometers to tens of nanometers compared that without Ca^{2+} addition at pH 8.5 (Figure 6.4b). The 100 mM Ca^{2+} addition almost led to the disappearance of the "pancake" domains as shown in Figure 6.6b. It has been reported that the electrostatic repulsive force between bitumen/asphaltenes and silica could be reduced by adding Ca^{2+}.[27,40] Therefore, in this study, the phenomenon

observed in the presence of Ca^{2+} could be possibly explained by the force between asphaltenes and mica surface which was an electrostatic repulsive force and was reduced by the addition of Ca^{2+}. More details are discussed in the later sections.

(a)   (b)
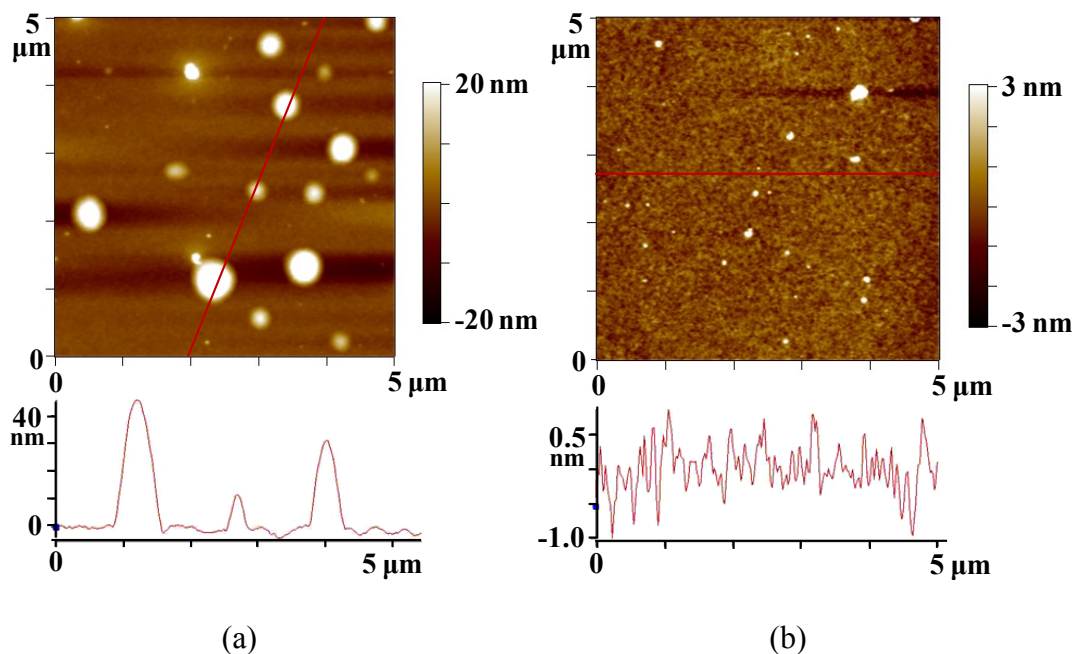
Figure 6.6 The morphology of the asphaltene film (20 nm) coated on hydrophobized mica with a contact angle of 40° and *in-situ* imaged in 1 mM NaCl solution at pH 8.5 with the addition of (a) 1 mM Ca^{2+} and (b) 100 mM Ca^{2+}. The diagrams below the AFM images show the height profiles in red lines.

6.3.4 The stability mechanisms of asphaltene film on mica surface in aqueous solutions

van der Waals interaction between mica and water across the asphaltene film

As discussed above, the water penetration could cause the asphaltene film to rupture on the freshly cleaved mica surface. The van der Waals interaction between

water and mica surface across the asphaltene film might be the reason for water to penetrate through. Therefore, we firstly calculated the van der Waals interactions between water and mica across the asphaltene film by determining the asphaltenes Hamaker constant. Using the reliable proportionality between Hamaker constant A and the non-polar surface energy component γ^d, the Hamaker constant of the asphaltene film $A_{asphaltene}$ can be determined by Eq. 6.1.[41,42] l_o is the minimum equilibrium distance, the value of which is reported to be 1.65 Å.[42] γ_a^d is the dispersive component of asphaltene film which can be obtained by measuring the contact angle of three different probe liquids on the asphaltene film. In the Good & Van Oss model,[36,37] the surface energy can be written as Eq. 6.2, where γ is the surface energy, γ^d the dispersive component (Lifshitz-van der Waals interactions), and γ^+ and γ^- are the polar components (Lewis acid-base).

$$A_{asphaltene} = 24\pi l_0^2 \gamma_a^d \tag{6.1}$$

$$\gamma = \gamma^d + 2\sqrt{\gamma^+ \gamma^-} \tag{6.2}$$

Eq. 6.3 describes the relationship between the surface energy of the solid surface, the surface tension of the liquid and the liquid contact angle on the solid surface, where l and s denote the liquid and solid respectively and θ_l is the liquid contact angle on the solid surface. In order to determine the surface energy components of the asphaltene surface, γ_a^d, γ_a^+ and γ_a^-, at least three different probe liquids of known energy components should be used in contact angle measurements and then three equations can be obtained. Thus, the energy components of the

150

asphaltene surface can be determined by Eq. 6.4, where $l1$, $l2$ and $l3$ denote the three different probe liquids, respectively. The measured contact angle and the surface energy components of these three liquids are listed in Table 6.1. By using Eq. 6.4 and Eq. 6.1, respectively, the dispersive component of asphaltene film γ_a^d was calculated to be 41.18 mJ/m^2, and the Hamaker constant of asphaltenes, $A_{asphaltene}$, was 8.45×10^{-20} J. Applying Eq. 6.5, the Hamaker constant between water and mica across the asphaltene film $A_{w\text{-}a\text{-}m}$ could be determined by using the Hamaker constant between mica and mica and the Hamaker constant between water and water.[43] Hence, $A_{w\text{-}a\text{-}m}$ was calculated to be -2.13×10^{-21} J and all the Hamaker constants obtained here are summarized in Table 6.2. The negative Hamaker constant $A_{w\text{-}a\text{-}m}$ obtained would result in a repulsive van der Waals interaction (Eq. 6.6) between water and bare mica across the asphaltene film suggesting that another mechanism should be involved here which induced the lifting of the asphaltene film.

$$\gamma_l(1+\cos\theta_l) = 2(\sqrt{\gamma_s^d\gamma_l^d} + \sqrt{\gamma_s^+\gamma_l^-} + \sqrt{\gamma_s^-\gamma_l^+}) \tag{6.3}$$

$$\begin{bmatrix} \gamma_a^d \\ \gamma_a^- \\ \gamma_a^- \end{bmatrix} = \left\{ \left[2 \begin{pmatrix} \sqrt{\gamma_{l1}^d} & \sqrt{\gamma_{l1}^-} & \sqrt{\gamma_{l1}^+} \\ \sqrt{\gamma_{l2}^d} & \sqrt{\gamma_{l2}^-} & \sqrt{\gamma_{l1}^-} \\ \sqrt{\gamma_{l3}^d} & \sqrt{\gamma_{l3}^-} & \sqrt{\gamma_{l1}^-} \end{pmatrix} \right]^{-1} \begin{pmatrix} \gamma_{l1}[\cos\theta_{l1}+1] \\ \gamma_{l2}[\cos\theta_{l2}+1] \\ \gamma_{l3}[\cos\theta_{l3}+1] \end{pmatrix} \right\}^2 \tag{6.4}$$

$$A_{w\text{-}a\text{-}m} = (\sqrt{A_{ww}} - \sqrt{A_{aa}})(\sqrt{A_{mm}} - \sqrt{A_{aa}}) \tag{6.5}$$

$$F_{VdW} = -\frac{A_{w\text{-}a\text{-}m}}{12\pi D^2} \tag{6.6}$$

151

Table 6.1 The surface energy and surface energy components of the three probe liquids in mJ/m^2 and their contact angles on the asphaltene surface.

Liquid	γ_l^d	γ_l^+	γ_l^-	γ_l	Contact angle θ
Glycerol	34.4	3.92	57.4	64.4	80.2
Ethylene glycol	29.0	1.92	47.0	48.0	74.0
Diiodomethane	50.8	0	0	50.8	36.8

Table 6.2 The Hamaker constants.

$A_{asphaltene}$	A_{mm}	A_{ww}	A_{w-a-m}
Asphaltenes-Asphaltenes	Mica-Mica	Water-Water	Water-Asphaltenes-Mica
8.45×10^{-20} J	9.72×10^{-20} J	3.68×10^{-20} J	-2.13×10^{-21} J

Water diffusion model through the asphaltene film

Due to the repulsive van der Waals interaction between water and mica surface across the asphaltene film, the possible mechanism for this phenomenon is proposed as the water diffusion process from the top of the asphaltene surface to the bare mica surface through the free volume inside the asphaltene thin film. It is similar to the water diffusion process through polymeric thin films which has been widely reported.[44-47] From the solution diffusion model, there are three stages of the permeation process of the solution molecules happening through the polymeric film.[44] Firstly the molecules are adsorbed on the polymer surface, and then the

molecules diffuse through the film followed by desorption from the other side of the surface. Based on the XPS spectrum of the asphaltenes (Figure 6.8) and reported literature, the asphaltenes should bear some polar groups such as cationic group RNH_3^+ and anionic groups of $RCOO^-$ and $ROSO_3^-$.[6,33,48,49] Therefore water molecules might adsorb to these polar groups first, and then the water diffused through the free volume of the asphaltene film. Finally, water spread on the bare mica surface and lifted up the asphaltene film. It has also been reported the diffusion process of water can be affected by the film thickness. Hence, for the thicker asphaltene film, water penetration was not observed through the top face of the asphaltene film probably because (1) observation time was not long enough to see the water drop to diffuse through the asphaltene film; (2) the higher asphaltene concentration would lead to a much denser asphaltene film which could also retard or inhibit the water diffusion process due to the lack of free volume. A schematic of penetration process of water into asphaltene film is illustrated in Figure 6.7.
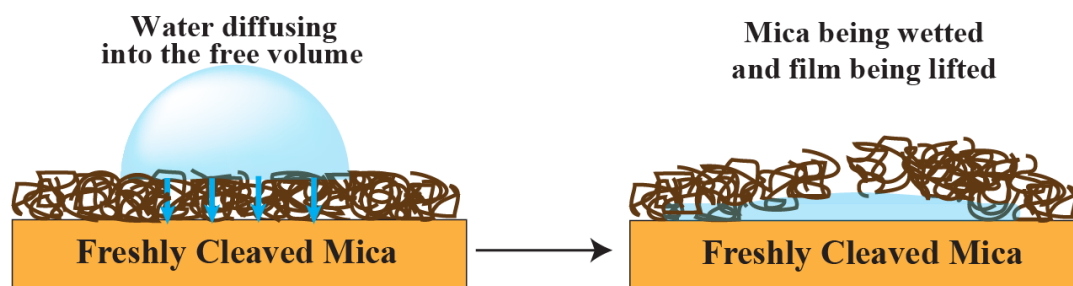
(a)
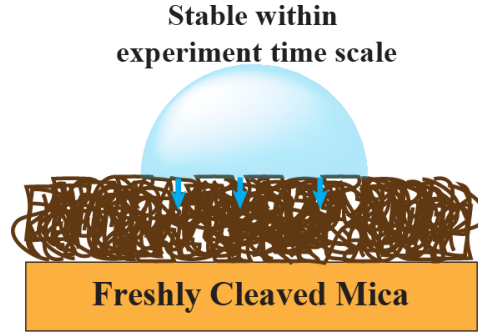
(b)

Figure 6.7 The schematic of the water penetration process for the asphaltene films with a thickness of 20 nm (a) and 40 nm (b) coated on the freshly cleaved mica surfaces.

Fickian's diffusion model, which is used to analyse the water diffusion through polymer films, is applied here to analyse the water diffusion process through asphaltene film shown in Eq. 6.7.[47,50]

$$\frac{M_t}{M_\infty} = 1 - \frac{8}{\pi^2} \sum_{n=0}^{\infty} \frac{1}{(2n+1)^2} \exp\left[-D(2n+1)^2 \pi^2 t / 4L^2\right] \tag{6.7}$$

$$\frac{M_t}{M_\infty} = 1 - \frac{8}{\pi^2} \exp(-\pi^2 D t / 4L^2) \tag{6.8}$$

where $M(t)$ and $M(\infty)$ are the water sorption at time t and water sorption at $t=\infty$, respectively. D is the diffusion coefficient with a unit of cm^2/sec and L is the film thickness. If $M(t)/M(\infty) > 0.52$, the Eq. 6.7 can be simplified to Eq. 6.8.[50] Assuming 99% of water was taken up by the asphaltene film of 20 nm in 13 s shown in Figure 6.1, the diffusion coefficient D of water diffusing through the asphaltene film can be

calculated to be 5.49×10^{-13} cm^2/sec. Since the thicker asphaltene film (40 nm) was denser, too little free volume might be available for water to diffuse through in short time. Therefore, a longer time might be needed and much smaller diffusion coefficient would be for the water diffusing through thicker asphaltene film.

For asphaltene film coated on hydrophobized mica surface with contact angle of 85°, very small amount of water might still diffuse into the free volume of the film, whereas water could not accumulate on and wet the mica surface attributed to the increased hydrophobicity of the mica surface.
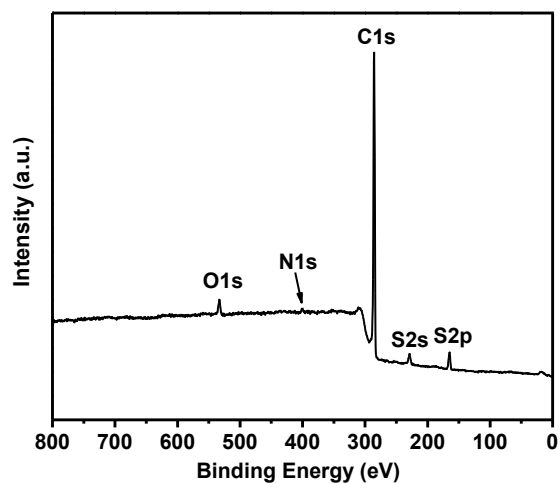
Figure 6.8 The XPS survey spectrum of the asphaltene film coated on a bare mica surface.

The impact of pH and addition of Ca^{2+} on the morphology of the asphaltene film (20 nm thick) coated on hydrophobized mica with contact angle θ=40°

The interaction mechanisms between asphaltenes and mica surface across brine solutions have been investigated and it was found the interactions between

155

asphaltene surface and mica surface was dominated by the electrostatic repulsive forces and significantly affected by the solution pH and salinity.[30] Therefore, based on the water diffusion process into the interspace of mica and asphaltene film, electrostatic interaction is proposed here to explain the mechanisms of "pancake" domains formation on the mica surface in aqueous solutions with different water chemistry. Although the presence of water could not cause the asphaltene film rupture on the hydrophobized mica surface with a contact angle of 40°, water could still diffuse through and enter in between the asphaltene film and the mica surface. Mica surface was partially hydrophobic and water could still stay on the hydrophilic part of the surface thereby lifted up part of the asphaltene film which appeared like "pancake" in 1 mM NaCl solution at pH 8.5 as shown in Figure 6.4b. The electrophoresis study on the asphaltene has been reported that asphaltenes carry negative charges under alkaline condition and the isoelectric point (i.e.p) is around pH=3~pH=4.[27] Therefore, the "pancake" formation of asphaltene film could be affected due to the electrostatic force between charged asphaltene film and negatively charged mica surface in the presence of water.[51] The decrease of the negative charges of both asphaltene and mica at pH 4.0 resulted in a decrease of the electrostatic repulsive force between each other, thus the entering of water was partially prevented and smaller size of "pancake" domains formed (Figure 6.6b). At pH 2.2, the asphaltene film was positively changed whereas mica remained negatively changed. In consequence, the electrostatic attractive force between the asphaltene film and mica surface prohibited the water entering in between leading to the disappearance of the "pancake" domains.

156

The effect of Ca^{2+} has been investigated on the behaviours of bitumen on solid surfaces in many different aspects. Kasongo *et al.* reported that the presence of calcium ions would depress the bitumen recovery during the flotation process which might be due to the enhanced adhesion between bitumen and solid surfaces.[52] Later on, Basu *et al.* investigated the effect of Ca^{2+} on the displacement of bitumen from glass surface and explained that the slow rate of recession of bitumen was due to the weakened repulsive force and strengthen adhesion force between bitumen and glass by the addition of Ca^{2+}.[53] Similar with the behaviour of bitumen, the Ca^{2+} could reduce the negative charges of asphaltene film by the interactions between calcium ions and carboxylic groups in the asphaltene film.[27] Therefore the reduced electrostatic repulsive force between asphaltene film and mica surface might reduce or prohibit the water entering resulting in the smaller "pancake" formation or no "pancake" formation.

6.4 Conclusions

The stability of the asphaltene thin films under various solution conditions on the surfaces with varying wettability was characterized. The results showed that the hydrophobicity of the substrate substantially affected the stability and the morphology of the asphaltene thin films and the water diffusion process was proposed. For asphaltenes coated on bare mica surface, a water drop could diffuse through the free volume of the thinner asphaltene film (20 nm) very quickly leading to the fracture of the film. For the thicker asphaltene film (40 nm), the water drop could not diffuse through the film on the top within the observation time because the

film was much denser and there was too little free volume for water to diffuse through.

Hydrophobized mica surface with a contact angle of 40° was obtained by 1-hour OTS treatment. The coated 20 nm-thick asphaltene film did not rupture in the presence of brine solutions. By the *in-situ* imaging using AFM, large "pancake" domains were observed in 1 mM NaCl solution at pH 8.5. It was proposed that water diffused through the free volume of the asphaltene film and stayed on the hydrophilic part of the mica surface lifting up part of the asphaltene film. The "pancake" pattern became less pronounced and even disappeared when the pH was decreased to 4.0 and 2.2, respectively. The different charges asphaltene carried at various pH values led to the different morphology change. The addition of Ca^{2+} also had an impact on the "pancake" pattern due to the reduced electrostatic repulsive forces between asphaltene film and mica surface. Our results provide insights into the fundamental understanding of the stability of asphaltenes on solid surfaces which could be further related to the bitumen liberation process and reservoir solids wettability change in the oil industry.

Supporting information

Movie S 6.1 The evolution of water contact angle on the asphaltene film with a thickness of 20 nm, which was spin-coated on a freshly cleaved mica surface.

Link for the video:

https://drive.google.com/open?id=0B7KQbCrdhB7IUnlDd3hvOTNfS3c

References

(1) Sheremata, J. M.; Gray, M. R.; Dettman, H. D.; McCaffrey, W. C. *Energ Fuel* **2004**, *18*, 1377-1384.

(2) Mullins, O. C. *Annu Rev Anal Chem* **2011**, *4*, 393-418.

(3) Wang, S. Q.; Liu, J. J.; Zhang, L. Y.; Masliyah, J.; Xu, Z. H. *Langmuir* **2010**, *26*, 183-190.

(4) Yarranton, H. W.; Hussein, H.; Masliyah, J. H. *J Colloid Interf Sci* **2000**, *228*, 52-63.

(5) Spiecker, P. M.; Kilpatrick, P. K. *Langmuir* **2004**, *20*, 4022-4032.

(6) Zhang, L. Y.; Xu, Z. H.; Mashyah, J. H. *Langmuir* **2003**, *19*, 9730-9741.

(7) Taylor, S. D.; Czarnecki, J.; Masliyah, J. *J Colloid Interf Sci* **2002**, *252*, 149-160.

(8) Buckley, J. S. *Rev I Fr Petrol* **1998**, *53*, 303-312.

(9) Jiang, T.; Hirasaki, G. J.; Miller, C. A.; Moran, K. *Energ Fuel* **2008**, *22*, 4158-4164.

(10) Angle, C. W.; Dabros, T.; Hamza, H. A. *Energ Fuel* **2007**, *21*, 912-919.

(11) Alvarez, G.; Jestin, J.; Argillier, J. F.; Langevin, D. *Langmuir* **2009**, *25*, 3985-3990.

(12) Saukowski, D. M.; Yarranton, H. W. *J Colloid Interf Sci* **2005**, *285*, 821-833.

(13) Liu, J. J.; Xu, Z. H.; Masliyah, J. *Can J Chem Eng* **2004**, *82*, 655-666.

(14) Sjöblom, J.; Hemmingsen, P. V.; Kallevik, H. In *Asphaltenes, Heavy Oils, and Petroleomics*; Springer, 2007; pp 549-587.

(15) Feng, X. H.; Mussone, P.; Gao, S.; Wang, S. Q.; Wu, S. Y.; Masliyah, J. H.; Xu, Z. H. *Langmuir* **2010**, *26*, 3050-3057.

(16) Gu, G.; Xu, Z.; Nandakumar, K.; Masliyah, J. H. *Fuel* **2002**, *81*, 1859-1869.

(17) McLean, J. D.; Kilpatrick, P. K. *J Colloid Interf Sci* **1997**, *189*, 242-253.

(18) Kumar, K.; Nikolov, A. D.; Wasan, D. T. *Ind Eng Chem Res* **2001**, *40*, 3009-3014.

(19) Czarnecki, J. *Energ Fuel* **2009**, *23*, 1253-1257.

(20) Czarnecki, J.; Moran, K. *Energ Fuel* **2005**, *19*, 2074-2079.

(21) Rudrake, A.; Karan, K.; Horton, J. H. *J Colloid Interf Sci* **2009**, *332*, 22-31.

(22) Dudasova, D.; Silset, A.; Sjoblom, J. *J Disper Sci Technol* **2008**, *29*, 139-146.

(23) Goual, L.; Horvath-Szabo, G.; Masliyah, J. H.; Xu, Z. H. *Langmuir* **2005**, *21*, 8278-8289.

(24) Ekholm, P.; Blomberg, E.; Claesson, P.; Auflem, I. H.; Sjoblom, J.; Kornfeldt, A. *J Colloid Interf Sci* **2002**, *247*, 342-350.

(25) Dudasova, D.; Simon, S.; Hemmingsen, P. V.; Sjoblom, J. *Colloid Surface A* **2008**, *317*, 1-9.

(26) Akhlaq, M. S.; Gotze, P.; Kessel, D.; Dornow, W. *Colloid Surface A* **1997**, *126*, 25-32.

(27) Abraham, T.; Christendat, D.; Karan, K.; Xu, Z.; Masliyah, J. *Ind Eng Chem Res* **2002**, *41*, 2170-2177.

(28) Basu, S.; Sharma, M. M. *Spe J* **1999**, *4*, 235-241.

(29) Liu, J. J.; Zhang, L. Y.; Xu, Z. H.; Masliyah, J. *Langmuir* **2006**, *22*, 1485-1492.

(30) Drummond, C.; Israelachvili, J. *J Petrol Sci Eng* **2002**, *33*, 123-133.

(31) Drummond, C.; Israelachvili, J. *J Petrol Sci Eng* **2004**, *45*, 61-81.

(32) Jada, A.; Debih, H. *Compos Interface* **2009**, *16*, 219-235.

(33) Zhang, L. Y.; Lawrence, S.; Xu, Z. H.; Masliyah, J. H. *J Colloid Interf Sci* **2003**, *264*, 128-140.

(34) Shi, C.; Cui, X.; Xie, L.; Liu, Q. X.; Chan, D. Y. C.; Israelachvili, J. N.; Zeng, H. B. *Acs Nano* **2015**, *9*, 95-104.

(35) Shi, C.; Chan, D. Y. C.; Liu, Q. X.; Zeng, H. B. *J Phys Chem C* **2014**, *118*, 25000-25008.

(36) Vanoss, C. J. *Colloid Surface A* **1993**, *78*, 1-49.

(37) Vanoss, C. J.; Good, R. J.; Chaudhury, M. K. *J Colloid Interf Sci* **1986**, *111*, 378-390.

(38) Buckley, J. S.; Lord, D. L. *J Petrol Sci Eng* **2003**, *39*, 261-273.

(39) Li, H. H.; Long, J.; Xu, Z. H.; Masliyah, J. H. *Can J Chem Eng* **2008**, *86*, 168-176.

(40) Liu, J. J.; Xu, Z. H.; Masliyah, J. *Langmuir* **2003**, *19*, 3911-3920.

(41) Van Oss, C. J. *Interfacial forces in aqueous media*; CRC press, 2006.

(42) Israelachvili, J. N. *Intermolecular and surface forces: revised third edition*; Academic press, 2011.

(43) Israelachvili, J. *Intermolecular and Surface Forces*; third ed.; Academic Press, 2011.

(44) Vanderhoff, J.; Bradford, E.; Carrington, W. In *Journal of Polymer Science: Polymer Symposia*; Wiley Online Library, 1973; Vol. 41; pp 155-174.

(45) Seo, J.; Han, H. *J Appl Polym Sci* **2001**, *82*, 731-737.

(46) Linossier, I.; Gaillard, F.; Romand, M.; Feller, J. F. *J Appl Polym Sci* **1997**, *66*, 2465-2473.

(47) Pereira, M. R.; Yarwood, J. *J Chem Soc Faraday T* **1996**, *92*, 2737-2743.

(48) Boukir, A.; Aries, E.; Guiliano, M.; Asia, L.; Doumenq, P.; Mille, G. *Chemosphere* **2001**, *43*, 279-286.

(49) Liu, J. J.; Zhou, Z.; Xu, Z. H. *Ind Eng Chem Res* **2002**, *41*, 52-57.

(50) Wind, M. M.; Lenderink, H. J. W. *Prog Org Coat* **1996**, *28*, 239-250.

(51) Nishimura, S.; Tateyama, H.; Tsunematsu, K.; Jinnai, K. *J Colloid Interf Sci* **1992**, *152*, 359-367.

(52) Kasongo, T.; Zhou, Z.; Xu, Z. H.; Masliyah, J. *Can J Chem Eng* **2000**, *78*, 674-681.

(53) Basu, S.; Nandakumar, K.; Lawrence, S.; Masliyah, J. *Fuel* **2004**, *83*, 17-22.

CHAPTER 7   CONCLUSIONS AND SUGGESTIONS

The challenging issues of stable water-in-oil (W/O) and oil-in-water (O/W) emulsions can be detrimental to the oil production from the reservoir to the downstream operations. Asphaltenes are believed one of the major components enhancing the stability of the emulsion drops and solid particles. Therefore, it drives us to fundamentally investigate the interactions of asphaltenes in various liquid media which may provide some insights into the mechanisms involved and ultimately solve the problems of the stable emulsion drops and solid particles due to the presence of asphaltenes. Moreover, the aggregation and adsorption/deposition behaviours of asphaltenes are also determined by the interactions between asphaltenes or between asphaltenes and solid surfaces and the involved mechanisms remain unclear, which require a deeper investigation for better understanding and may provide useful clues in solving the asphaltene destabilization and fouling issues during oil production.

In this study, the interaction between asphaltene surfaces was measured in heptol (toluene/n-heptane mixture) solvent by surface forces apparatus (SFA) and the effect solvent condition was investigated. Micropipette and 4-roll mill techniques were also applied to further provide implications to the stability mechanisms of W/O emulsions. For investigating the asphaltenes adsorption mechanisms in the organic solvent, the adsorption of asphaltenes on silica surfaces in toluene was studied using quartz crystal microbalance with dissipation monitoring (QCM-D) and SFA. The interaction mechanisms between asphaltene surfaces were also elucidated in aqueous

solutions using SFA and AFM and the impacts of solution pH, salinity and calcium addition were determined. Additionally, asphaltene film stability on solid surfaces in various aqueous solutions was studied by AFM and contact angle goniometer. The major conclusions from these studies are summarized below.

7.1 Major conclusions

(1) The SFA results revealed that the solvent condition could significantly impact on the interactions between asphaltenes. As the weight fraction of n-heptane in heptol increased, the interaction between asphaltene surfaces gradually changed from pure repulsion to weak attraction. The repulsive forces measured were mainly due to the steric interaction between the swelling asphaltene molecules and aggregates. In good solvent toluene, the measured repulsion also well agreed with the results from micropipette tests and 4-roll mill tests, which demonstrated that asphaltenes could adsorb onto the water/oil interfaces and inhibit the coalescence of the emulsions. The results from 4-roll mill tests also suggested that proper collision angles and compression were required to cause interfacial sliding or shearing which locally destabilized the protective interfacial asphaltene layers and thus enhanced the coalescence probability of the W/O emulsion drops. The results provide insights into the fundamental understanding of molecular interaction mechanisms of asphaltenes in organic solvents and stabilization/destabilization behaviors of W/O emulsions with asphaltenes.

(2) The QCM-D results showed that asphaltenes precipitated from crude oil (A) could continuously adsorb on silica surface in toluene whereas asphaltenes

precipitated from bitumen (B) saturated the silica surfaces shortly in toluene. Combined with the SFA adsorption measurement, it was found the adsorption behaviour of asphaltenes A was different under flow condition and static condition. A fraction in asphaltenes A tended to form aggregates even at very low concentration (50 mg/L) in toluene which was evident from the AFM imaging. The larger amounts of Ca and O found in the adsorbed layer compared to the bulk asphaltenes revealed that the existence of Ca and O might play a key role in the aggregate formation of asphaltenes A, resulting in the continuous adsorption under flow condition in toluene. The results provide some insights into the fundamental understanding of adsorption mechanisms of asphaltenes on solid surfaces, with implications for the wettability change of the solid surface as well as the fouling problems due to asphaltenes.

(3) The surface force measurement between asphaltenes showed that repulsion was measured during approach and adhesion was detected during separation under all the aqueous solution conditions tested. The repulsions could be influenced by the solution pH, salinity and Ca^{2+} addition whereas the repulsions measured could not be described by the DLVO theory, which was mainly due to the pancake-like domains formed on asphaltene surfaces in aqueous solutions as evident from the AFM imaging. The AFM force measurement results revealed that there was a DLVO origin between asphaltenes at nanoscale in aqueous solutions. By further studying the morphology of asphaltene surfaces in aqueous solutions, it was found that water drop could diffuse through the thin asphaltene film (~20 nm) very quickly on the bare mica surface leading to the fracture of the film and the stability of the

asphaltene thin film could be affected by the hydrophobicity of the substrate. The pancake-like domains were observed on asphaltene film coated on a hydrophobized mica surface in aqueous solutions and these pancake domains could be affected by the solution pH and addition of Ca^{2+}. Our results provide insights into an improved understanding of the interaction mechanisms between asphaltene surfaces and between asphaltenes and solid substrates in aqueous solutions, with implications for the stabilization mechanism of O/W emulsions in the presence of asphaltenes and solid particles. The results might be further correlated to the bitumen liberation process and wettability change of reservoir solids.

7.2 Major contributions

(1) It was the first time the interactions between asphaltene surfaces has been quantitatively measured as a function of absolute separation distance in heptol solvent with varying n-heptane content. It was found that the interactions between asphaltene surfaces gradually changed from pure repulsion to weak adhesion as the weight ratio of toluene (ω) in heptol decreased from $\omega=1$ to 0, which provide some insights into the understanding the stabilization mechanisms between W/O emulsions in the presence of asphaltenes.

(2) A device called computer-controlled 4-roll mill fluidic device was in-house built and applied to investigate the stability of W/O emulsion drops in the presence of asphaltenes under various flow conditions for the first time. The results from 4-roll mill tests suggested that proper collision angles and compression were required to cause interfacial sliding or shearing which locally destabilized the protective

interfacial asphaltene layers and thus enhanced the coalescence probability of the water-in-oil emulsion drops. This instrument can also be extended to other suspension systems to study the interactions among particles or drops under various flow conditions which will be more closely related to the real flow systems in industries.

(3) The interactions between asphaltene surfaces have been measured quantitatively as a function of absolute separation distance by SFA for an improved understanding of the interaction mechanisms between asphaltene surfaces at much larger scale in aqueous solutions. Solution conditions were found to significantly affect the interactions between asphaltene surfaces and an interesting phenomenon was also observed in the surface force measurement. The asphaltene surface showed substantial morphology change in aqueous solutions which was dependent on the hydrophobicity of the substrate as well as the solution conditions. To the best our knowledge, it was the first time this phenomenon was observed on asphaltene films and systematically investigated which provides some insights into an improved understanding of the wettability change of solid surfaces due to asphaltenes as well as the bitumen liberation process during the oil sands extraction process.

7.3 Suggestions for future work

(1) Investigate the stability among W/O emulsion drops in a more real industrial environment by using the in-house built 4-roll mill device. Toluene was used in this study as the organic phase which cannot fully represent the complex liquid surroundings in oil production system. Real dilutes used in industry can be

applied, such as naphtha. Moreover, the flow patterns can also be modified to mimic the flow conditions applied in industrial or can be improved based on the industrial condition to help destabilize the emulsion drops. Commonly used demulsifiers can also be incorporated into the system to investigate the stability of emulsion drops in the presence of demulsifiers and to further understand the demulsification mechanisms under flow conditions.

(2) Measure the interactions of sub-fractions of asphaltenes in different liquid media. Asphaltenes are known as a complex mixture which contains different sub-fractions. Understanding the interaction mechanisms between sub-fractions will provide us a more complete understanding on the "real component" in asphaltenes that plays the key role in aggregation, precipitation and surface adsorption as well as emulsion stabilization due to the presence of asphaltenes.

BIBLIOGRAPHY

(1) Hirschberg, A.; Dejong, L. N. J.; Schipper, B. A.; Meijer, J. G. Soc Petrol Eng J 1984, 24, 283-293.

(2) Hammami, A.; Phelps, C. H.; Monger-McClure, T.; Little, T. M. Energ Fuel 2000, 14, 14-18.

(3) Buckley, J. S. Rev I Fr Petrol 1998, 53, 303-312.

(4) Sjoblom, J.; Aske, N.; Auflem, I. H.; Brandal, O.; Havre, T. E.; Saether, O.; Westvik, A.; Johnsen, E. E.; Kallevik, H. Adv Colloid Interfac 2003, 100, 399-473.

(5) Czarnecki, J.; Moran, K. Energ Fuel 2005, 19, 2074-2079.

(6) Czarnecki, J. Energ Fuel 2009, 23, 1253-1257.

(7) Yan, J. N.; Plancher, H.; Morrow, N. R. Spe Prod Facil 1997, 12, 259-266.

(8) Chang, C. L.; Fogler, H. S. Fuel Sci Techn Int 1996, 14, 75-100.

(9) Al-Sahhaf, T. A.; Fahim, M. A.; Elkilani, A. S. Fluid Phase Equilibr 2002, 194, 1045-1057.

(10) Tharanivasan, A. K., UNIVERSITY OF CALGARY, 2012.

(11) Mullins, O. C.; Sheu, E. Y. Structures and dynamics of asphaltenes; Springer Science & Business Media, 2013.

(12) Yen, T. F.; Boucher, L. J.; Dickie, J. P.; Tynan, E. C.; Vaughan, G. B. J I Petrol 1969, 55, 87-&.

(13) Kuznicki, T.; Masliyah, J. H.; Bhattacharjee, S. Energ Fuel 2008, 22, 2379-2389.

(14) Durand, E.; Clemancey, M.; Lancelin, J. M.; Verstraete, J.; Espinat, D.; Quoineaud, A. A. Energ Fuel 2010, 24, 1051-1062.

(15) Aguilera-Mercado, B.; Herdes, C.; Murgich, J.; Muller, E. A. Energ Fuel 2006, 20, 327-338.

(16) Ruiz-Morales, Y.; Mullins, O. C. Energ Fuel 2007, 21, 256-265.

(17) Schneider, M. H.; Andrews, A. B.; Mitra-Kirtley, S.; Mullins, O. C. Energ Fuel 2007, 21, 2875-2882.

(18) Groenzin, H.; Mullins, O. C. Energ Fuel 2000, 14, 677-684.

(19) Gawrys, K. L.; Blankenship, G. A.; Kilpatrick, P. K. Langmuir 2006, 22, 4487-4497.

(20) Gray, M. R. Energ Fuel 2003, 17, 1566-1569.

(21) Murgich, J.; Abanero, J. A.; Strausz, O. P. Energ Fuel 1999, 13, 278-286.

(22) Long, J.; Xu, Z. H.; Masliyah, J. H. Langmuir 2007, 23, 6182-6190.

(23) Mullins, O. C. Spe J 2008, 13, 48-57.

(24) Mullins, O. C.; Sheu, E. Y.; Hammami, A.; Marshall, A. G. Asphaltenes, heavy oils, and petroleomics; Springer Science & Business Media, 2007.

(25) Yarranton, H. W. J Disper Sci Technol 2005, 26, 5-8.

(26) Mullins, O. C. Energ Fuel 2010, 24, 2179-2207.

(27) Mullins, O. C. Annu Rev Anal Chem 2011, 4, 393-418.

(28) Andreatta, G.; Bostrom, N.; Mullins, O. C. Langmuir 2005, 21, 2728-2736.

(29) Andreatta, G.; Goncalves, C. C.; Buffin, G.; Bostrom, N.; Quintella, C. M.; Arteaga-Larios, F.; Perez, E.; Mullins, O. C. Energ Fuel 2005, 19, 1282-1289.

(30) Zeng, H.; Song, Y. Q.; Johnson, D. L.; Mullins, O. C. Energ Fuel 2009, 23, 1201-1208.

(31) Lisitza, N. V.; Freed, D. E.; Sen, P. N.; Song, Y. Q. Energ Fuel 2009, 23, 1189-1193.

(32) Rogel, E.; Leon, O.; Torres, G.; Espidel, J. Fuel 2000, 79, 1389-1394.

(33) Castillo, J.; Fernandez, A.; Ranaudo, M. A.; Acevedo, S. Petrol Sci Technol 2001, 19, 75-106.

(34) Andersen, S. I.; Christensen, S. D. Energ Fuel 2000, 14, 38-42.

(35) Rogel, E. Langmuir 2004, 20, 1003-1012.

(36) Rogel, E. Langmuir 2002, 18, 1928-1937.

(37) Merino-Garcia, D.; Murgich, J.; Andersen, S. I. Petrol Sci Technol 2004, 22, 735-758.

(38) Agrawala, M.; Yarranton, H. W. Ind Eng Chem Res 2001, 40, 4664-4672.

(39) Duda, Y.; Lira-Galeana, C. Fluid Phase Equilibr 2006, 241, 257-267.

(40) Merino-Garcia, D.; Andersen, S. I. J Disper Sci Technol 2005, 26, 217-225.

(41) Groenzin, H.; Mullins, O. C. J Phys Chem A 1999, 103, 11237-11245.

(42) Adams, J. J. Energ Fuel 2014, 28, 2831-2856.

(43) Simon, S.; Jestin, J.; Palermo, T.; Barre, L. Energ Fuel 2009, 23, 306-313.

(44) Yarranton, H. W.; Alboudwarej, H.; Jakher, R. Ind Eng Chem Res 2000, 39, 2916-2924.

(45) Tanaka, R.; Sato, E.; Hunt, J. E.; Winans, R. E.; Sato, S.; Takanohashi, T. Energ Fuel 2004, 18, 1118-1125.

(46) Espinat, D.; Fenistein, D.; Barre, L.; Frot, D.; Briolant, Y. Energ Fuel 2004, 18, 1243-1249.

(47) Peramanu, S.; Singh, C.; Agrawala, M.; Yarranton, H. W. Energ Fuel 2001, 15, 910-917.

(48) Spiecker, P. M.; Gawrys, K. L.; Trail, C. B.; Kilpatrick, P. K. Colloid Surface A 2003, 220, 9-27.

(49) Gawrys, K. L.; Spiecker, P. M.; Kilpatrick, P. K. Petrol Sci Technol 2003, 21, 461-489.

(50) Speight, J. G.; Long, R. B. Fuel Sci Techn Int 1996, 14, 1-12.

(51) Carbonezi, C. A.; de Almeida, L. C.; Araujo, B. C.; Lucas, E. F.; Gonzalez, G. Energ Fuel 2009, 23, 1249-1252.

(52) Auflem, I. H.; Havre, T. E.; Sjoblom, J. Colloid Polym Sci 2002, 280, 695-700.

(53) Hong, E.; Watkinson, P. Fuel 2004, 83, 1881-1887.

(54) Angle, C. W.; Long, Y. C.; Hamza, H.; Lue, L. Fuel 2006, 85, 492-506.

(55) Maqbool, T.; Balgoa, A. T.; Fogler, H. S. Energ Fuel 2009, 23, 3681-3686.

(56) Pineda, L. A.; Trejo, F.; Ancheyta, J. Petrol Sci Technol 2007, 25, 105-119.

(57) Joshi, N. B.; Mullins, O. C.; Jamaluddin, A.; Creek, J.; McFadden, J. Energ Fuel 2001, 15, 979-986.

(58) Wang, J. X.; Buckley, J. S. Energ Fuel 2003, 17, 1445-1451.

(59) Andersen, S. I. Energ Fuel 1999, 13, 315-322.

(60) Buckley, J. S. Fuel Sci Techn Int 1996, 14, 55-74.

(61) Leontaritis, K. J.; Amaefule, J. O.; Charles, R. E. Spe Prod Facil 1994, 9, 157-164.

(62) Hammami, A.; Changyen, D.; Nighswander, J. A.; Stange, E. Fuel Sci Techn Int 1995, 13, 1167-1184.

(63) Stachowiak, C.; Viguie, J. R.; Grolier, J. P. E.; Rogalski, M. Langmuir 2005, 21, 4824-4829.

(64) Porte, G.; Zhou, H. G.; Lazzeri, V. Langmuir 2003, 19, 40-47.

(65) Buckley, J. S.; Hirasaki, G. J.; Liu, Y.; Von Drasek, S.; Wang, J. X.; Gil, B. S. Petrol Sci Technol 1998, 16, 251-285.

(66) Buckley, J. S. Energ Fuel 1999, 13, 328-332.

(67) Wang, J. X.; Buckley, J. S. Energ Fuel 2001, 15, 1004-1012.

(68) Wang, J. X.; Buckley, J. J Disper Sci Technol 2007, 28, 425-430.

(69) Pazuki, G. R.; Nikookar, M. Fuel 2006, 85, 1083-1086.

(70) Johansson, B.; Friman, R.; Hakanpaa-Laitinen, H.; Rosenholm, J. B. Adv Colloid Interfac 2009, 147-48, 132-143.

(71) Alboudwarej, H.; Pole, D.; Svrcek, W. Y.; Yarranton, H. W. Ind Eng Chem Res 2005, 44, 5585-5592.

(72) Dudasova, D.; Simon, S.; Hemmingsen, P. V.; Sjoblom, J. Colloid Surface A 2008, 317, 1-9.

(73) Ekholm, P.; Blomberg, E.; Claesson, P.; Auflem, I. H.; Sjoblom, J.; Kornfeldt, A. J Colloid Interf Sci 2002, 247, 342-350.

(74) Dudasova, D.; Silset, A.; Sjoblom, J. J Disper Sci Technol 2008, 29, 139-146.

(75) Farooq, U.; Sjoblom, J.; Oye, G. J Disper Sci Technol 2011, 32, 1388-1395.

(76) Kokal, S.; Tang, T.; Schramm, L.; Sayegh, S. Colloid Surface A 1995, 94, 253-265.

(77) Castro, M.; de la Cruz, J. L. M.; Buenrostro-Gonzalez, E.; Lopez-Ramirez, S.; Gil-Villegas, A. Fluid Phase Equilibr 2009, 286, 113-119.

(78) Xie, K.; Karan, K. Energ Fuel 2005, 19, 1252-1260.

(79) Goual, L.; Abudu, A. Energ Fuel 2010, 24, 469-474.

(80) Syunyaev, R. Z.; Balabin, R. M.; Akhatov, I. S.; Safieva, J. O. Energ Fuel 2009, 23, 1230-1236.

(81) Acevedo, S.; Ranaudo, M. A.; Garcia, C.; Castillo, J.; Fernandez, A. Energ Fuel 2003, 17, 257-261.

(82) Balabin, R. M.; Syunyaev, R. Z.; Schmid, T.; Stadler, J.; Lomakina, E. I.; Zenobi, R. Energ Fuel 2011, 25, 189-196.

(83) Acevedo, S.; Ranaudo, M. A.; Garcia, C.; Castillo, J.; Fernandez, A.; Caetano, M.; Goncalvez, S. Colloid Surface A 2000, 166, 145-152.

(84) Acevedo, S.; Ranaudo, M. A.; Escobar, G.; Gutierrez, L.; Ortega, P. Fuel 1995, 74, 595-598.

(85) Marczewski, A. W.; Szymula, M. Colloid Surface A 2002, 208, 259-266.

(86) Goual, L.; Horvath-Szabo, G.; Masliyah, J. H.; Xu, Z. H. Langmuir 2005, 21, 8278-8289.

(87) Zahabi, A.; Gray, M. R. Energ Fuel 2012, 26, 1009-1018.

(88) Drummond, C.; Israelachvili, J. J Petrol Sci Eng 2004, 45, 61-81.

(89) Abdallah, W. A.; Taylor, S. D. J Phys Chem C 2008, 112, 18963-18972.

(90) Rudrake, A.; Karan, K.; Horton, J. H. J Colloid Interf Sci 2009, 332, 22-31.

(91) Jouault, N.; Corvis, Y.; Cousin, F.; Jestin, J.; Barre, L. Langmuir 2009, 25, 3991-3998.

(92) Carbognani, L. Petrol Sci Technol 2000, 18, 335-360.

(93) Alvarez-Ramirez, F.; Garcia-Cruz, I.; Tavizon, G.; Martinez-Magadan, J. M. Petrol Sci Technol 2004, 22, 915-926.

(94) Yeung, A.; Dabros, T.; Masliyah, J.; Czarnecki, J. Colloid Surface A 2000, 174, 169-181.

(95) Moran, K.; Yeung, A.; Masliyah, J. Langmuir 1999, 15, 8497-8504.

(96) Zhang, L. Y.; Lopetinsky, R.; Xu, Z. H.; Masliyah, J. H. Energ Fuel 2005, 19, 1330-1336.

(97) Bouriat, P.; El Kerri, N.; Graciaa, A.; Lachaise, J. Langmuir 2004, 20, 7459-7464.

(98) Tsamantakis, C.; Masliyah, J.; Yeung, A.; Gentzis, T. J Colloid Interf Sci 2005, 284, 176-183.

(99) Rane, J. P.; Pauchard, V.; Couzis, A.; Banerjee, S. Langmuir 2013, 29, 4750-4759.

(100) Sztukowski, D. M.; Yarranton, H. W. Langmuir 2005, 21, 11651-11658.

(101) Liu, J. J.; Xu, Z. H.; Masliyah, J. Can J Chem Eng 2004, 82, 655-666.

(102) Liu, J. J.; Xu, Z. H.; Masliyah, J. Colloid Surface A 2005, 260, 217-228.

(103) Long, J.; Zhang, L. Y.; Xu, Z. H.; Masliyah, J. H. Langmuir 2006, 22, 8831-8839.

(104) Liu, J. J.; Zhang, L. Y.; Xu, Z. H.; Masliyah, J. Langmuir 2006, 22, 1485-1492.

(105) Wang, S. Q.; Liu, J. J.; Zhang, L. Y.; Xu, Z. H.; Masliyah, J. Energ Fuel 2009, 23, 862-869.

(106) Wang, S. Q.; Liu, J. J.; Zhang, L. Y.; Masliyah, J.; Xu, Z. H. Langmuir 2010, 26, 183-190.

(107) Abraham, T.; Christendat, D.; Karan, K.; Xu, Z.; Masliyah, J. Industrial & engineering chemistry research 2002, 41, 2170-2177.

(108) Natarajan, A.; Xie, J. G.; Wang, S. Q.; Liu, Q. X.; Masliyah, J.; Zeng, H. B.; Xu, Z. H. J Phys Chem C 2011, 115, 16043-16051.

(109) Zhang, L. Y.; Lawrence, S.; Xu, Z. H.; Masliyah, J. H. J Colloid Interf Sci 2003, 264, 128-140.

(110) Tabor, D.; Winterto.Rh Proc R Soc Lon Ser-A 1969, 312, 435-&.

(111) Israelachvili, J.; Tabor, D. Nature 1972, 236, 106-106.

(112) Israelachvili, J.; Tabor, D. In Proceedings of the Royal Society of London A: Mathematical, Physical and Engineering Sciences; The Royal Society, 1972; Vol. 331; pp 19-38.

(113) Israelachvili, J. N.; Adams, G. E. Nature 1976, 262, 773-776.

(114) Israelachvili, J. N. Faraday Discuss 1978, 65, 20-24.

(115) Israelachvili, J. N.; Mcguiggan, P. M. J Mater Res 1990, 5, 2223-2231.

(116) Israelachvili, J.; Min, Y.; Akbulut, M.; Alig, A.; Carver, G.; Greene, W.; Kristiansen, K.; Meyer, E.; Pesika, N.; Rosenberg, K.; Zeng, H. Rep Prog Phys 2010, 73.

(117) Mcguiggan, P. M.; Israelachvili, J. N. J Mater Res 1990, 5, 2232-2243.

(118) Zeng, H.; Tian, Y.; Anderson, T. H.; Tirrell, M.; Israelachvili, J. N. Langmuir 2008, 24, 1173-1182.

(119) Teng, F. C.; Zeng, H. B.; Liu, Q. X. J Phys Chem C 2011, 115, 17485-17494.

(120) Natarajan, A.; Kuznicki, N.; Harbottle, D.; Masliyah, J.; Zeng, H. B.; Xu, Z. H. Langmuir 2014, 30, 9370-9377.

(121) Faghihnejad, A.; Zeng, H. Soft Matter 2012, 8, 2746-2759.

(122) Israelac.Jn J Colloid Interf Sci 1973, 44, 259-272.

(123) Israelachvili, J. Intermolecular and Surface Forces; third ed.; Academic Press, 2011.

(124) Heuberger, M.; Zäch, M.; Spencer, N. Science 2001, 292, 905-908.

(125) Strausser, Y. E.; Heaton, M. G. Am Lab 1994, 26, 20-&.

(126) Giessibl, F. J. Rev Mod Phys 2003, 75, 949-983.

(127) Oliver, R. A. Rep Prog Phys 2008, 71.

(128) Alexander, J.; Magonov, S.; Moeller, M. J Vac Sci Technol B 2009, 27, 903-911.

(129) Binnig, G.; Rohrer, H. Helv Phys Acta 1982, 55, 726-735.

(130) Binnig, G.; Quate, C. F.; Gerber, C. Phys Rev Lett 1986, 56, 930-933.

(131) Zeng, H. Polymer adhesion, friction, and lubrication; John Wiley & Sons, 2013.

(132) Leckband, D.; Israelachvili, J. Q Rev Biophys 2001, 34, 105-267.

(133) Hannisdal, A.; Ese, M. H.; Hemmingsen, P. V.; Sjoblom, J. Colloid Surface A 2006, 276, 45-58.

(134) Binazadeh, M.; Zeng, H.; Unsworth, L. D. Acta Biomater 2014, 10, 56-66.

(135) Voinova, M. V.; Rodahl, M.; Jonson, M.; Kasemo, B. Phys Scripta 1999, 59, 391-396.

(136) Wang, S. S.; Zhang, L.; Yan, B.; Xu, H. L.; Liu, Q. X.; Zeng, H. B. J Phys Chem C 2015, 119, 7327-7339.

(137) Bentley, B. J.; Leal, L. G. J Fluid Mech 1986, 167, 219-240.

(138) Bentley, B. J.; Leal, L. G. J Fluid Mech 1986, 167, 241-283.

(139) Leal, L. G. Phys Fluids 2004, 16, 1833-1851.

(140) Borrell, M.; Leal, L. G. Langmuir 2007, 23, 12497-12502.

(141) Rumschel.F; Mason, S. G. J Coll Sci Imp U Tok 1961, 16, 238-&.

(142) Zhang, L.; Shi, C.; Lu, Q. G.; Liu, Q. X.; Zeng, H. B. Langmuir 2016, 32, 4886-4895.

174

(143) Sheremata, J. M.; Gray, M. R.; Dettman, H. D.; McCaffrey, W. C. Energ Fuel 2004, 18, 1377-1384.

(144) Gu, G.; Zhang, L.; Xu, Z.; Mashyah, J. Energ Fuel 2007, 21, 3462-3468.

(145) Yarranton, H. W.; Hussein, H.; Masliyah, J. H. J Colloid Interf Sci 2000, 228, 52-63.

(146) Pekdemir, T.; Akay, G.; Dogru, M.; Merrells, R. E.; Schleicher, B. Separ Sci Technol 2003, 38, 1161-1183.

(147) Feng, X. H.; Mussone, P.; Gao, S.; Wang, S. Q.; Wu, S. Y.; Masliyah, J. H.; Xu, Z. H. Langmuir 2010, 26, 3050-3057.

(148) Kumar, K.; Nikolov, A. D.; Wasan, D. T. Ind Eng Chem Res 2001, 40, 3009-3014.

(149) Kilpatrick, P. K.; Spiecker, P. M. Asphaltene emulsions. In Encyclopedic Handbook of Emulsion Technology; Sjoblom, J., Ed.; Marcel Dekker: New York, 2001, pp 707-730.

(150) McLean, J. D.; Kilpatrick, P. K. J Colloid Interf Sci 1997, 189, 242-253.

(151) Angle, C. W.; Dabros, T.; Hamza, H. A. Energ Fuel 2007, 21, 912-919.

(152) Verruto, V. J.; Kilpatrick, P. K. Langmuir 2008, 24, 12807-12822.

(153) Jestin, J.; Simon, S.; Zupancic, L.; Barre, L. Langmuir 2007, 23, 10471-10478.

(154) Alvarez, G.; Jestin, J.; Argillier, J. F.; Langevin, D. Langmuir 2009, 25, 3985-3990.

(155) Wu, X. Energ Fuel 2003, 17, 179-190.

(156) Chang, C.-L.; Fogler, H. S. Langmuir 1994, 10, 1749-1757.

(157) Roux, J. N.; Broseta, D.; Deme, B. Langmuir 2001, 17, 5085-5092.

(158) Sheu, E. Y.; Detar, M. M.; Storm, D. A.; Decanio, S. J. Fuel 1992, 71, 299-302.

(159) Mitchell, D. L.; Speight, J. G. Fuel 1973, 52, 149-152.

(160) Mullins, O. C.; Sabbah, H.; Eyssautier, J.; Pomerantz, A. E.; Barre, L.; Andrews, A. B.; Ruiz-Morales, Y.; Mostowfi, F.; McFarlane, R.; Goual, L.; Lepkowicz, R.; Cooper, T.; Orbulescu, J.; Leblanc, R. M.; Edwards, J.; Zare, R. N. Energ Fuel 2012, 26, 3986-4003.

(161) Rane, J. P.; Harbottle, D.; Pauchard, V.; Couzis, A.; Banerjee, S. Langmuir 2012, 28, 9986-9995.

(162) Pauchard, V.; Rane, J. P.; Zarkar, S.; Couzis, A.; Banerjee, S. Langmuir 2014, 30, 8381-8390.

(163) Sjöblom, J.; Aske, N.; Auflem, I. H.; Brandal, Ø.; Havre, T. E.; Sæther, Ø.; Westvik, A.; Johnsen, E. E.; Kallevik, H. Advances in Colloid and Interface Science 2003, 100, 399-473.

(164) Shi, C.; Zhang, L.; Xie, L.; Lu, X.; Liu, Q.; Mantilla, C.; van den Berg, F. G.; Zeng, H. Langmuir 2016.

(165) McLean, J. D.; Kilpatrick, P. K. J Colloid Interf Sci 1997, 196, 23-34.

(166) Spiecker, P. M.; Kilpatrick, P. K. Langmuir 2004, 20, 4022-4032.

(167) Zhang, L.; Zeng, H. B.; Liu, Q. X. J Phys Chem C 2012, 116, 17554-17562.

(168) Lu, Q. Y.; Wang, J.; Faghihnejad, A.; Zeng, H. B.; Liu, Y. Soft Matter 2011, 7, 9366-9379.

(169) Zeng, H. B.; Kristiansen, K.; Wang, P.; Bergli, J.; Israelachvili, J. Langmuir 2011, 27, 7163-7167.

(170) Zeng, H. B.; Hwang, D. S.; Israelachvili, J. N.; Waite, J. H. P Natl Acad Sci USA 2010, 107, 12850-12853.

(171) Wang, J.; Opedal, N. V.; Lu, Q. Y.; Xu, Z. H.; Zeng, H. B.; Sjoblom, J. Energ Fuel 2012, 26, 2591-2599.

(172) Israelachvili, J.; Min, Y.; Akbulut, M.; Alig, A.; Carver, G.; Greene, W.; Kristiansen, K.; Meyer, E.; Pesika, N.; Rosenberg, K. Rep Prog Phys 2010, 73, 036601.

(173) Zeng, H. B.; Maeda, N.; Chen, N. H.; Tirrell, M.; Israelachvili, J. Macromolecules 2006, 39, 2350-2363.

(174) Degennes, P. G. Adv Colloid Interfac 1987, 27, 189-209.

(175) Lowrey, D. D.; Tasaka, K.; Kindt, J. H.; Banquy, X.; Belman, N.; Min, Y.; Pesika, N. S.; Mordukhovich, G.; Israelachvili, J. N. Tribol Lett 2011, 42, 117-127.

(176) Akbulut, M.; Alig, A. R. G.; Min, Y.; Belman, N.; Reynolds, M.; Golan, Y.; Israelachvili, J. Langmuir 2007, 23, 3961-3969.

(177) Dechaine, G. P.; Gray, M. R. Energ Fuel 2010, 24, 2795-2808.

(178) Saukowski, D. M.; Yarranton, H. W. J Colloid Interf Sci 2005, 285, 821-833.

(179) Jiang, T.; Hirasaki, G. J.; Miller, C. A.; Moran, K. Energ Fuel 2008, 22, 4158-4164.

(180) Marchal, C.; Abdessalem, E.; Tayakout-Fayolle, M.; Uzio, D. Energ Fuel 2010, 24, 4290-4300.

(181) Nassar, N. N. Energ Fuel 2010, 24, 4116-4122.

(182) de la Cruz, J. L. M.; Castellanos-Ramirez, I. V.; Ortiz-Tapia, A.; Buenrostro-Gonzalez, E.; Duran-Valencia, C. D.; Lopez-Ramirez, S. Colloid Surface A 2009, 340, 149-154.

(183) Abudu, A.; Goual, L. Energ Fuel 2009, 23, 1237-1248.

(184) Labrador, H.; Fernandez, Y.; Tovar, J.; Munoz, R.; Pereira, J. C. Energ Fuel 2007, 21, 1226-1230.

(185) Acevedo, S.; Castillo, J.; Fernandez, A.; Goncalves, S.; Ranaudo, M. A. Energ Fuel 1998, 12, 386-390.

(186) Piro, G.; Canonico, L. B.; Galbariggi, G.; Bertero, L.; Carniani, C. Spe Prod Facil 1996, 11, 156-160.

(187) Wang, J.; Lu, Q. Y.; Harbottle, D.; Sjoblom, J.; Xu, Z. H.; Zeng, H. B. J Phys Chem B 2012, 116, 11187-11196.

(188) Faghihnejad, A.; Zeng, H. B. Soft Matter 2012, 8, 2746-2759.

(189) Dutta, A. K.; Belfort, G. Langmuir 2007, 23, 3088-3094.

(190) Kwon, W. T.; Park, K.; Han, S. D.; Yoon, S. M.; Kim, J. Y.; Bae, W.; Rhee, Y. W. J Ind Eng Chem 2010, 16, 684-687.

(191) Kallevik, H.; Kvalheim, O. M.; Sjöblom, J. J Colloid Interf Sci 2000, 225, 494-504.

(192) Dai, Q.; Chung, K. H. Fuel 1996, 75, 220-226.

(193) Kim, B.-Y.; Moon, J. H.; Sung, T.-H.; Yang, S.-M.; Kim, J.-D. Separ Sci Technol 2002, 37, 1307-1320.

(194) Kralova, I.; Sjoblom, J.; Oye, G.; Simon, S.; Grimes, B. A.; Paso, K. Adv Colloid Interfac 2011, 169, 106-127.

(195) Kumar, K.; Nikolov, A.; Wasan, D. Ind Eng Chem Res 2001, 40, 3009-3014.

(196) Pekdemir, T.; Akay, G.; Dogru, M.; Merrells, R.; Schleicher, B. Separ Sci Technol 2003, 38, 1161-1183.

(197) Sparks, B. D.; Kotlyar, L. S.; O'Carroll, J. B.; Chung, K. H. J Petrol Sci Eng 2003, 39, 417-430.

(198) Kotlyar, L. S.; Sparks, B. D.; Woods, J. R.; Chung, K. H. Energ Fuel 1999, 13, 346-350.

(199) Yan, N. X.; Gray, M. R.; Masliyah, J. H. Colloid Surface A 2001, 193, 97-107.

(200) Zhang, W. B.; Shi, Z.; Zhang, F.; Liu, X.; Jin, J.; Jiang, L. Adv Mater 2013, 25, 2071-2076.

(201) Kilpatrick, P. K.; Spiecker, P. M.; Marcel Dekker: New York, 2001; Vol. 3; pp 707-730.

(202) Sjoblom, J. Encyclopedic handbook of emulsion technology; CRC Press, 2001.

(203) Gafonova, O. V.; Yarranton, H. W. J Colloid Interf Sci 2001, 241, 469-478.

(204) Czarnecki, J.; Tchoukov, P.; Dabros, T. Energ Fuel 2012, 26, 5782-5786.

(205) Higaki, Y.; Hatae, K.; Ishikawa, T.; Takanohashi, T.; Hayashi, J.-i.; Takahara, A. ACS applied materials & interfaces 2014, 6, 20385-20389.

(206) Kaminski, T. J.; Fogler, H. S.; Wolf, N.; Wattana, P.; Mairal, A. Energ Fuel 2000, 14, 25-30.

(207) Mullins, O. C.; Sabbah, H.; Eyssautier, J. l.; Pomerantz, A. E.; Barré, L.; Andrews, A. B.; Ruiz-Morales, Y.; Mostowfi, F.; McFarlane, R.; Goual, L. Energ Fuel 2012, 26, 3986-4003.

(208) Jiang, T.; Hirasaki, G. J.; Miller, C. A.; Ng, S. Energ Fuel 2011, 25, 2551-2558.

(209) Zhang, L. Y.; Xu, Z. H.; Mashyah, J. H. Langmuir 2003, 19, 9730-9741.

(210) Shi, C.; Chan, D. Y. C.; Liu, Q. X.; Zeng, H. B. J Phys Chem C 2014, 118, 25000-25008.

(211) Shi, C.; Cui, X.; Xie, L.; Liu, Q. X.; Chan, D. Y. C.; Israelachvili, J. N.; Zeng, H. B. Acs Nano 2015, 9, 95-104.

(212) Li, L.; Yan, B.; Yang, J. Q.; Chen, L. Y.; Zeng, H. B. Adv Mater 2015, 27, 1294-1299.

(213) Israelachvili, J. N. Intermolecular and surface forces: revised third edition; Academic press, 2011.

(214) Alcantar, N. A.; Park, C.; Pan, J.-M.; Israelachvili, J. N. Acta materialia 2003, 51, 31-47.

(215) Alcantar, N.; Israelachvili, J.; Boles, J. Geochimica et Cosmochimica Acta 2003, 67, 1289-1304.

(216) Yang, D. Z.; Xie, L.; Bobicki, E.; Xu, Z. H.; Liu, Q. X.; Zeng, H. B. Langmuir 2014, 30, 10809-10817.

(217) Drelich, J.; Long, J.; Yeung, A. The Canadian Journal of Chemical Engineering 2007, 85, 625-634.

(218) Das, S.; Thundat, T.; Mitra, S. K. Fuel 2013, 108, 543-549.

(219) Ducker, W. A.; Clarke, D. R. Colloids and Surfaces A: Physicochemical and Engineering Aspects 1994, 93, 275-292.

(220) Yan, L.; Englert, A. H.; Masliyah, J. H.; Xu, Z. Langmuir 2011, 27, 12996-13007.

(221) Yang, D.; Xie, L.; Bobicki, E.; Xu, Z.; Liu, Q.; Zeng, H. Langmuir 2014, 30, 10809-10817.

(222) Ducker, W. A.; Senden, T. J.; Pashley, R. M. Langmuir 1992, 8, 1831-1836.

(223) Liu, J. J.; Xu, Z. H.; Masliyah, J. Langmuir 2003, 19, 3911-3920.

(224) Liu, J.; Zhang, L.; Xu, Z.; Masliyah, J. Langmuir 2006, 22, 1485-1492.

(225) Taylor, S. D.; Czarnecki, J.; Masliyah, J. J Colloid Interf Sci 2002, 252, 149-160.

(226) Sjöblom, J.; Hemmingsen, P. V.; Kallevik, H. In Asphaltenes, Heavy Oils, and Petroleomics; Springer, 2007; pp 549-587.

(227) Gu, G.; Xu, Z.; Nandakumar, K.; Masliyah, J. H. Fuel 2002, 81, 1859-1869.

(228) Akhlaq, M. S.; Gotze, P.; Kessel, D.; Dornow, W. Colloid Surface A 1997, 126, 25-32.

(229) Basu, S.; Sharma, M. M. Spe J 1999, 4, 235-241.

(230) Drummond, C.; Israelachvili, J. J Petrol Sci Eng 2002, 33, 123-133.

(231) Jada, A.; Debih, H. Compos Interface 2009, 16, 219-235.

(232) Vanoss, C. J. Colloid Surface A 1993, 78, 1-49.

(233) Vanoss, C. J.; Good, R. J.; Chaudhury, M. K. J Colloid Interf Sci 1986, 111, 378-390.

(234) Buckley, J. S.; Lord, D. L. J Petrol Sci Eng 2003, 39, 261-273.

(235) Li, H. H.; Long, J.; Xu, Z. H.; Masliyah, J. H. Can J Chem Eng 2008, 86, 168-176.

(236) Van Oss, C. J. Interfacial forces in aqueous media; CRC press, 2006.

(237) Vanderhoff, J.; Bradford, E.; Carrington, W. In Journal of Polymer Science: Polymer Symposia; Wiley Online Library, 1973; Vol. 41; pp 155-174.

(238) Seo, J.; Han, H. J Appl Polym Sci 2001, 82, 731-737.

(239) Linossier, I.; Gaillard, F.; Romand, M.; Feller, J. F. J Appl Polym Sci 1997, 66, 2465-2473.

(240) Pereira, M. R.; Yarwood, J. J Chem Soc Faraday T 1996, 92, 2737-2743.

(241) Boukir, A.; Aries, E.; Guiliano, M.; Asia, L.; Doumenq, P.; Mille, G. Chemosphere 2001, 43, 279-286.

(242) Liu, J. J.; Zhou, Z.; Xu, Z. H. Ind Eng Chem Res 2002, 41, 52-57.

(243) Wind, M. M.; Lenderink, H. J. W. Prog Org Coat 1996, 28, 239-250.

(244) Nishimura, S.; Tateyama, H.; Tsunematsu, K.; Jinnai, K. J Colloid Interf Sci 1992, 152, 359-367.

(245) Kasongo, T.; Zhou, Z.; Xu, Z. H.; Masliyah, J. Can J Chem Eng 2000, 78, 674-681.

(246) Basu, S.; Nandakumar, K.; Lawrence, S.; Masliyah, J. Fuel 2004, 83, 17-22.